Doctoral Theses at NTNU, 2008:201

Daniel Stanghelle

High temperature filtration of biomass combustion and gasification processes

NTNU
Norwegian University of
Science and Technology

NTNU
Norwegian University of
Science and Technology

NTNU
Norwegian University of
Science and Technology
Thesis for the degree of
philosophiae doctor
Faculty of Engineering Science and Technology
Department of Energy and Process Engineering

Daniel Stanghelle

Doctoral Thesis

Theses at NTNU, 2008:201

NTNU

ISBN 978-82-471-1085-0 (printed ver.)
ISBN 978-82-471-1086-7 (electronic ver.)
ISSN 1503-8181

NTNU
Norwegian University of
Science and Technology

Daniel Stanghelle

High temperature filtration of biomass combustion and gasification processes

Thesis for the degree of philosophiae doctor

Trondheim, October 2008

Norwegian University of
Science and Technology
Faculty of Engineering Science and Technology
Department of Energy and Process Engineering

NTNU
Norwegian University of
Science and Technology

NTNU
Norwegian University of Science and Technology

Thesis for the degree of philosophiae doctor

Faculty of Engineering Science and Technology
Department of Energy and Process Engineering

ISBN 978-82-471-1085-0 (printed ver.)
ISBN 978-82-471-1086-7 (electronic ver.)
ISSN 1503-8181

Theses at NTNU, 2008:201

Printed by Tapir Uttrykk

Preface

This thesis is submitted in partial fulfillment of the requirements for the degree of Philosophiae Doctor at the Norwegian University of Science and Technology (NTNU). The work was carried out at the Department of Energy and Process Engineering at the Faculty of Engineering Science and Technology. Professor Johan E. Hustad has supervised the work and professor Otto K. Sønju has been the co-supervisor. The research was funded by the Nordic Graduate School of Biofuel Science and Technology.

Acknowledgments

I would like to thank my academic advisers Professor Johan E. Hustad and Otto K. Sønju for their support and encouragement. Their enthusiasm and scientific skills have been important for my motivation during my PhD study.

I also want to thank Professor Gernot Krammer for his willingness to discuss scientific problems as well as his precise and constructive criticism of my work during many discussions.

I would like to thank Torbjørn Slungaard, Arnstein Norheim and Kjell Myrland for their invaluable help during the experimental work. I would also like to thank the staff of the laboratory at the Department of Energy and Process Engineering for their practical help and support, especially Jan Erik Molde and Reidar Tellebon who participated in the testing outside the laboratory in addition to Øyvind Skreiberg and Roger Khalil for their contribution to the BioSOFC project. Furthermore, I would like to thank Magnus Paulsen and Ingunn Natvig who worked with me and wrote their Master theses as well as Ronny Schimpke who worked with me during his project report.

Special thanks to the administration staff for their assistance on all practical matters.

I also want to thank my present and past colleagues at the department for the practical solutions found during "coffee discussions".

Finally, I want to thank my wife Monica for always being there for me. She has given up a lot in order to give me the opportunity to complete this work. Without her patience and endless support, this work would have been stranded years ago.

Abstract

This thesis describes the theoretical background, including the current status of the panel bed filter before focusing on the experimental investigation done in order to further develop the granular panel bed filter. The experimental investigation was done on four different filters and include:

- The laboratory study of a new louver design.
- The prototype study of high temperature filtration of biomass gasification producer gas.
- The demonstration plant study of a new puffback geometry as well as the startup and the running of the first experimental series of a commercial plant.

The laboratory study of a new louver design was performed with ISO-standard dust at ambient temperature. Several filtration experiments were preformed with different dust concentration (3.53 - 7.01 g/m^3) and filtration velocities (3.87 - 14.8 cm/s). The results showed a high collection efficiency above 99.071% and a significant reduction in the the residual pressure compared to older louver designs.

The high temperature prototype study was done on a slipstream from the biomass gasification plant in Güssing, Austria. The purpose of the tests were to clean the producer gas from particles in order to utilize the gas in a Solid Oxide Fuel Cell. Two panel bed filters were tested separately with a filtration temperature of 500-550°C. The filter operation was not influenced by the high tar content of the producer gas of 1 - 2 g/m^3. Several hours of testing on the two filters with a fluctuating dust concentration (2 - 3 g/m^3 or 7 - 11 g/m^3 depending on the sampling line) resulted in a collection efficiency above 99.98%.

The demonstration plant study was performed at 190°C on a slipstream from the biomass furnace at Bjertnæs Sag AS in Jevnaker, Norway. The furnace burns wood chip residue from the wood panel production plant and delivers district heating to a local heating system. A new puffback geometry was developed which reduced the height of of the filter with approximately 1 meter (a reduction of the puffback geometry height of approximately 70%) compared to the earlier designs. The filter module was design for a maximum flow of 375 Nm^3/h. The results from the filtration tests showed a collection efficiency of 98.23% with an inlet concentration fluctuation between 0.15-0.17 g/m^3.

Abstract

Contents

Nomenclature

Latin Letters

a	Constant	[-]
A	Area	[m^2]
C	Concentration	[g/m^3]
CV	Calorific value	[J]/[kg]
dp	Particle diameter	[m]
Ec	Collection efficiency	[-]
f	Hydraulic friction factor	[-]
h	Weight fraction of hydrogen (equation 2.6)	[-]
I_p	Specific impulse	[kg m/s]
K	Equilibrium constant (reaction kinetics)	[-]
K_1	Residual resistance of filter	[m/m^2]
K_2	Specific resistance of dust cake	[m/kg]
K_1^*	Residual resistance of filter normalized by the gas viscosity	[kg/m^2 s]
K_2^*	Specific resistance of the filter cake normalized by the gas viscosity	[s^{-1}]
L	Lenght	[m]
m	Mass	[kg]
M_2/M_1	Sphere size distribution in equation 3.13	[-]
n	Total number (of particles)	[-]
P	Pressure	[Pa]
Q	Volume flow	[m^3/s]
$q_r(x)$	Frequency particle size distribution curve	[-]
$Q_r(x)$	Cumulative particle size distribution curve	[-]
S	Surface	[m^2]
t	Time	[s]
t_a	Active time	[s]
T	Temperature	[^{o}C]
V	Volume	[m^3]
$vol\%$	Volume prosentaile	[-]
w	Moisture fraction	[kg]$_{water}$/[kg]$_{sample}$
$\overline{W}_A$	Average accumulated mass of dust per filter area	[kg/m^2]
$wt\%$	Weight prosentaile	[-]
X	Weight fraction	[-]

Greek Letters

α	Constant	[-]
β	Constant	[-]
Δ	Difference	[-]
π	Constant	[-]
κ	Permeability	[m]
μ	Dynamic viscosity	[Pa s]
ς	Resistance coefficient	[-]
ω	Angle	[°]
ϵ	Porosity	[-]
ψ	Spericity	[-]

Subscripts and superscripts

$^{-}$	Average
c	Container weight in equation refeq:moisture
cs	Cross section
el	Electricity
f	Final value (equation refeq:moisture)
fr	Friction
FC	Fixed carbon
gf	Granular filter
h	Hydraulic
i	Integer number or initial value equation refeq:moisture
l	Liquid
min	Minimum
n	Number (of sampling size)
p	Particle
peak	Maximum
R	Residual (pressure)
s	Surface area
sf	Superficial
tot	Totale
VM	Volatile matter

Abbreviations

ASTM	American Society for Testing and Materials
BFB	Bubbling Fluidized Bed
BGPG	Biomass Gasification Producer Gas
CFB	Circulating Fluidized Bed
CV	Calorific value
d.a.f	Dry Ash Free
db	Dry basis
ESP	Electrostatic precipitation
EU	European Union
FFR	Filtration area to Frontal area Ratio
GCV	Gross calorific value or higher heating value
HHV	Higher heating value or gross calorific value
HTHP	High temperature high pressure
ISO	International Organization for Standardization
LHV	Lover heating value or net calorific value
MSW	Municipal Solid Waste
NTNU	Norwegian University of Science and Technology
PBF	Panel Bed Filter
PCL	Pressurized Control Loop
RES	Renewable Energy Sources
RES-E	Electricity generation from Renewable Energy Sources
SB	Sintered Bauxite
SFT	Norwegian Pollution Control Authority
SOFC	Solid Oxide Fuel Cell
wb	Wet basis
WW2	Second World War

List of Figures

List of Tables

Chapter 1

Introduction

"Change starts when someone sees the next step"

William Drayton (1776-1846)
US Congressman

1.1 Background

Currently, non renewable fossil fuels are the predominant energy carrier in global energy production. However, high oil prices, increased demand, as well as a growing concern for the environmental impact caused by human activity have all resulted in a renewed interest in the renewable energy carriers.

In 2007, the European Union (EU) set a new renewable energy target of a 20% share of the total EU energy consumption by 2020 [34]. The utilization of biomass both as gasification and combustion as well as biomass co-combustion with other fuels is an interesting and important alternative in this respect.

The utilization of renewable energy carriers is in accordance with the laws and legislations regarding gaseous and particulate emissions. The emission limits have become stricter in recent years and are currently 50 mg/m^3 but can be stricter as the emissions level from Norwegian industry is case dependent and set by the Norwegian Pollution Control Authority (SFT).

Gas cleaning from industrial applications has become the topic of world-wide research which is also the motivation for this work. This work focuses on the use of the panel bed filter. The panel bed filter is a granular filter which operates in surface filtration mode. The filter design allows for regeneration of the filter surface by a pressure pulse in the reverse direction of the normal flow which allows for continuous operation of the filter.

1.2 Objectives of the work

This experimental investigation focuses on further development of the panel bed filter. The main objectives have been to:

- Conduct a laboratory study of a panel bed filter with the new filter tray louver design. This includes building, instrumenting and operating the filter in order to investigate the new louver design.
- Investigate two prototype panel bed filters designed for high temperature applications. The study includes building, instrumenting and operating the filters above 500°C in order to filtrate out the particles from a slipstream of a biomass gasification plant. The gas must be cleaned and prepared in order to be utilized in a Solid Oxide Fuel Cell (SOFC).
- Build and operate an industrial scale panel bed filter designed to clean the flue gas from the biomass furnace at Bjertnæs Sag AS in Jevnaker, Norway. The study includes designing and instrumenting the filter, designing and building the regeneration of the filter media and the start-up of the filter on-site.
- Program the control system for all filters which will include the data handling and operation of the axillary equipment.

The scope of this PhD is clearly experimental in design. The time and energy used for on-site testing and laboratory experiments have resulted in a large amount of experimental knowledge which can hardly be communicated in a written document.

1.3 Survey of thesis

Chapter 2 describes woody biomass and gives an overview of the standards for fuel analysis of biomass and biomass energy conversion with an emphasis on gasification.

Chapter 3 gives an overview of particle properties. The basic theory of hydraulic resistance of flow through granular material is presented before focusing on the theory and earlier experimental work within granular bed gas-solid filtration.

Chapter 4 describes the history of the panel bed filter. Earlier designs are described as well as the principles of cake removal from the panel bed filter. The current status is given and some of the future challenges are highlighted.

Chapter 5 contains experimental setups and results.

Chapter 6 contains the conclusion and scope for further work.

Chapter 7, 8, 9, 10 and 11 reprints the scientific publications published based on this work.

Chapter 2

Biomass

"As the kindled fire consumes the fuel, so in the flame of wisdom the embers of action are burnt to ashes"

Bhagavad Gita
Old Hindu text

Thermal conversion of biomass has been a subject of research at the Norwegian University of Science and Technology (NTNU) for many years. Grønli [41] produced a detailed study of the thermal degradation of several biomass materials. Skreiberg [123] focused on NO_x emissions from incomplete wood log combustion. Sørum [138] focused on the environmental aspects of thermal degradation of multicipal solid waste (MSW). Barrio [7] and Fossum [37] investigated biomass gasification processes. Risnes [110] focused on high temperature filtration of biomass combustion and gasification. Adam [2] investigated catalytic conversion of biomass to produce liquid biofuels and Norheim [92] investigated Solid Oxide Fuel Cells (SOFC) on biomass gasification producer gas.

This work is a natural continuation of the previous work at the Department of Energy and Process Engineering, not focusing on the thermal degradation of the biomass, but rather on the high temperature cleaning process of biomass gasification producer gas before it is utilized.

2.1 Introduction

Fossil fuels such as oil, gas and coal are the most used energy carriers on a global scale as shown in figure 2.1. However, growing concern for energy security (security of supply) and the environmental impact due to increased CO_2 concentrations in the atmosphere, figure 2.2, are resulting in an increased interest in the utilization of renewable energy carriers. The EU has agreed to increase the use of Renewable Energy Sources (RES) from 6% in 1997 to 12% in 2010. The target for electricity generation from Renewable Energy Sources (RES-E) is to increase the production from 14% in 1997 to 22% in 2010. The focus on renewable energy within the EU has resulted in technological development, improved energy security, and it has reduced the environmental impacts of power production. In 2007, the EU council proposed a new renewable energy target of a 20% share of the total EU

energy consumption by 2020. All 27 member states supported the proposal which will be a natural extention of the 2010 targets [34]. The largest contribution of renewable energy production in the EU comes from combustible renewables and waste, figure 2.3.
The EU defined biomass as the biodegradable fraction of products, waste and residues from agriculture (including vegetal and animal substances), forestry and related industries, as well as the biodegradable fraction of industrial and municipal waste [33]. This definition includes trees, arable crops, algae and other plants; agricultural and forest residues; effuents, sewage sludge, manures, industrial by-products and the organic fraction of municipal solid waste. In this work biomass will only refer to wood and wood residues.

2.2 Wood composition

The energy in woody biomass is a result of the photosynthesis process shown in equation 2.1. Burning or digesting the biomass releases the bounded organic carbon back into the environment. The net increase of CO_2 in the environment is zero as long as the CO_2 emissions from biomass consumption is equal to or lower than the CO_2 production from new biomass growth.

$$CO_2 + H_2O + Light + Chlorophyll = CH_2O + O_2 \tag{2.1}$$

A live tree consists mainly of dead cells. Only the cambium (Fig. 2.4) contains living cells. Phloem (inner bark) is produced on the outer edge of the cambium, while wood material (xylem) is produced at the inner edge. The xylem grows in annual increments or growth rings. The growth rings consist of the lighter early wood that is formed during the high growth season (rain season, spring and summer), and the darker and shorter late wood. Rays stretch from the outer bark either to the pith (primary rays) or to the annual ring (secondary rays). The pith is located in the core of the tree trunk and represents the tree tissue formed during the first year of growth [41].

Wood can be divided into two broad classes (Fig. 2.5), softwood (gymnosperms) and hardwood (angiosperms). The terms have no reference to the actual hardness of the wood. Softwood (like pine and fir) are generally nonporous and do not contain vessels [145]. Softwood has a relatively simple structure and consists of 90-95 vol% longitudinal cells called tracheids [36].
Hardwoods (like oak and beech) generally have a more complex structure compared to softwoods. Several kinds of longitudinal cells create more intercellular volume and the radial ray volume can exceed 25 vol% [47][145].

Both softwoods and hardwoods are made up of cellulose, hemicellulose, lignin, extractives and ash. The main species cellulose, hemicellulose and lignin consist of approximately 95 vol% of the woody biomass material [41].

Cellulose is a linear polysaccharide and the main component of the wood fiber cell walls. The polymer is the main source of the high tensile strength in wood and consists of repeating units of cellobiose molecules in the range of 7500-15000

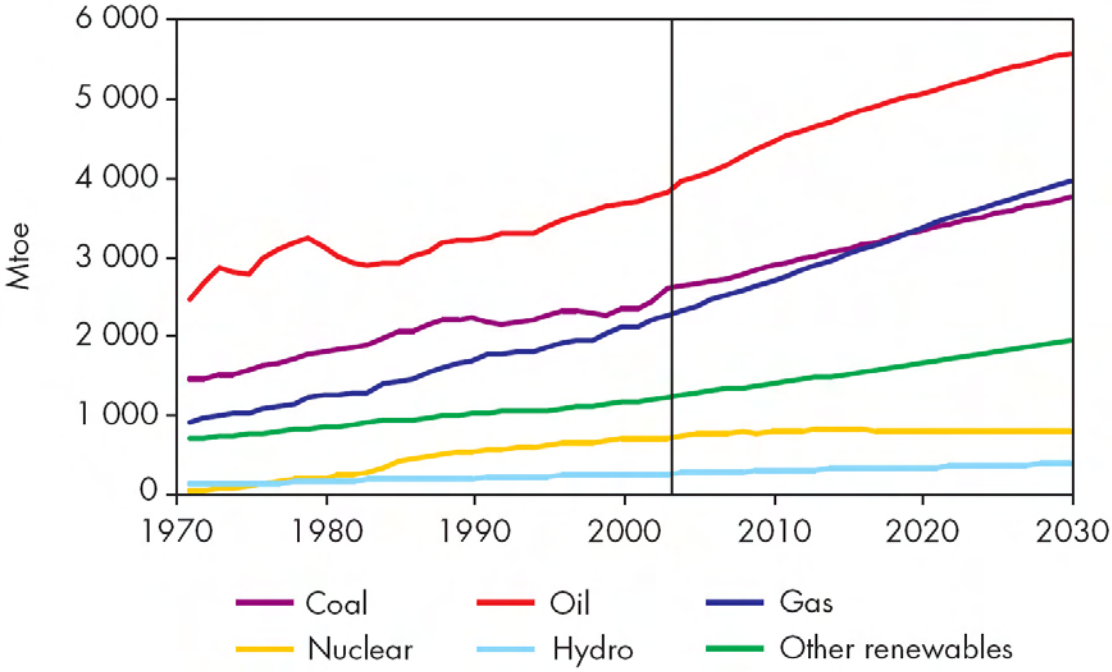

Figure 2.1: World energy usage [55]

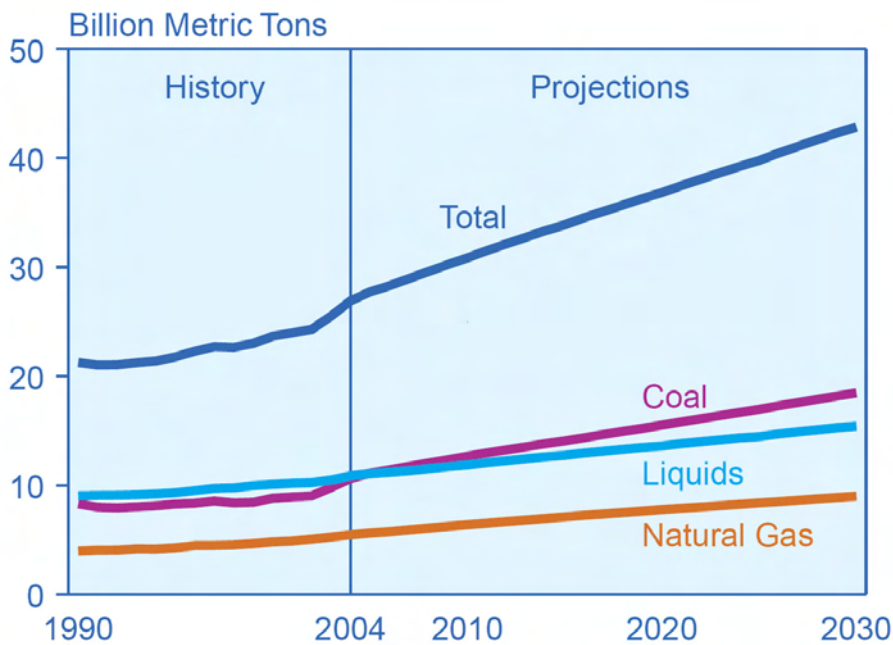

Figure 2.2: Emission of CO_2 equivalent [146]

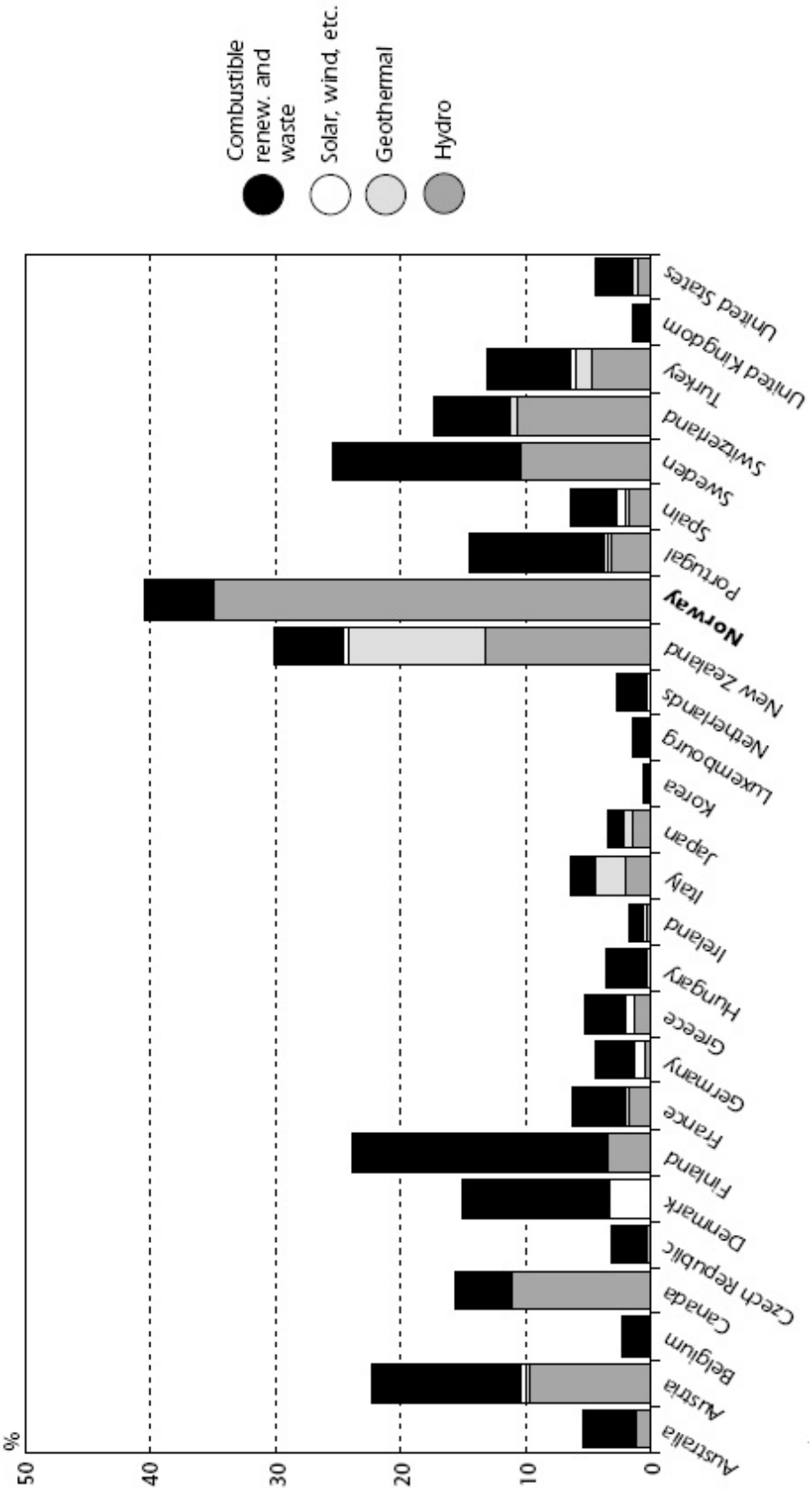

Figure 2.3: Renewable energy production as % of total production [54]

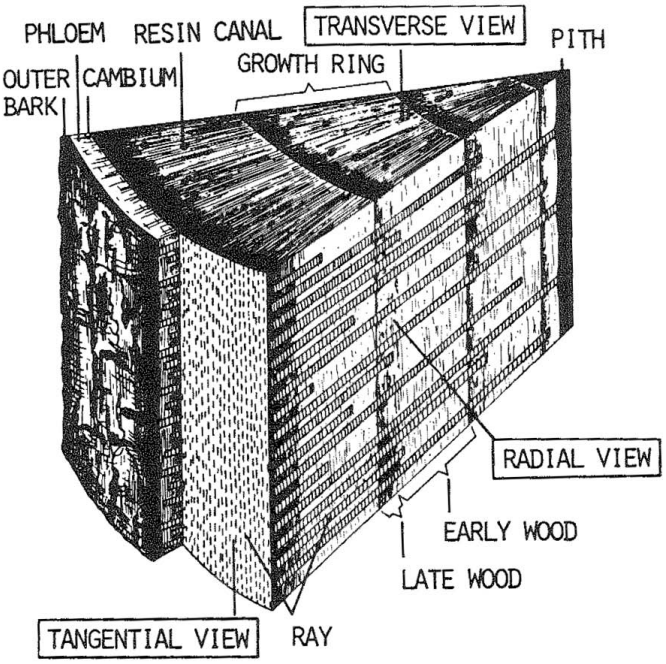

Figure 2.4: Section of a four-year-old stem [122]

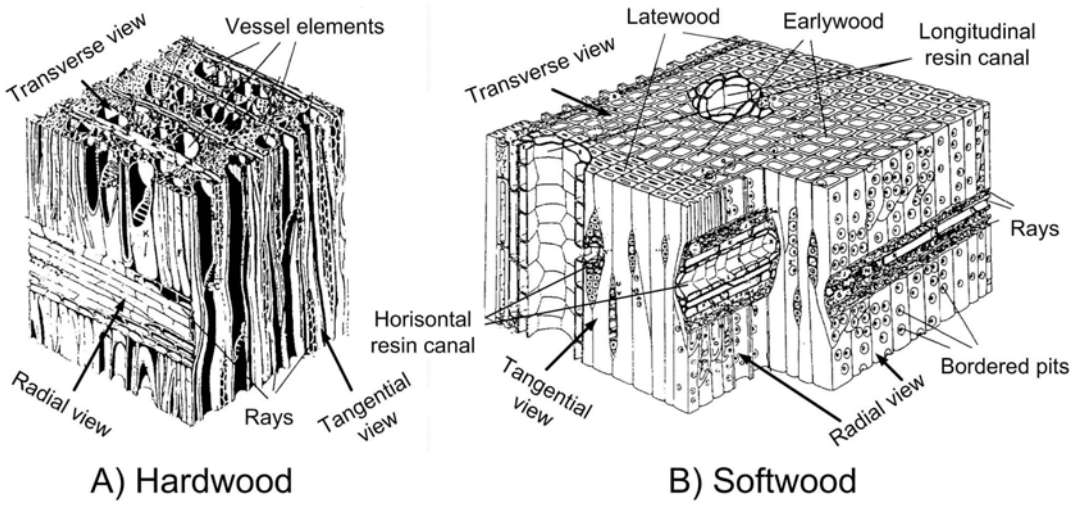

Figure 2.5: Hardwood and softwood structures [120]

in plant cellulose. The elemental formula of cellulose is ($C_6H_{10}O_5$) [2][41][47].

Hemicellulose is an amorphous heterogeneous group of branched polysaccharides consisting primarily of five- and six-carbon sugars [85]. Hemicellulose is more soluble and easier to degrade chemically compared to cellulose. The hemicellulose consists of 50 to 200 units that might be randomly branched [41][92].

Lignin binds the wood cells together and is responsible for the rigidity of the cell walls. Lignin is a complex three dimensional polymer [41] and is believed to be made of a three carbon chain attached to rings of six carbon atoms called phenyl-propanes [85]. The solubility of lignin is very poor in most solvents [4]. It is hard to isolate lignin in wood without altering the chemical structure i.e. many bonds are broken in order to separate the substance [41].

Extractives include aliphatic, aromatic and alicyclic compounds, hydrocarbons, alcohols, ketones and various acids, esters, phenolic componds, resins, terpenes and many more. These components can be separated from the wood using an organic solvent or water [41].

Ash in wood contains the heavy metals, alkali metals, sulphur, chlorine and silicates. The ash content of wood is normally less than 1% by weight [41].

2.2.1 Fuel analysis of biomass

The proximate and ultimate fuel analysis are standardized tests (ASTM 870-82) for comparing fuels. The tests are commonly presented with the measured heating value of the fuel.

Proximate Analysis

Proximate analysis of wood fuels quantifies key parameters such as *the moisture content* (ASTM E871), *the volatile content* (ASTM E872), *the fixed carbon content*, and *the ash content* (ASTM D1102).

The moisture content, w, is defined as the water to biomass weight ratio. The weight can be referred to on a wet basis (wb), dry basis (db) or on a dry and ash free (d.a.f.) basis [66]. The moisture is defined according to the ASTM tests after drying the wood at $103 \pm 1°C$ for approximately 24 hours.

$$w = \frac{w_i - w_f}{w_i - w_c} \tag{2.2}$$

The moisture can be divided into extrinsic and intrinsic moisture. The intrinsic moisture only concerns the moisture in the biomass, while the extrinsic moisture takes into consideration the weather during harvest [85]. The intrinsic moisture consists of hygroscopic bounded water in the solid structure, capillary or free water in the pores and water vapor in the pores [10] [12] [41].

The volatile matter (VM) of wood is determined by weight after heating a sample in a covered crucible of 950±20°C in an inert atmosphere for 7 min. Since no air is added the fuel sample is not burned, but carbonized, and both the char and the ash fraction remain in the crucible. The weight fraction of volatile matter, X_{VM}, in the sample is:

$$X_{VM} = \frac{m_{VM}}{m_{sample}} \tag{2.3}$$

The ash fraction is determined by heating the sample in an open crucible at 600±20°C for 4 to 6 hours. Only the ash will remain in the crucible after the burnout, giving the ash weight fraction, X_{Ash}, as:

$$X_{Ash} = \frac{m_{Ash}}{m_{sample}} \tag{2.4}$$

The fixed carbon content, X_{FC},of the fuel sample can then be calculated as:

$$X_{FC} = 100 - (X_{VM} - X_{Ash}) \tag{2.5}$$

Heating value

The heating value describes the energy content per unit mass from stocheometric adiabatic combustion. The heating value can be expressed either as the higher heating value (HHV) or the lower heating value (LHV). The higher heating value quantifies the energy including the latent heat from the combustion assuming all water to be in vapor phase. The higher heating value can be determined by a bomb calorimeter and is in the range of 18-21 MJ/kg.

$$\begin{aligned} LHV &= HHV\left(1 - \frac{w_{w.b.}}{100}\right) - 2.447\left(\frac{w_{w.b.}}{100}\right) \\ &\quad - 2.447\left(\frac{h}{100}\right) 8.99\left(1 - \frac{w_{w.b.}}{100}\right) [MJ/kg, w.b] \end{aligned} \tag{2.6}$$

The lower heating value quantifies the fuel energy assuming that all water is in a liquid phase after combustion. The lower heating value can be calculated from the higher heating value as shown in equation 2.6, where $w_{w.b.}$ and h are the weight fraction of fuel moisture (wt% wet basis) and hydrogen of the fuel (wt% dry basis) respectively.
Proximate analysis of different biomass fuels together with the measured heating values are given in table 2.1.

Ultimate Analysis

Ultimate analysis is the determination of the elements in the sample presented by weight percentage. The elements in biomass are mainly carbon, hydrogen, oxygen and nitrogen. Additional varying quantities of sulphur, chlorine, alkali metals and heavy metals might be present in the sample. Results from ultimate analysis from different biomass fuels are given in table 2.2.

Material	Proximate Analysis Moisture (wt%)	VM (wt%)	FC (wt%)	Ash (wt%)	Heating value (MJ/kg)	Ref
Alfaalfa stems	-	78.92	15.81	5.27	HHV 18.67	[58]
Weat straw	-	75.27	17.71	7.02	HHV 17.94	[58]
Rice hulls	-	63.52	16.22	20.26	HHV 15.84	[58]
Willow	-	82.22	11.95	2.7	HHV 19.59	[58]
Fir	6.5	82.0	17.2	0.8	HHV 21.00	[85]
Danish pine	8.0	71.6	19.0	1.6	HHV 21.20	[85]
Cereal straw	6.0	79.0	10.7	4.3	HHV 17.30	[85]
Barley straw	30	46.0	18.0	6.0	LHV 16.10	[85]
Lignite	34.0	29.0	31.0	6.0	LHV 26.80	[85]
Bituminous coal	11.0	35.0	45.0	9.0	LHV 34.00	[85]
Pine	5.5	81.2	12.1	1.2	HHV 18.30	[113]
Miscanthus	6.1	67.9	13.1	12.9	HHV 15.40	[113]
Willow	7.2	78.1	13.7	1.0	HHV 17.80	[113]

Table 2.1: Proximate Analysis

	Ultimate Analysis (wt%) C	H	N	O	S	Cl	Ash	Ref
Alfaalfa stems	47.17	5.99	2.68	38.19	0.20	0.50	5.27	[58]
Weat straw	44.92	5.46	0.44	41.77	0.16	0.23	7.02	[58]
Rice hulls	38.83	4.75	0.52	35.47	0.05	0.12	20.26	[58]
Willow	49.9	5.9	0.61	41.8	0.07	<0.01	1.71	[58]
Cypress	55.0	6.5	-	38.1	-	-	0.4	[85]
Ash	49.7	6.9	-	43.0	-	-	0.3	[85]
Beech	51.6	6.3	-	41.4	-	-	-	[85]
Miscanthus	48.1	5.4	0.5	42.2	<0.1	-	2.8	[85]
Barley straw	45.7	6.1	0.4	38.3	0.1	-	6.0	[85]
Rice straw	41.4	5.0	0.7	39.9	0.1	-	-	[85]
Bituminous coal	73.1	5.5	1.4	8.7	1.7	-	9.0	[85]
Lignite	56.4	4.2	1.6[1]	18.4	-	-	5.0	[85]
Pine	49.8	8.1	-	38.3	-	-	1.2	[113]
Miscanthus	39.9	6.3	-	34.8	-	-	12.9	[113]
Willow	45.9	6.6	-	39.3	-	-	1.0	[113]

[a] Combined N and S

Table 2.2: Ultimate Analysis

The carbon content of hardwood species is on average 47-50%, whereas softwoods average 50-53% carbon content due to the varying content of lignin and extractives [104]. The sulphur content for most woody biomass materials is below 0.5%

and the nitrogen content is in the range of 0.1-1% [92].
The amount of ash formed by biomass combustion is highly dependant on the type of biomass, but is generally lower than for coal. Biomass fuels with higher concentrations of alkaline metals reduce the ash melting temperature. This might result in higher ash deposits and more fouling in the boilers as well as on the heat exchanger surfaces [31].

2.3 Biomass energy conversion

The chemically stored energy in biomass has to be converted to usable forms of energy. The conversion can be done directly or indirectly through an intermediate state depending on the end purpose. Grønli [41] divided the conversion into three different types of conversion techniques:

- Biochemical conversion using microorganisms
- Physical/chemical processing
- Thermal conversion using heat treatment

Biochemical and physical/chemical conversion are not within the scope of this Ph.D. thesis and will not be commented on further.

2.3.1 Thermal conversion of biomass

Thermal conversion can be divided into four different types of heat treatments; *pyrolysis*, *gasification*, *combustion* and *liquefaction* , as illustrated by Grønli [41] in figure 2.6.
Several of the heat treatments might occur simultaneously in a thermal conversion reactor. The products from all the thermal conversion methods are a combination of [7];

- Solid residue, called *char*
- Gas product, called *product gas*
- Liquid product, called *tar*, has a complex composition. Different parts of the tar might be present in the vapor phase depending on the process temperature.

The characteristics of the products depend on many different factors such as the heating rate, the chemical and physical characteristics of the feedstock, the initial and final process temperature, the pressure, and the type of reactor [7].

2.3.2 Pyrolysis

Pyrolysis is the thermal devolatilization in an environment without an oxidizing agent, or with an oxidizing agent in such a limited supply that gasification does not occur to any considerable extent [38]. Drying and pyrolysis will always occur prior to any biomass combustion or gasification [41]. The thermal degradation of the biomass starts at 200-550°C and continues up to 700°C [40]. Lignin decomposes over a wider temperature range than cellulose and hemicellulose giving the impression of thermal stability during pyrolysis [17]. Pyrolysis of biomass leads to the production of char, tar and product gas. The characteristics and proportions of the products are strongly dependent on the reactor conditions like temperature, pressure, heating rate and reaction time [41]. The heating rate can be used to characterize the pyrolysis process into slow or fast pyrolysis [82]. Slow pyrolysis produces more char and less liquid than fast pyrolysis [40] [103] [95]. During fast pyrolysis the liquid yield is dependent on the temperature [11]. A case study by Bridgwater [18] shows that fast pyrolysis of waste wood gives a very good control of contaminants. The use of catalysts has shown a higher liquid yield [1] [115].
The char from pyrolysis might be used for domestic cooking fuel, barbecuing, refined to activated carbon or used in the metallurgical industry. The product gases might be synthesised to produce ammonia or methanol, while the liquid product

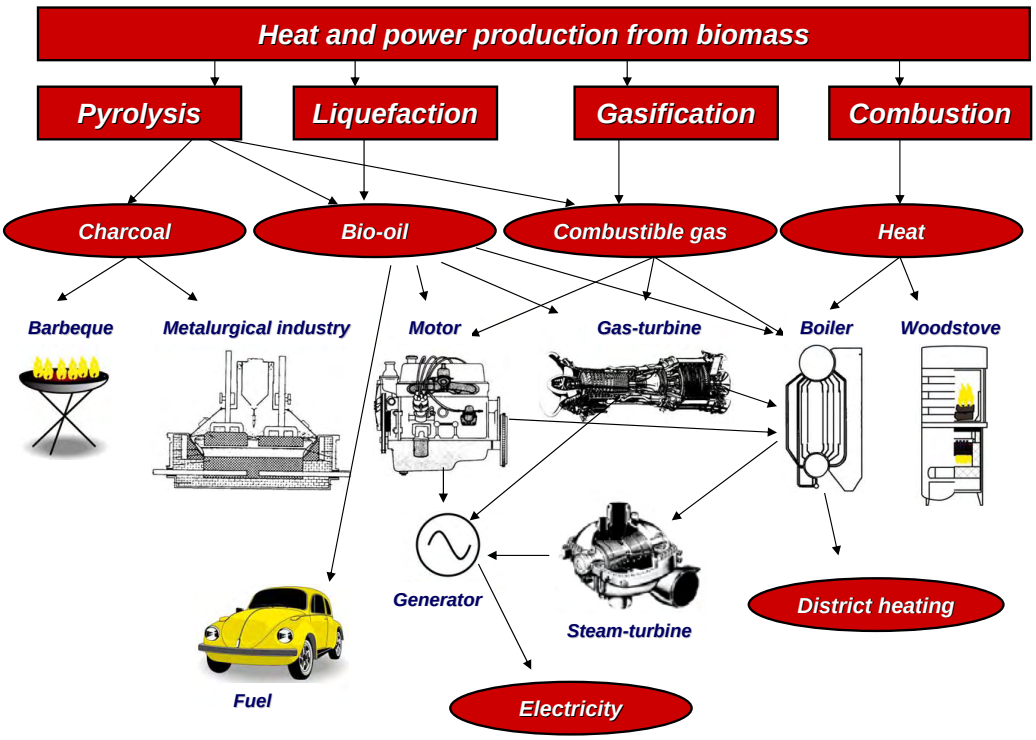

Figure 2.6: Thermal conversion [41]

may be upgraded to high grade liquid fuels for combustion engines, or both the gas and liquid yield might be combusted to produce heat [41].

2.3.3 Gasification

The objective of biomass gasification is to maximize the yield of product gas that typically takes place between 800-1100°C. The product gas contains CO, CO_2, H_2, H_2O, CH_4, N_2, H_2S, char, particles and traces of different alkaline metals. The name "biomass gasification" is a common name for the complex processes of drying, pyrolysis, thermal cracking of vapors, char gasification and partial oxidation of combustible gas, vapor and char which occurs simultaneously in most reactors. The endothermic char gasification where the solid char residue is transformed into a gaseous mixture in a reducing atmosphere is described in detail in chapter 2.4.

The product gas can either be upgraded to a liquid, burned in a boiler, gas turbine, or gas engine, or utilized in a fuel cell [7] [66].

2.3.4 Combustion

Combustion is the complete oxidation of the fuel. Biomass combustion produces hot gases at temperatures in the range of 800-1000°C and was the first human controlled source of heat. The energy in biomass can be utilized in many ways, from the traditional wood stove to industrial plants in the range of 100 kW - 550 MW_{th} [86] [96].

2.3.5 Liquefaction

The main goal of the liquefaction process is to maximize the liquid yield. The thermo chemical conversion of biomass to a liquid phase is conducted at low temperature, 250-350°C, and high pressure, 100-200 bar. High partial pressure of hydrogen and/or a catalyst might be used to enhance the reaction rate and control the composition of the products [63] [155]. The higher heating values of the liquid products are higher from liquefaction, 35-40 MJ/kg, than from pyrolysis, 20-25 MJ/kg [41]. The liquid product becomes more stable and easier to upgrade to a commercial fuel for transport applications due to the low oxygen content [41].

2.4 Biomass gasification

In earlier days, pyrolysis of wood and later coal was the main form of tar production. The first utilization of pyrolysis gas for lighting took place in England in 1792. The gas was produced by coal pyrolysis in air-tight furnaces. The first factories that used gas for lighting were installed by Murdoch in 1802 in Sohofoundry near Birmingham. Gas production went commercial with the foundation of the London Gas, Light and Coke Company in 1812.

Fuel shortages during the World Wars put an emphasis on gasification of both charcoal and wood. During World War II (WW2) approximately one million wood and charcoal gasifiers were used to drive cars, trucks, boats, trains and electricity

generators in Europe. From WW2 to the 1990s, the only time there was an increased interest in gasification was during the oil crisis in the 1970s. From the 1990s and onwards, environmental awareness and a growing concern for energy sustainability have been the main driving forces for gasification [66].

Fossum [37] lists several advantages of biomass gasification compared to direct combustion:

- More options for power production like fuel cells, gas turbines and gas engines, while direct combustion is limited to steam processes, Stirling engines and indirectly fired gas turbines.
- Higher combustion control due to the fact that gaseous fuels are easier to control and optimize than solid fuels.
- Relatively lower emission due to the fact that some components can be removed in the gasifier in addition to the gas cleaning system.
- Integration or co-firing is made possible in existing natural gas or coal power plants thus reducing the net CO_2 emissions.
- Possibility of hydrogen production with the production of a hydrogen rich gas mixture.
- Basis for further chemical synthesis which can be used to produce a wide range of products

2.4.1 Overview of the gasification kinetics

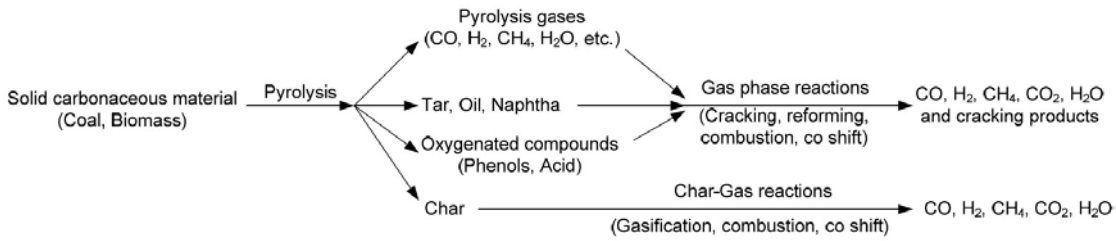

Figure 2.7: Overview of reactions before gasification [46]

The principle chemical reactions involving carbon, carbon monoxide, carbon dioxide, hydrogen, water (or steam) and methane are the same in coal, coke, or char gasification [46]. Gasification is the endothermic process where the solid char residue is transformed into a gaseous mixture in a reducing atmosphere, with little or no oxygen, as seen in figure 2.7. The needed energy can either be provided by partial oxidation or by an external source. Gasification done with heat from partial oxidation is referred to as autothermal or direct gasification. The energy needed is provided by equation 2.8 and equation 2.9 and describes the partial oxidation on the char surface. Gasification with heat from an external source is

called allothermal or indirect gasification. The heat is then provided through a heat exchanger or an indirect process which can be any process with separation of the gasification and the combustion zone.

$$C + O_2 = CO_2 + 393.8kJ/mol \tag{2.8}$$

$$C + \frac{1}{2}O_2 = CO + 123.1kJ/mol \tag{2.9}$$

The heterogeneous (i.e., gas and solid phase) Boudouard equation (Eq. 2.10) and the water gas reaction (Eq. 2.11) are the most important endothermic reduction reactions. The reactions are controlled by temperature and pressure according to Le Chatelier's principle where higher temperatures and lower pressures will increase the gasification rate. The water vapor in equation 2.11 comes from the material drying process or it is introduced as the gasification agent.

$$C + CO_2 + 159.9kJ/mol = 2CO \tag{2.10}$$

$$C + H_2O + 118.5kJ/mol = CO + H_2 \tag{2.11}$$

Another reaction in the reduction zone is the methanation reaction (Eq. 2.12). Methanation becomes more distinguished during high pressurized gasification.

$$C + 2H_2 = CH_4 + 87.5kJ/mol \tag{2.12}$$

Products from gasification can undergo further reactions, unlike combustion which only produces a hot gas product [87]. The most important ones are the water gas shift reaction (Eq. 2.13) and the methane reforming reaction (Eq. 2.14) [66].

$$CO + H_2O = CO_2 + H_2 + 41kJ/mol \tag{2.13}$$

$$CH_4 + H_2O = CO + 3H_2 + 206kJ/mol \tag{2.14}$$

In addition to equation 2.8 and equation 2.9, heat can be produced through equation 2.15 and equation 2.16 in the gas phase if oxygen is present. These reactions are not desired since they reduce the heating value of the product gas.

$$CO + \frac{1}{2}O_2 = CO_2 + 283.9kJ/mol \tag{2.15}$$

$$H_2 + \frac{1}{2}O_2 = H_2O + 285.9kJ/mol \tag{2.16}$$

A simplification of the biomass composition in order to calculate the minimum amount of oxygen needed to gasify the biomass into CO and H_2 is expressed as $CH_{1.4}O_{0.6}$. The simplified ideal biomass expression is used to simplify the gasification to one single reaction as shown in equation 2.18 [7]:

$$CH_{1.4}O_{0.6} + 0.2O_2 = CO + 0.7H_2 \tag{2.17}$$

In practical operations, more oxygen is needed, giving the simplified equation 2.18 [7]:

$$CH_{1.4}O_{0.6} + 0.4O_2 = 0.7CO + 0.3CO_2 + 0.6H_2 + 0.1H_2O \tag{2.18}$$

Agent	Advantages	Disadvantages	Gas heating value
Air	Inexpensive	Low heating values	4-7 MJ/Nm^3
Oxygen	N_2 free product gas Medium heating value	Expensive	10-18 MJ/Nm^3
Steam	N_2 free product gas Medium heating value Enhanced H_2 content	Very endothermic process	10-18 MJ/Nm^3

Table 2.3: Comparison of gasification agents [7]

2.4.2 Gasification agents

Table 2.3 shows the comparison of the different gasification agents. Air is cheap and always accessible, but the high nitrogen content in air lowers the heating value of the product gas. The nitrogen content in the product gas from air gasification can be up to 50%-vol [7][87].
The use of steam or oxygen removes the nitrogen from the gasification agent and the nitrogen content in the product gas then only comes from the fuel. The nitrogen reduction reduces the NO_x emission and increases the product gas heating value. In addition, using steam or oxygen as the gasification agent creates a product gas that can be used for further refining (Methanol production, hydrogen production, Fischer-Tropsch liquid fuels).

2.4.3 Gasification reactors

There are two main types of biomass gasification technologies; fixed bed and fluidized bed gasifiers. The fixed bed reactors have a fixed bed of fuel moving downwards in a reactor as it is being thermally converted. The different conversion stages can be located in different places in the fixed bed reactor as shown in Figure 2.8.

The fluidized bed reactors, in contrast to the fixed bed reactors, have a dynamic bed with multiple conversion reactions at any given location. The bed has a high thermal mass that mainly consists of inert materials like fine grain sand, dolomite or alumina and only a small percentage of fuel material. The high thermal mass makes the fluidized bed capable of gasifying low calorific materials as well as fuel blends. The fluidization process also blends the materials and creates an approximately uniform temperature in the reactor [87].

In addition, entrained flow gasifiers are commercially available for coal gasification (Shell, Destec, Kellogg, Lurgi, Texaco, Krupp-Uhde, Nodell). The entrained flow gasifiers have pulverized coal which is blown or slurry fed into the gasifier in direct gasification mode, but these will not work with more than 10-15% biomass in a coal blend [66].

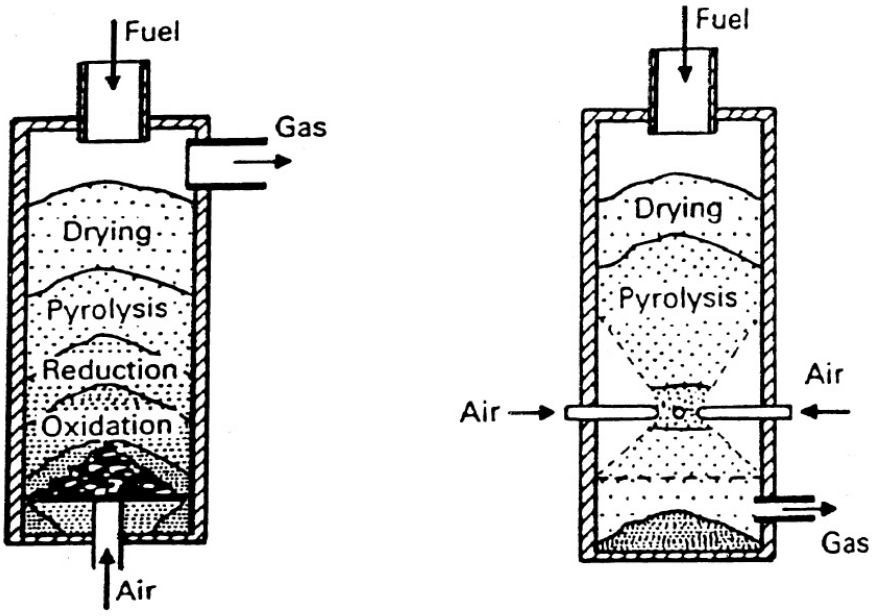

Figure 2.8: Fixed bed: updraft (left) and downdraft (right) [151]

Fixed Bed gasification

The fixed bed reactors have been the traditional reactors used for gasification. The reactors have a simpler design and are easier to operate than the fluidised bed reactors [86]. They are suitable for small scale applications and generally operate at temperatures around 1000°C [87]. The size of the fixed bed reactors is below 1 MW in most designs. Increasing the reactor diameter might cause problems in establishing the required high temperature zones to crack the tar content in the product gas [7]. The reactors are further classified according to the flow direction of the gasification agent into updraft, downdraft and crossdraft gasifiers.

Updraft gasifiers or counter current gasifiers have fuel fed from the top while the gasification agent is fed from the lower part of the reactor, as shown in Figure 2.8 (left). The volatiles will move up with the gasifying agent, allowing vaporous tars from the pyrolysis to either condense on the cool descending fuel or be carried out of the reactor with the product gas [16]. This results in a relatively high heating value in the product gas, due to high levels of tars and hydrocarbons. The high tar content is challenging for the gas cleaning and downstream process equipment. The low temperature of the exiting product gas results in a high thermal efficiency of the process [87], and biomass containing up to 50% moisture can still be gasified without any feed preheating [8].

Downdraft gasifiers or co-current gasifiers have the same flow direction of the fuel and the gasification agent. The most popular design is the Imbert gasifier, Figure 2.8 (right), recognized by a diameter reduction just below the introduction

of the gasification agent [7]. The diameter reduction creates a high temperature zone which allows tar cracking to occur. Drying and pyrolysis take place above the narrowing of the reactor, forcing the volatiles from the pyrolysis to pass the high temperature zone before exiting. This results in a higher exit gas temperature with a lower tar content than the updraft gasifier. The downdraft gasifiers have a limited scale up potential with low maximum size due to the physical limitations of the reactor diameter and particle size relations [16].

Cross draft gasifiers have the inlet and outlet of the gasification agent placed at the same height in the gasifier. The fuel is fed from the top and combusted close to the inlet of the gasification agent. The fuel is dried and pyrolysed above or in front of this high temperature zone. The vaporous tars from the pyrolysis are transported with the gasification agent. The tars are avoiding high temperature zones like in the updraft gasifiers, resulting in a product gas with high levels of tars and hydrocarbons. The product gas leaves the gasifier at temperatures around 800-900°C, giving a low overall energy efficiency [87].

Fluidized Bed gasification

Fluidized bed gasification has been used for coal gasification for many years [87], and is regarded by many as the best design option for biomass gasification [92]. Fluidized bed gasifiers can be classified as Bubbling Fluidized Bed (BFB) and Circulating Fluidized Bed (CFB). Their main advantage compared to the fixed bed gasifiers is the approximate uniform temperature distribution in the gasification zone and their upscaling potential. The uniform temperature is maintained by fluidizing the reactor bed, thereby creating excellent gas-solid mixing characteristics and high reaction rates. The bed material usually consists of silica sand with added fuel, although alumina and other refractory oxides have been used to avoid sintering [16]. The high thermal mass of fluidized bed reactors makes them suitable for blended fuels and fuels with low calorific value. Catalysts can be added to lower the tar content and modify the product gas composition. Fluidized bed gasifiers have a high fuel flexibility with few preprocessing limitations. The product gas leaves at a high temperature (800-1000°C) with a generally higher particle concentration than the fixed beds. The high exit temperature might result in a higher alkali content in the product gas due to limited condensation of alkali rich phases.

Bubbling fluidized bed, figure 2.9 (left), the gasification agent is fed through the bottom of the reactor at moderate velocities. This fluidizes the bed material into a bubbling bed that occupies the lower part of the gasifier. Pyrolysis of the biomass material starts on contact with the hot, inert bed material, normally kept at 700-900°C. The char gasification and cracking of the tar from pyrolysis occurs in the hot bed. The exiting product gas normally contains low tar concentrations.

The Circulating fluidized bed, figure 2.9 (right), is fluidized by a high velocity gasification agent. The fluidized bed occupies the whole gasification reactor, en-

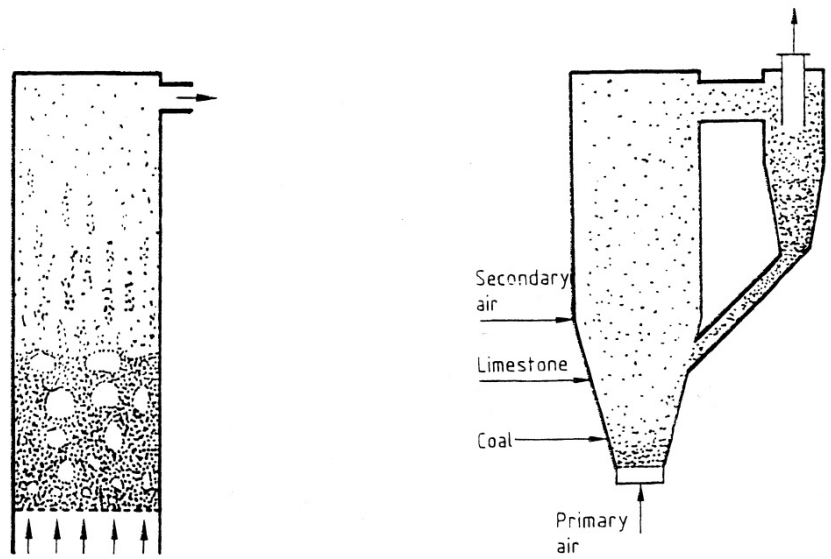

Figure 2.9: Fluidized bed: bubbling bed (left) and circulating bed (right) [151]

hancing the heat transfer between biomass and the gasification agent. The bed material will follow the gas stream out of the reactor. A cyclone separates the product gas from the bed material and the bed material is returned to the gasification chamber.

Entrained flow gasification

Commercial entrained flow gasifiers use pulverized coal that is pneumatically fed into the reactor in a similar manner to pulverized coal fired stations, normally with oxygen or highly enriched air as gasification agents [53]. The small particles ($<$ 100μm) have a short residence time and the gasification yields high temperatures in the gasifier (1300-1600°C) [66]. The high operation temperatures increases the carbon conversion. The fuel feeding allows for high pressure gasification and large capacities ($>$ 100 MW) [66].

Since 2000, experiments with solid biomass in coal entrained flow gasifiers have been conducted at Buggenum, the Netherlands, and Puertollano, Spain [66].

Other gasification processes

Fixed bed reactors and fluidized bed reactors are the most used process solutions for gasification of biomass. Fixed bed and fluidized bed processes use well known technology, as shown in figure 2.10. However, other gasification solutions based on existing technologies are also used such as the entrained flow, the multiple hearth, the moving bed, the rotary kiln and the screw/auger kiln [37]. In addition, results from ongoing R&D have resulted in improved gasification processes like the fast internally circulating fluidized bed gasifier from the University of Vienna [48][49][50][51][52], the two step gasification process from DTU, Denmark [45]

and the downdraft gasifier with internal pre-combustion of pyrolysis gases developed at Twente University, The Netherlands [84].

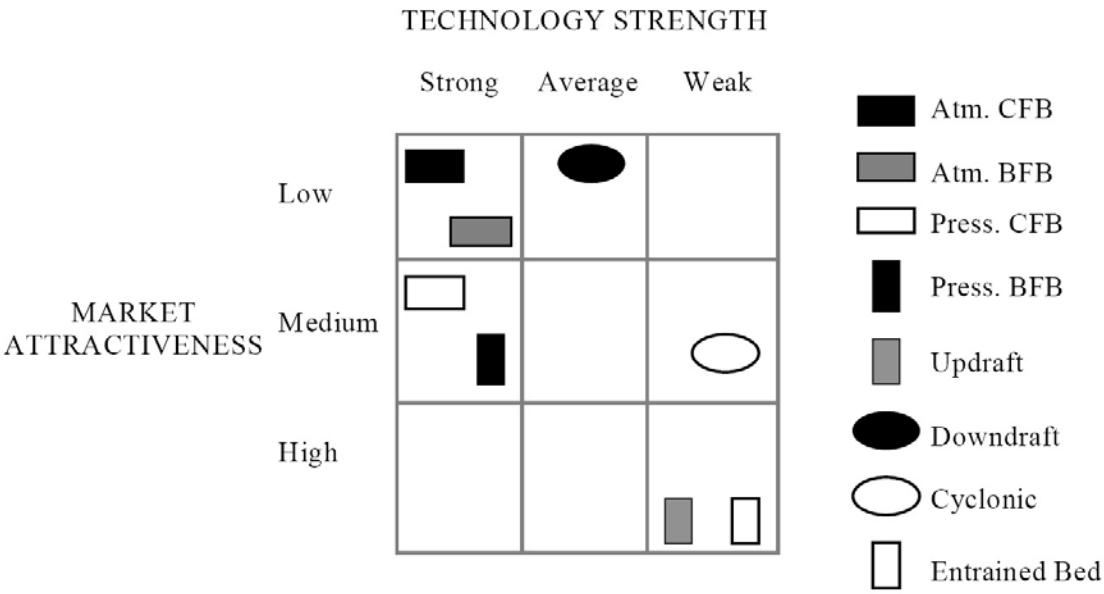

Figure 2.10: Overview of gasification technologies [83]

Chapter 3

Granular filtration

"An hour in the library can save you a year working in the laboratory"

Anonymous

3.1 Introduction

Granular filtration is a process for separating solids suspended in a fluid (gas or liquid). Different types of granular filters exists (moving-bed, fluidized bed and fixed bed), but only gas-solid separation in fixed bed filters is within the scope of this work.

Granular fixed bed filters and other barrier filters (e.g. fibrous, ceramic and metallic) have been reported with a high mass collection efficiency in the literature [23] [25] [43] [107]. The barrier filters normally operate through surface filtration whereby the collection efficiency is enhanced by cake filtration.

Schmidt [117] categorized the main parameters influencing the operational behavior of surface filtration into five groups by examining bag house filters as described below and illustrated in figure 3.1.

- *Gas*
  The parameters influencing the incoming gas depend on the specific filtration process and have been monitored/controlled separately for each of the different PBF setups in this thesis.

- *Particles*
  The parameters characteristic of gas suspended particles are dependent on the specific filtration process and are presented in chapter 3.2.

- *Operation*
  The operation parameters are dependent on the specific filtration process, the filter medium and the configuration of the filter. The operation parameters have been monitored/controlled separately for each of the different PBF setups in this thesis.

- *Filter medium*
  The filter medium is made up of unbound particles. Chapter 3.2 describes

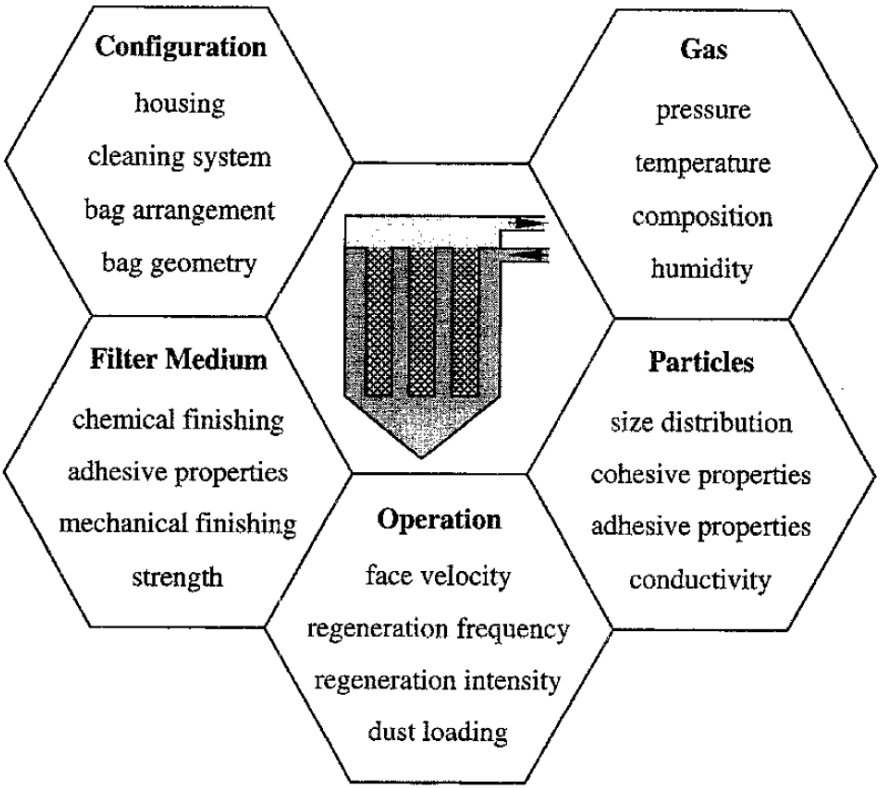

Figure 3.1: Parameters influencing the operational behavior of cake forming filters [117]

the particle properties, while the hydraulic resistance from the flow through the bed is described in chapter 3.3.

- *Configuration*
  The configuration parameters differ and are described individually for each experimental setup. The configuration of the setups used for the experimental work of this thesis is described in chapter 5.

Chapter 3 describes the general principles of granular filtration while chapter 4 describes the granular Panel Bed Filter.

3.2 Particle properties

The term "particles" describes a discrete portion of matter ranging from subatomic nuclear particles to lumps of materials in the range of several millimeters. The properties of the particles suspended in the fluid (gas or liquid) will effect the filter cake that influences the filter performance.

Geometric equivalent diameters		
Diameter of the sphere with the same volume	dp_V	
Diameter of the sphere with the same surface area	dp_S	
Diameter of the sphere with the same specific surface area	dp_{SV}	
Diameter of the circumscribing sphere	dp_{en}	
	Particle orientation	
Equivalent diameters from particle projection	Stable	Average
Diameter of the circle with the same area	$dp_{P.S}$	$dp_{P.M}$
Diameter of the circle with the same perimeter	$dp_{PE.S}$	$dp_{PE.M}$
Diameter of the inscribed circle	$dp_{IN.S}$	$dp_{IN.M}$
Diameter of the circumscribed circle	$dp_{CI.S}$	$dp_{CI.M}$
Hydrodynamic equivalent diameters		
Diameter of the sphere with the same resistance (drag)	dp_D	
Diameter of the sphere with the same thermal velocity	dp_u	
Diameter of the sphere with the same thermal velocity in the Stokes law range (Stokes law)	dp_{St}	
Other equivalent diameters		
Diameter of the sphere scattering light at the same intensity	dp_{sca}	
Diameter of the sphere causing the same change in electrical resistance (coulter counter)	dp_{el}	

Table 3.1: Equivalent diameters [112]

Particle diameter

Spherical particles with only a slight variation in size can be defined with an average diameter, $\bar{dp}$, as shown in equation 3.1.

$$\bar{dp} = \frac{1}{n}\sum_{i=1}^{n} dp_i \tag{3.1}$$

dp_i is the diameter of particle number i whereas n is the total number of particles. The sample of n particles must be a representative selection of the granular filter.

Only perfect spheres or perfect cubes can be defined by a single geometrical value. The size description of a non spherical or non cubical particle can only be derived by measuring a size-dependent property of the particle and relating it to one singular dimension, also known as an equivalent diameter. Table 3.1 shows equivalent diameters frequently used in the literature.

The sphericity is a measure of how spherical (round) a particle is. Wadell [147] defined the sphericity, ψ, as shown in equation 3.2:

$$\psi = (\frac{dp_S}{S_P})^2 \tag{3.2}$$

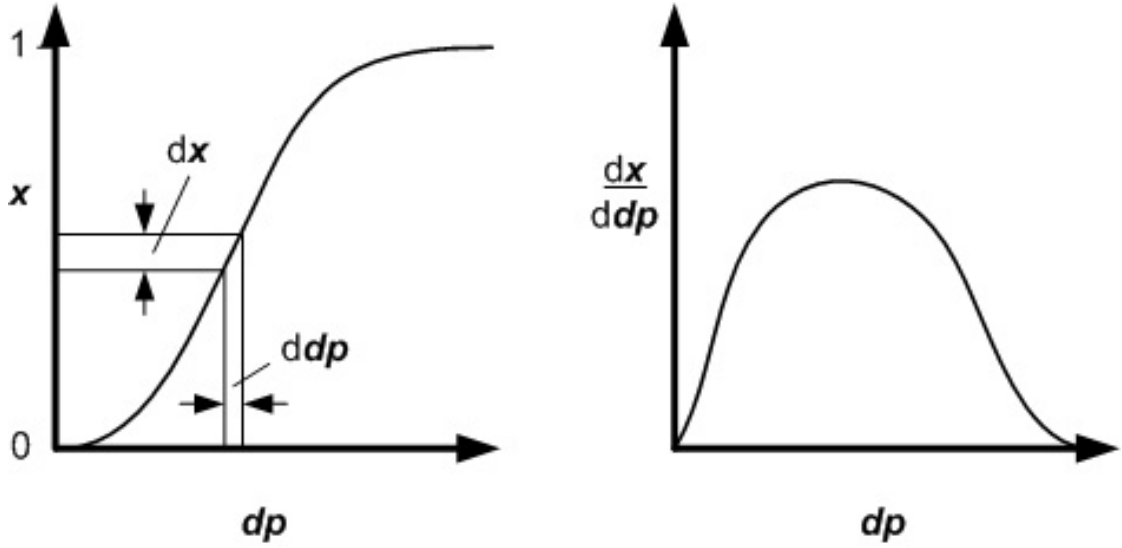

Figure 3.2: Size distribution curves, cumulative (left) and frequency (right) [108]

Where dp_S is the surface area of a sphere having the same volume as the particle and S_P is the actual surface area of the particle. The sphericity can be further used to compare different equivalent diameters as shown in equation 3.3.

$$dp_S = dp_{P.M} = dp_{St}\ \psi^{-\frac{3}{4}} = dp_V\ \psi^{-\frac{1}{2}} \tag{3.3}$$

Most practical granular filters, however, have a random packing which make the influence of particle orientation negligable [124].

The different equivalent diameters and the techniques used to quantify them are described in detail in the literature and will not be discussed further in this thesis.

Particle size distribution

Particles in any system will have a mean size within the particle rage. The particle size distribution visually shows the mean size and the spread of sizes. The size distribution can be presented as a cumulative curve (figure 3.2 left) or as a frequency curve (figure 3.2 right).

The cumulative curve plots the proportion of particles, x, smaller than a certain particle size, dp, plotted against that particle size.

The size frequency curve plots the slope, $\mathrm{d}\boldsymbol{x}/\mathrm{d}\boldsymbol{dp}$, of the cumulative curve plotted against the particle size. The frequency curve normally gives one peak for naturally occurring particles [108].

The cumulative curve is most commonly presented as $Q_r(x)$ and the frequency curve as $q_r(x)$. Equation 3.4 shows how the cumulative distribution function can be obtained from the population density by integration.

$$Q_r(x) = \int_{x_{min}}^{x} q_r(x) \tag{3.4}$$

The particle size distribution can be measured and plotted in different ways:

- `By numbers`. Counting the particles and presenting the population by numbers is indicated with the denomination m^0.

- `By length`. Giving the denomination m^1.

- `By area`. Giving the denomination m^2.

- `By volume`. Giving the denomination m^3.

The subscript r in equation 3.4 determines the denomination of the curve where 0 represents distribution by numbers, 1 by length, 2 by area and 3 by volume. The cumulative and frequency curves are most commonly presented by volume and will be plotted by volume in the remaining part of this thesis.

Adhesive and cohesive particle properties (forces)

The term adhesion is used in several scientific fields with different concepts, or ideas, depending on whether the subjective view is on a molecular, microscopic, or macroscopic point of view [89]. Adhesion forces can be defined as the attractive forces between particles or between particles and a wall [112]. The adhesion forces can arise through capillary forces [57] [88], van der Waals forces [108] and electrostatic forces [119]. Stickiness due to molten ash will also have an effect on the adhesion of particles [157].

Cohesive forces can be defined as the adhesive forces between particles of the same substance [89]. The influence of cohesive forces will increase with a reduction in particle size [59].

Adhesion of particles before the filter enhances the filtration due to an increase in the diameter of the aggregated particles. Increased surface roughness reduces the contact area between the particles and can reduce the adhesion forces [39]. Fayed [35], Mittal [89] and Rumph [112] discuss the topics of adhesion and cohesion in detail.

Strength of bed particles

Table 3.2 shows the ISO and ASTM standards for measuring particle strength (hardness). Table 3.3 shows the older Moh scale that measures the material hardness by identifying the hardest material that the given material can scratch, and/or the softest material that can scratch the given material. The scale classifies soft materials as 1 to 3, intermediate hardness as 4 to 6 and hard materials as 7 to 10 [99].

The hardness of the bed material used during the experimental part of this thesis is presented by using the Moh scale and the % of crushed material at given pressures from the suppliers as shown in Appendix A.

Hardness test	Standard	
	ISO	ASTM
Brinell	ISO 6506-(1-4)	E10
Vickers	ISO 6507-(1-4)	E92
Rockwell	ISO 6508-(1-3)	E18

Table 3.2: Standards of measuring material strength

1	Talc	6	Feldspar
2	Gypsum	7	Quartz
3	Calcite	8	Topaz
4	Fluoride	9	Corundum
5	Apatite	10	Diamond

Table 3.3: Moh Scale [99]

Packing of particles

The packing of the particles in a granular filter is an important factor used to characterize the filter and to estimate the pressure drop. The filters' void or porosity are defined to be the volume not occupied by the granular filter material. A filter made of spherical shaped particles will normally be limited by the two cases shown in Figure 3.3. The face-centered cubic packing, figure 3.3 a, represents the most dense packing possible, while figure 3.3 b represents the unlikely, but theoretically possible, most loose packing. The porosity, ϵ, can be mathematically

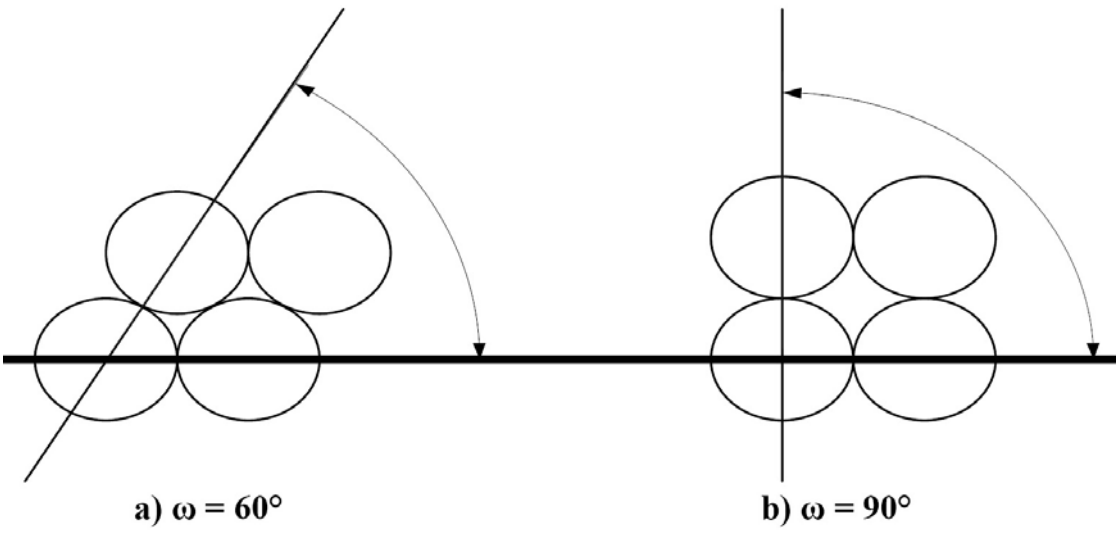

Figure 3.3: Packing of spherical particles [124]

expressed with the center core angle, ω:

$$\epsilon = 1 - \frac{1}{6\left(1 - cos\left(\omega\right)\right)\sqrt{1 + 2cos\left(\omega\right)}} \tag{3.5}$$

Equation 3.5 gives a void range for the spherical particles from 0.260 for face-centered cubic packing up to a theoretical maximum of 0.476. Mechanical vibration can be used to pack granular materials and decrease the porosity. Low sphericity tends to give higher porosities, while a large variation in size distribution can give low porosity [124].

The particle properties (*diameter*, *size distribution*, *cohesive and adhesive forces*, *strength* and *packing*) are discussed in detail by Allan [3], Richardson [108] and Rumpf [112].

3.3 Hydraulic resistance of granular materials

Basic pressure drop theory for incompressible fluids

The classical formulation of an incompressible fluid flowing through a tube has pressure losses both because of friction to the walls and because of resistance to the flow such as sudden contractions, expansions, changes in flow direction and so on. These losses are due to transformation from mechanical energy to heat and cannot be recovered. A resistance coefficient, ζ, is often used and defined as:

$$\zeta = \frac{\Delta P}{\frac{1}{2}\rho_f u^2} \tag{3.6}$$

Where ΔP is the pressure drop and ρ_f is the density of the fluid flowing with a velocity u. Further, the resistance coefficient can be divided into two parts. The resistance coefficient due to friction can be expressed by the hydraulic friction factor, f, as:

$$\zeta_{fr} = f\frac{L}{d_h} \tag{3.7}$$

Where L is the tube length and d_h is the hydraulic diameter. The resistance coefficient for the single resistances in the system can then be added up and together with the friction express the resistance coefficient for the whole system and the total pressure loss for the system as shown in equation 3.8 and equation 3.9 respectively.

$$\zeta_{tot} = \zeta_{fr} + \sum \zeta_{single} \tag{3.8}$$

$$\Delta P = \zeta_{tot}\rho_f\frac{u^2}{2} \tag{3.9}$$

The hydraulic resistance in a granular filter is normally given by one total hydraulic resistance coefficient [124]:

$$\Delta P = \zeta_{gf}\rho_f\frac{u^2}{2} = f_{gf}\frac{L_{gf}}{d_h}\rho_f\frac{u^2}{2} \tag{3.10}$$

The subscript *gf* means granular filter. The hydraulic diameter is usually replaced by a correlation containing particle diameter and porosity [124].

General theory

Darcy measured the flow of water in vertical homogeneous sand filters as described by Carman [21]. Darcy found out that the volume flow, Q, is proportional to the cross sectional area, A_{cs}, proportional to the pressure difference between the static fluid pressure before the filter, P_1, and the static pressure after the filter, P_2 and inversely proportional to the filter length, L. Using κ as the permeability of the filter material and μ as the fluids dynamic viscosity we get the Darcy equation 3.11:

$$Q = -\frac{\kappa A_{CS}}{\mu}\frac{(P_2 - P_1)}{L} \tag{3.11}$$

Darcy's law is widely used for describing laminar, single-phase flow in porous media. If the porous media consists of many individual particles, the permeability can be related to the particle diameter and the porosity. The Blacke-Kozeney equation (Eq. 3.12) a special form of Darcy's law, provides a more explicit relationship in these cases [81].

$$\frac{\Delta P}{L_{gf}} = \alpha\frac{(1-\epsilon)^2}{\epsilon^3}\frac{\mu u_{sf}}{dp^2} \tag{3.12}$$

$$\alpha = 150$$

The mathematical expression in equation 3.12 was first described by Kozeny [142]. Kozeny determined α to be 64 based on the view that a porous media is a bundle of capillaries with equal length and diameter. MacDonald [81] showed a mathematical derivate of equation 3.12 for spheres:

$$u_{sf} = \frac{2}{9\ i^2\mu}\frac{\epsilon^3}{(1-\epsilon)^2}\left(\frac{M_2}{M_1}\right)^2\frac{\Delta P}{L_{gf}} \tag{3.13}$$

u_{sf} is the superficial velocity defined as the volume flow divided on the cross sectional area of the flow and the ratio M_2 over M_1 represents the sphere size distribution. When the size distribution gets narrower, the ratio M_2 over M_1 approaches a single value dp [81]. Rearranging equation 3.13 shows that α was much lower than even Kozeny originally estimated. This is due to the simplified analysis, not accounting for tortuosity [81], the converging-diverging nature of the channels in the bed of spheres [98] and the interconnecting channels within the bed [91]. Due to the simplifications, MacDonald [80] concluded it was better to use an experimentally derived value for α. Carman [21] found α to be 180 through experimental data and this value has later been supported by MacDonald [80].

The Darcy equation has shown a valid linear relationship as long as the Reinhold number based on the average particle grain does not exceed 10 [124]. The reason for this is due to the transition from flow controlled by viscous forces at low Reynolds numbers to flow controlled by initial forces at high Reynolds numbers.

When viscous forces control the flow, the pressure loss is proportional to the velocity (Darcy's law), and when inertial forces control the flow, the pressure loss is proportional to the square of the velocity. This transformation is not necessarily connected to the onset of turbulence. A more useful relationship between pressure drop and velocity for a large range of Reynolds numbers can therefore be expressed written in the general form [124]:

$$\Delta P = a_1 u_{sf} + a_2 u_{sf}^2 \tag{3.14}$$

Where a_1 and a_2 are constants consisting of the density, porosity, viscosity, particle diameter and the proportionality constant α. The commonly used resistance model [153] for flow through granular media has the form of equation 3.14 and was presented by Ergun in 1952 [32]:

$$\frac{\Delta P}{L_{gf}} = 150\frac{(1-\epsilon)^2}{\epsilon^3}\frac{\mu u_{sf}}{dp^2} + 1.75\frac{(1-\epsilon)}{\epsilon^3}\frac{\rho_f u_{sf}^2}{dp} \tag{3.15}$$

$$0.4 < \epsilon < 0.65$$
$$0.4 < Re < 1380$$

The first part of the Ergun equation consists of the Blacke-Kozeney equation and represents the viscous energy loss primarily in laminar flow and the pressure drop for a low Reynolds number. The second part consists of the Burke-Plummer equation (Eq. 3.16) and represents the kinetic energy loss primarily occurring in turbulent flow and the pressure drop for Reynolds numbers higher than 100 [153].

$$\frac{\Delta P}{L_{gf}} = 1.75\frac{(1-\epsilon)}{\epsilon^3}\frac{\rho_f u_{sf}^2}{dp} \tag{3.16}$$

The pressure drop calculated with the Ergun equation with constants of 150 and 1.75 fits experimental data for beds of equal size spheres very well. Ergun constants are able to predict the pressure drop in beds composed of spherical particles within 10% [20][69][80][90].

MacDonald [80] measured the pressure drop over silica sand beds and based the empirical equation 3.17 on the results. The MacDonald equation uses a variable for the particle roughness,β, that varies from 1.8 to 4. The MacDonald equation shows better correlation with results from sand experiments [142].

$$\frac{\Delta P}{L_{gf}} = 180\frac{(1-\epsilon)^2}{\epsilon^3}\frac{\mu u_{sf}}{dp^2} + \beta\frac{(1-\epsilon)}{\epsilon^3}\frac{\rho_f u_{sf}^2}{dp} \tag{3.17}$$

$$0.123 < \epsilon < 0.919$$
$$0.01 < Re < 5000$$

The packing of granular material is related to the porosity and strongly influences the pressure drop over the bed. The literature reveals several empirically derived equations estimating the pressure drop for different materials properties [142].

Wall effects on the pressure drop due to local higher porosities is small compared to the variation in the pacing of the bed particles and can be neglected for granular filters where the L_{gf}/dp ratio is higher than 20 [44]. The topic of fluid flow through granular material is discussed in further detail by Carman [21], Liu [78] and Tien [142].

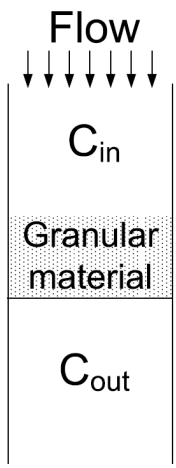

Figure 3.4: Granular bed

3.4 Granular bed filtration

During granular bed filtration the suspended particles are being separated from the fluid as it passes through a bed of unbound granular filter material as shown in figure 3.4. The collection efficiency, E_c, of the filter is given by equation 3.18 where C_{in} and C_{out} are the particle concentrations in and out of the filter.

$$E_c = 1 - \frac{C_{out}}{C_{in}} \tag{3.18}$$

During filtration the suspended particles have to get out of the streamlines of the gas first in order to make physical contact with the granular bed material. Then, the particles have to avoid re-entering the gas by sticking to the bed material or to other deposited particles [139].

Figure 3.5 illustrates the collection mechanisms. The collection mechanisms (impaction, diffusion (sub-micron particles), interception (geometrical effect) and electrostatic, magnetic and acoustic fields) are described in detail in the literature (e.g. Lee [73] [74] and Tien [142] [143]).

The retention of particles hitting a filter granule is governed by a balance between particle kinetic energy and adhesion energy [26]. The re-entrainment of the particles can occur when the Stokes' number is sufficiently large. The high impact velocity might lead the particle to bounce off the granular material and re-enter the gas stream [149]. Impact studies on two particles indicate that the angle of collision is critical for tangential rebound [67].

Most granular filters are based on the principle of deep bed filtration where the particle penetrates deep into the filtration medium [110]. Deep bed filtration has a pronounced dip in the collection efficiency for particle sizes in the range of 0.1-5 μm [42] as shown in figure 3.6. Lee [76] concluded that the dominating collection mechanisms acting on potential penetrating particles depended on the operating flow and the granule size. The important collection mechanisms for large bed

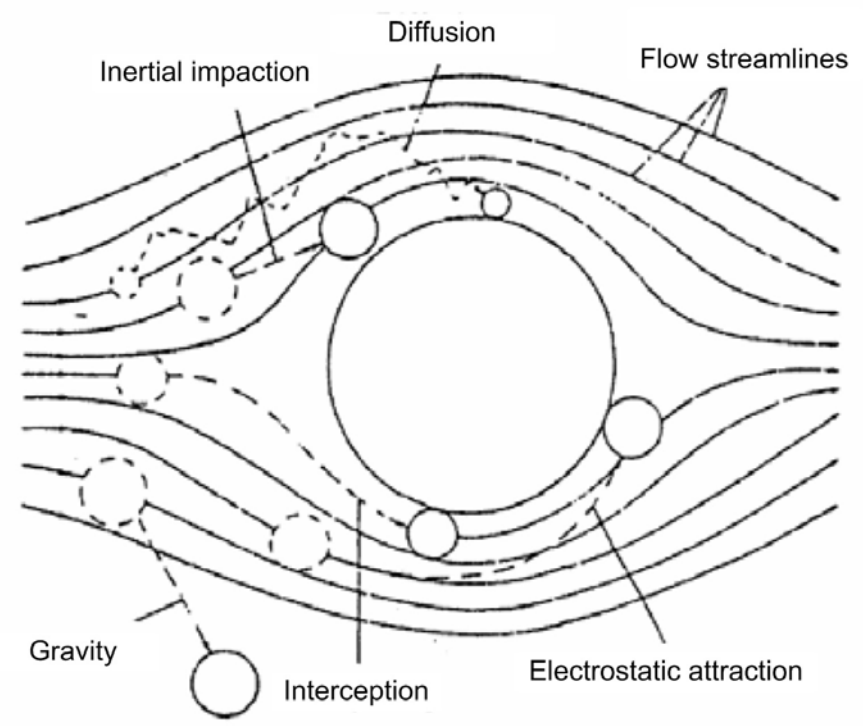

Figure 3.5: Particle forces [110]

materials and low filtration velocities are Brownian diffusion and gravitational sedimentation, while Brownian diffusion and interception become dominant for a bed of small granules operating at high velocity. Furthermore, the minimum collection efficiency can be increased by operating at lower velocity or using a filter media with a smaller diameter. Increased collection efficiency can also be reached by applying an electrical field in the bed material [6] [119]. Filter granules with a lower sphericity yield a higher collection efficiency due to an increase in the combination of diffusion and direct interception [64].

Formation of filter cake

Granular fixed bed filtration is inherently a time dependent process [142]. During the filtration process the filter medium accumulates the particles deposited from the fluid. The deposited particles will clog the filter medium over time and the creation of a filter cake might occur [73] [74] [110] [111].

The mechanics of filter cake construction on a clean granular filter depends upon the adhesivity of the incoming particles in the gas [74]. The processes of cake foundation can be divided into three stages as shown in figure 3.7 [73] [74] [111]:

- *Clean bed filtration* (Figure 3.7 A)
  Clean bed filtration is the first stage in a filtration process. The suspended particles in the gas tend to penetrate into the bed for a distance of a number of granular particle layers. This deep bed filtration results in the granular

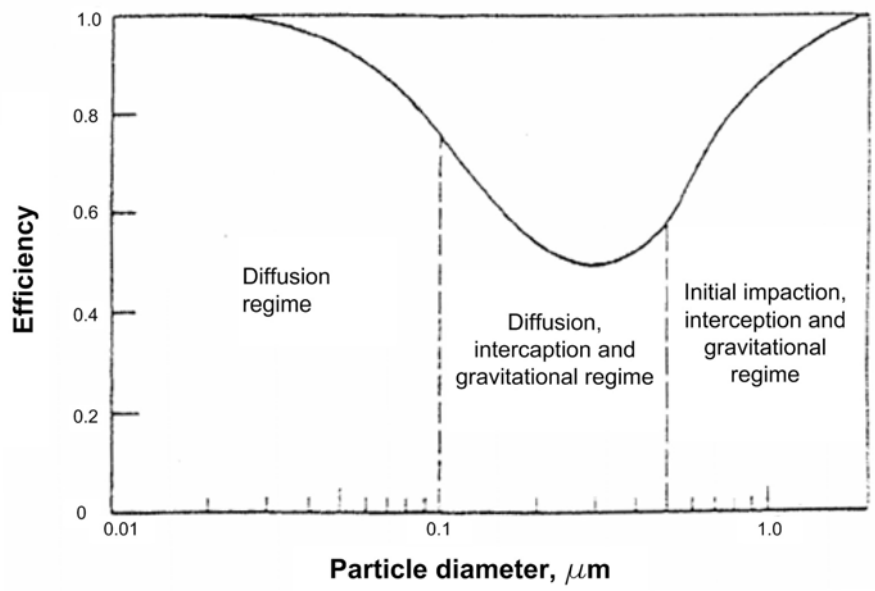

Figure 3.6: Collection efficiency of a typical barrier filter [75]

filter having its lowest collection efficiency during this deep bed filtration.

- *Rooting cake filtration* (Figure 3.7 B)
  Rooting cake filtration gradually occurs when enough particles are deposited into the filter media to start the agglomeration of deposited particles. The agglomerates of deposited particles grow fastest when diffusional deposition prevails, moderate for interception and slowest for the inertial deposition regime [62]. The collection efficiency is significantly increased.

- *Surface cake filtration* (Figure 3.7 C)
  Surface cake filtration is achieved when enough particles are deposited in the top layers of the filter medium so that new particle deposits will occur on the smooth surface of the filter medium. The highest collection efficiency for the

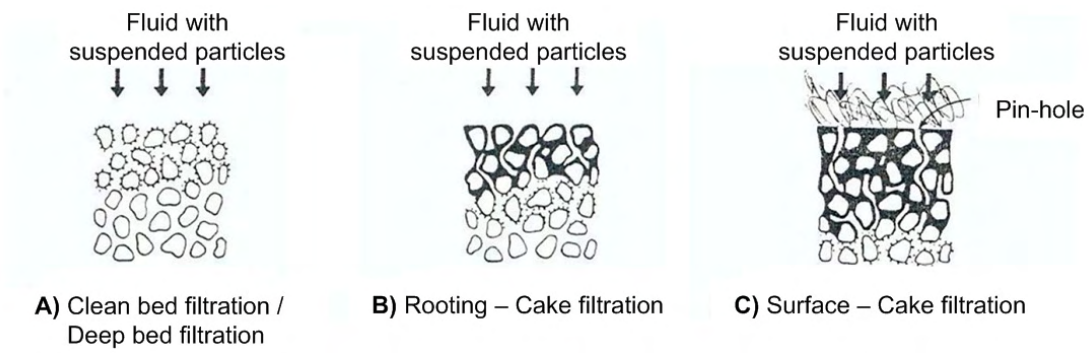

Figure 3.7: Cake regimes [74]

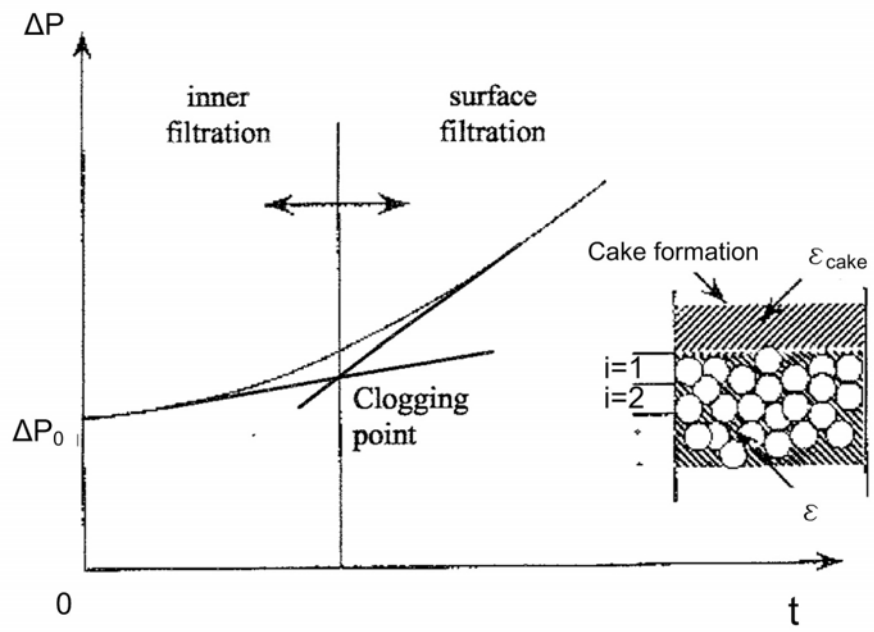

Figure 3.8: Schematic pressure drop versus particle [110]

filter after this point is due to the efficient sieving mechanisms. The sieving mechanisms can be compared to a permanently loaded bag filter [74]. The filter cake growth from this point (on the surface) can be compared to the cakes created on other barrier filters [110].

Figure 3.8 shows the pressure buildup over the filter unit, ΔP, during the formation of a filter cake. The "Clogging point" in the figure refers to the onset of cake filtration and is defined as the point where the deep bed and cake filtration slopes meet. The rooting cake filtration regime can be identified with the difference between the measured pressure buildup and the deep bed and cake filtration slopes.

Penetration of particles

Some particles will always penetrate the filter media during operation independent of filter type. Lee [74] compared granular cake filtration to bag filtration to describe three mechanisms for penetration:

Straight through penetration
Straight-through penetration is highest for clean bed filtration and for the panel bed filter immediately after it has removed the filter cake by puffback (Chapter 4.3). This type of penetration occurs when the particles pass through the filter without stopping. The particles then follow the streamlines of the gas through the filter. The collection efficiency for small particles will be lower as described above for deep bed filtration.

See page penetration (bleeding penetration)
Deposited particles on or between the filter media will be subject to an increasing force due to pressure buildup over the filter when the cake thickness increases. This might cause the deposited particles to loosen and penetrate the filter. Furthermore, it may be more pronounced in the case of spherical or smooth surfaced, regular particles and/or in granular filters where the adhesion forces are low.

Pinhole plug penetration
Pinhole plug penetration, shown in figure 3.7 C, occurs as a plug of deposited particles dislodge from the dust deposit and pass through the filter all at once. The possibility of pinhole creation might increase with increased pressure buildup over the filter due to cake growth [111] or during puffback cleaning [5]. Once a pinnhole is formed it tends to remain and acts as a bypass around the filter cake for further straight-through penetration.

Filter cake characteristics

On-line measurements of cake parameters (e.g. cake thickness, cake porosity, cake permeability etc.) have not been feasible in most operational systems. This has resulted in the development of several models predicting the pressure resistance due to cake growth over the filter unit that is based on easily measured parameters (e.g. particle concentration, gas flow rate, temperature, absolute pressure and the pressure drop over the filter) [110].

The general approximation for the pressure drop over a plain filter is that it consists of the sum of the pressure drop over the granular medium, P_{gf}, and the filter cake, P_{cake}, as shown in equation 3.19.

$$\Delta P = \Delta P_{gf} + \Delta P_{cake} \tag{3.19}$$

Applying Darcys law to equation 3.19 and introducing K_1 and K_2 as the specific resistance of the filter medium and the specific cake resistance gives equation 3.20.

$$\Delta P = K_1 \cdot \mu \cdot u + K_2 \cdot \mu \cdot u \cdot \overline{W}_A \tag{3.20}$$

where μ is the gas dynamic viscosity, u the gas velocity across the exposed filter surface and $\overline{W}_A$ is the mass of dust cake per unit area in a time period as given by equation 3.21.

$$\overline{W}_A = C_{in} \cdot u \cdot \Delta t \tag{3.21}$$

Combining equations 3.19 and equation 3.20 while replacing the product of the specific resistance and the dynamic viscosity with K^* gives an expression for the specific cake resistance, equation 3.22.

$$K_2^* = \frac{\Delta P_{cake}}{\Delta t \cdot u^2 \cdot C_{in}} \tag{3.22}$$

Figure 3.9 shows a physical determination of the specific cake resistance where ΔP_1 and ΔP_2 are the pressure drop values at the beginning and end of the first cleaning cycle. ΔP_R is the residual pressure drop after cleaning and ΔP_H is an auxiliary value used to determine the slope of the graph during cake filtration.

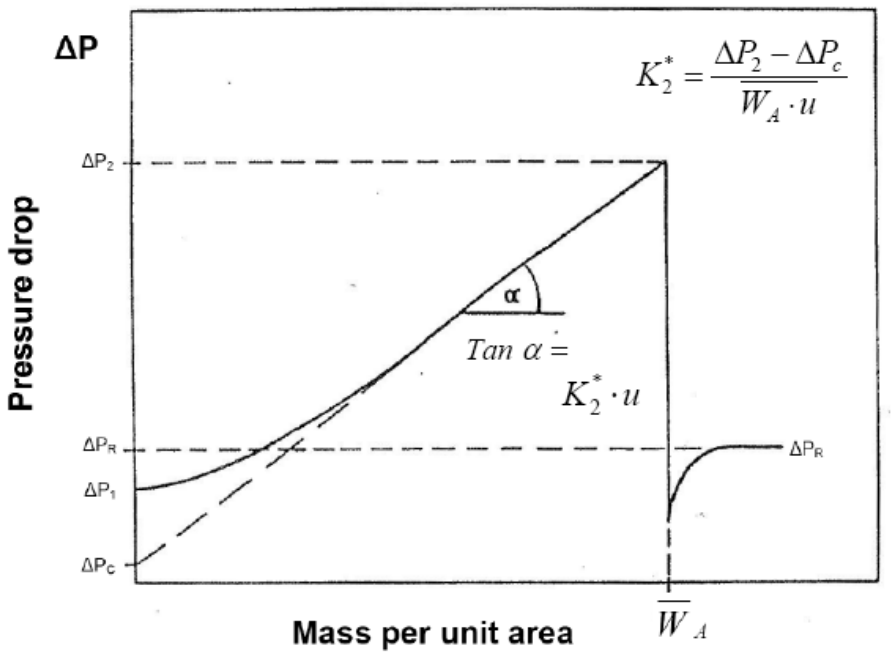

Figure 3.9: Physical determination of K_1^* and K_2^* [79]

The value of K_2 depends on the deposited particles in the cake regardless of the supporting media, and can therefore only be calculated for barrier filters in surface cake filtration mode [65]. The K_2^* value is therefore a function of the filter cake structure and the physical properties of the suspended particles [110].

Increasing filtration temperature increases the viscosity of the gas and results in a higher pressure drop over the filter. Furthermore, the increased viscosity strongly affect the K_2^* value. Peukert [101] [100] and Hajek [43] both show that K_2^* increases with temperature. Peukert [100] also shows that the diffusion range is significantly improved with increasing temperature. Increased temperatures also lowered the separation efficiency for particles larger than 5 μm due to a reduction in the initial collection efficiency. Risnes [110] therefore concluded that comparing K_2 might be a more representative parameter when comparing various filtration temperatures since K_2 is more closely connected to the structure of the filter cake.

Klingel [65] dispersed limestone (dp = 5 μm) filtration and showed that K_2 increases with higher filtration velocities.

Silva [121] investigated cake formation of dispersed photosphatic rock (dp = 20 μm). Increasing filtration velocities (u = 4.8-8.9 cm/s) decreased the cake porosity while the cake specific resistance increased with increasing filtration velocity.

Berbner [9] used quarts dust, brown coal fly ash and hard coal fly ash to investigate the temperature influence on dust cake formation and concluded that a higher temperature leads to a more porous dust cake. The porous dust cake will counteract some of the influence the increased temperature has on the gas viscosity thereby influencing the pressure drop over the filter. Smidt [117] [118] investigated the cake buildup of limestone (dp = 2 and 3.5 μm) and concluded

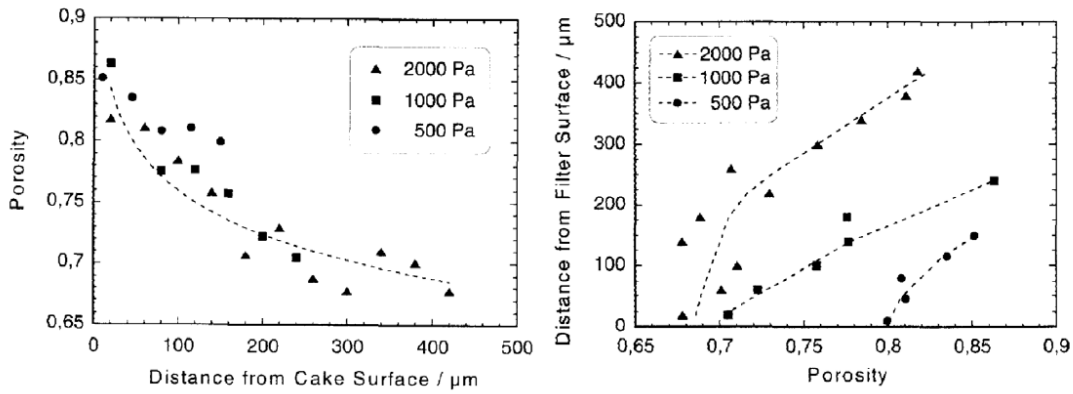

Figure 3.10: Change in cake porosity over the height of dust cake formed under different limiting pressure losses [118]

that the cake porosity is not uniform, but locally dependent of the cake thickness, filtration time and pressure drop over the filter as shown in figure 3.10. The cake porosity decreases with an increasing total pressure drop over the filter. Choi [22] found filter cakes from irregular particles to be more compressible than spherical ones after investigate ashes from a conventional power plant (dp = 19.15 μm), fluidized bed combustion (dp = 45.68 μm) and paint incinerator (dp = 37.55 μm). Choi [23] used three types of fly ash from a coal power plant (dp = 1.2, 2.2 and 3.6 μm) to show increased cake compression with higher filtration velocities. Song [126] investigated cake formation using 13 different sizes of polystyrene latex (dp = 0.135 - 2 μm). The results clearly showed that the pressure drop rate is smaller for higher particle size under similar filtration conditions. Furthermore, the porosity of the filter cakes decreases with larger particles sizes. Kono [68] used particles (30 %-wt carbon and 70 %-wt ash) from coal gasification to make and examine filter cakes. The filter cake porosity depended on the filtration velocity, but was independent of the temperature and absolute pressure.

Chapter 4

Panel Bed Filter

"An expert is a man who has made all the mistakes that can be made in a very narrow field"

Niels Bohr (1885-1962)
Danish physicist

4.1 Introduction

This chapter describes the current status of the Panel Bed Filter (PBF). The filter is a fixed bed granular filter which uses surface filtration to separate particles as described in chapter 3.

The unbound granular material in the PBF is held in place by louvers. The louvers are stacked on top of each other into tall, relatively narrow "panels" that create a vertical wall of granular beds illustrated in figure 4.1 A. The use of louvers is not a new concept [152] and different louver designs are summarized in chapter 4.2.

The first PBF patent was made by Squires [127] after he discovered that a sufficiently sharp reverse puff of gas, referred to as a puffback, could renew the surfaces on the gas entry side through a new mode of soil failure [72]. The puffback, or pulse back for liquid filtration [156], opens for continuous filtration through periodic removal of the filter cake during granular bed filtration. Figure 4.1 B (upper drawing) shows normal operation. The gas flows horizontally through the PBF and the dust deposits form a filter cake on the bed surface. The filter cake is removed periodically with a puffback. During the puffback the medium undergoes a mass movement towards its free surface that removes the filter cake with some of the granular medium as shown in figure 4.1 B (lower drawing). The puffback theory is described in more detail in chapter 4.3. The current status of the PBF is presented in chapter 4.4 together with potential future markets for commercialization.

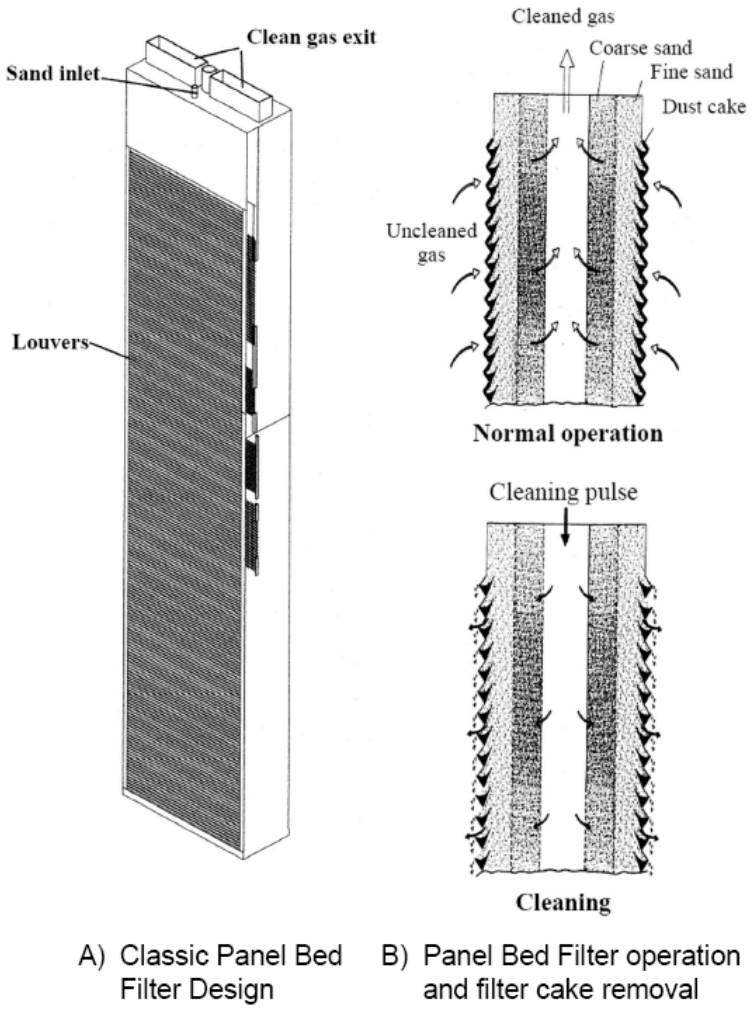

Figure 4.1: Illustration of Panel Bed Filter design and operation from 1997 [93]

4.2 Louver designs

The early work done by Squires [128] [129] and Lee [73] [74] resulted in the Wishbone louver, figure 4.4 E, that has been used as a reference for comparing all future front louvers. The article collection by Lee [72], Squires [131], Rodon [111], Wu [154] and Yang[156] presents the current status of the PBF, including the work done at NTNU (Appendix B) which resulted in the L10-56 design [110].

This section gives a brief summary of earlier investigations from the first PBF patent shown in figure 4.2 to the latest Filter Trays design. Both the front and back louvers (wire mesh in figure 4.2) support the granular filter material, but have different designs and design criteria as described below.

Front louver designs

New front louver designs should aim at improving the bed stability, smoothing the replacements of filter granules during puffbacks, increasing the area of bed surface

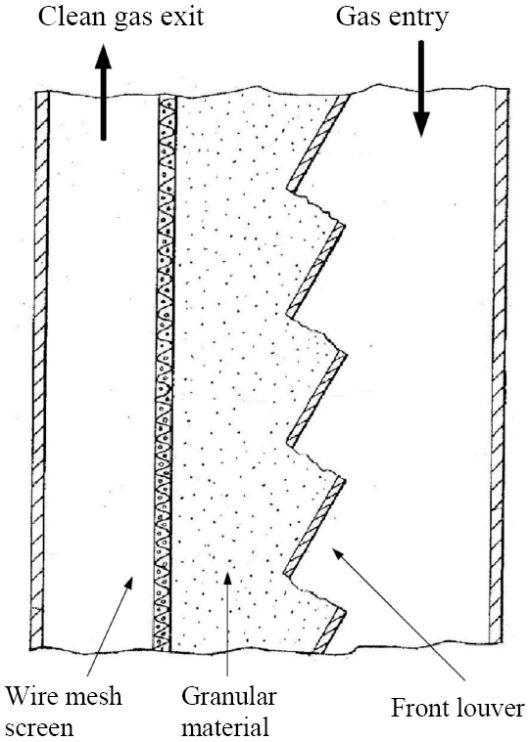

Figure 4.2: The first patented louver geometry [128]

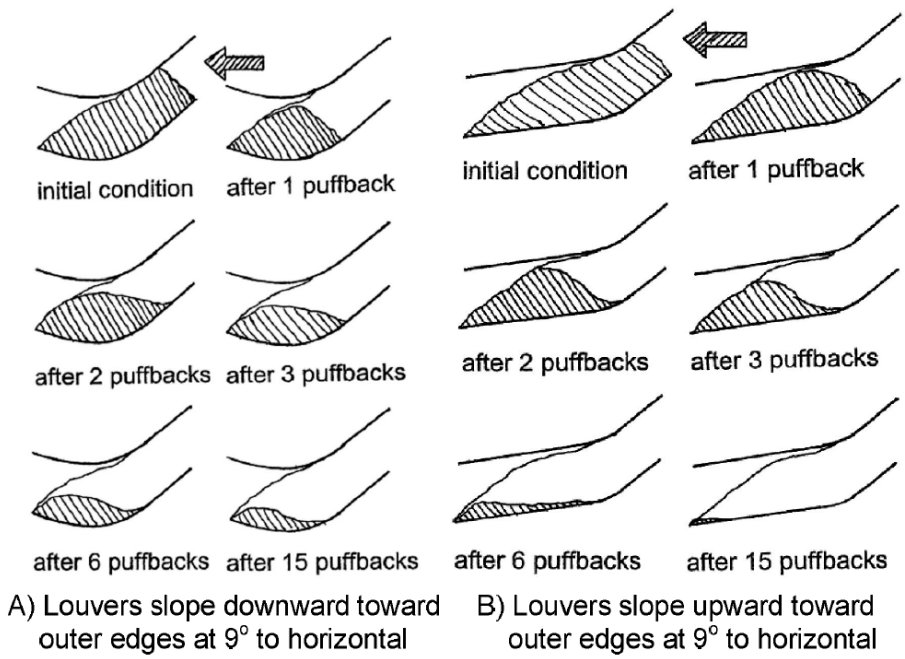

Figure 4.3: Tracings of photographs of a gas-entry sand face during a sequence of 15 puffbacks (air flowing in direction of hatched arrow). Shaded areas are olivine sand darkened by heating to 700 C [131].

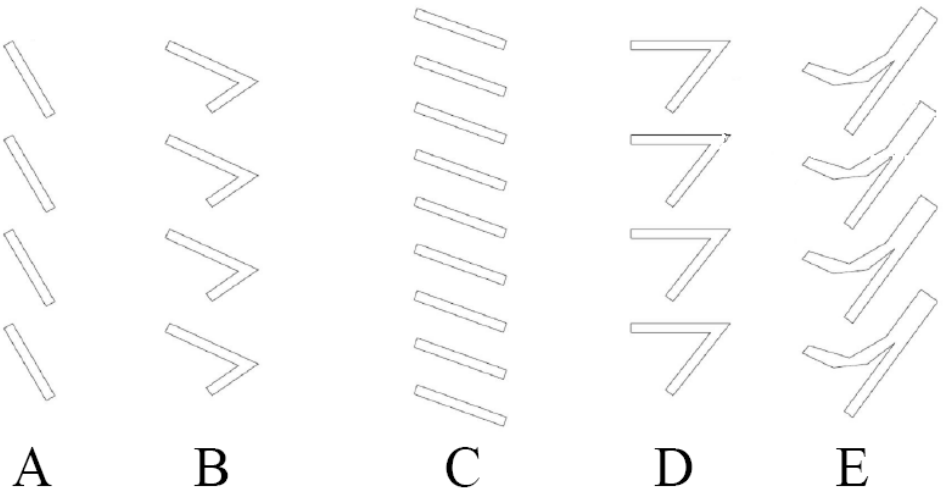

Figure 4.4: Early louver designs by Squires [127] [128] [129] and Lee [73] [74]

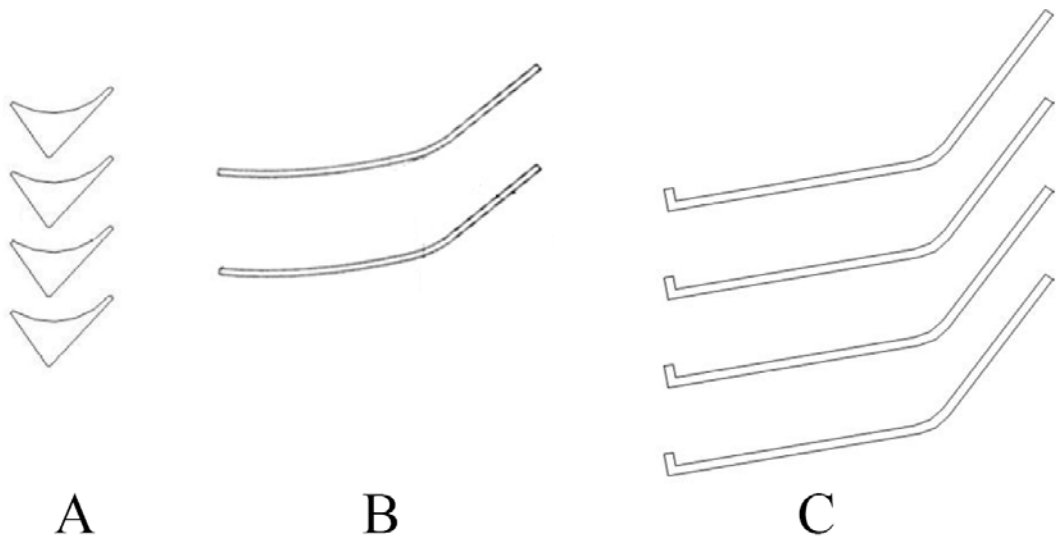

Figure 4.5: Norwegian louver designs by Nos [93] and Risnes [110]

per louver, lowering the initial pressure drop and maintaining a uniform spill of bed material during puffback.

- *Bed stability*
  The front louvers have to support a stable bed of granular media. The stability depends on the properties of the filter granules, the distance between the louvers and the angle of the louver slope toward the outer edge (the louver surface angle).Sand has traditionally been used as the granular media with an angle of repose between 30-35% depending on the sand properties. The angle of repose affects the maximum distance between the louvers and the louver surface angle.

- *Replacements of filter granules*
  Figure 4.3 illustrates the replacement of filter granules during 15 puffbacks [131]. The figure clearly shows that the up-sloping louvers (left) retain more of the original filter material than the down-sloping louvers (right). The static sand (or "heels")are not participating in the puffback created body movement and can be an indication of poor filter regeneration [131].

- *Area of granular bed per louver*
  Increasing the area of the granular bed per louver increases the filtration area per louver and implicitly the filter capacity. This might be utilized by reducing the production costs (fewer louvers needed to filtrate a given flow rate) or by increasing the time between puffbacks. Decreasing the puffback frequency might increase the collection efficiency of the filter since the particle penetration is highest during and right after a puffback (clean bed) [73].

- *Low initial pressure drop*
  Low initial pressure drop will allow for longer filtration cycles if initiated at a given ΔP. Equation 3.19 ($\Delta P = \Delta P_{gf} + \Delta P_{cake}$) shows that this is due to the reduced initial pressure drop, ΔP_{gf}.

- *Uniform spill of bed material during puffback*
  A uniform spill of bed material during puffback is important to ensure clean filter surfaces (avoiding patchy cleaning) and to reduce static sand areas (or "heels"). Patchy cleaning might result in high local filtration velocities [29] [30].

The louver designs in figure 4.4 show the front louvers tested by Lee [73] [74] and Squires [129]. Design A was the first louver to be studied in the PBF. Design B was designed to concentrate the cleaning pulse during puffback and to reduce the redeposition of dust during puffback. Designs C and D were designed to increase the bed surface area but gave poor puffback results. Design E, the Wishbone louver, improved the performance and is used as a reference for later designs.

Figure 4.5 shows front louver designs that were made and tested at NTNU [110]. Design A , the Folla design, was used during the commercial scale testing at the Folla plant [109]. This louver has similar properties as the wishbone louver but is easier to manufacture. Design B, the R-2 louver, was designed to further ease

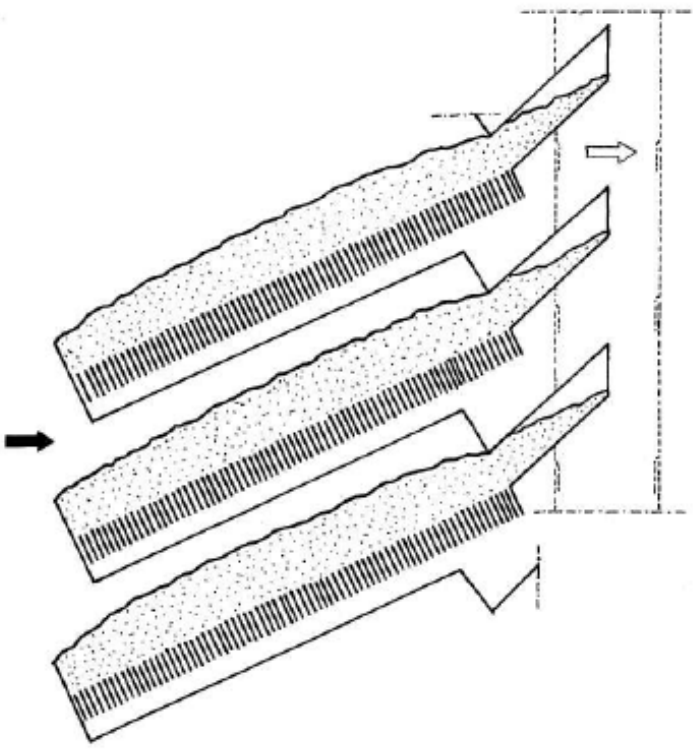

Figure 4.6: Cross-section of three Filter Trays [131]

the manufacturing process. Design C, the L10-56 louver, was designed to further increase the bed surface area. Risnes' [110] results with the L10-56 louvers showed a uniform sandspill during puffback and increased time between each filtration cycle compared to the wishbone louvers under equal filtration conditions. The L10-56 louvers were used for the high temperature filtration of biomass gasification producer gas described in chapter 8. L10-56 louvers with a small modification (closer vertical distance between the louvers to increase stability) was used for the industrial scale field testing as described in chapter 5.4.

Figure 4.6 shows the new louver design by Squires [130], called the Filter Trays. The design increases the ratio of gas entry surface to projected vertical area of the filter by 544% compared to the wishbone louver [131]. Squires calculated that the initial pressure drop would be 75% of the wishbone using sand as granular medium [131], although no laboratory testing was conducted. Chapter 5.2 describes the filter built using Filter Trays modified for use with Sintered Bauxite 20/40. Chapter 7 presents and compares these results to the results obtained from the wishbone and L10-56 designs under equal operation conditions.

Back louver design

New back louver designs should aim at maintaining the back boundary of the bed material, evenly distributing the pressure from the puffback pulse and minimizing the pressure resistance for the cleaned gas.

- *Back boundary of the bed material*
  The back louvers have to hold the granular material in place in order to create the boundary between the granular material and the clean gas volume. This includes the boundary between different granular materials used in the PBF as illustrated in figure 4.7 B.

- *Evenly distribute the pressure from the puffback pulse*
  Equally distributing the pressure pulse throughout the clean side of the granular bed should lead to an equal distribution of the spill during puffback.

- *Minimize pressure drop for the cleaned gas*
  High pressure drop over the back louvers is not desirable since it will increase the total pressure drop over the filter unit ΔP.

Figure 4.7 A shows the usage of the historical back louvers [129]. Lee's studies reported problems with maintaining the back boundaries due to fluidization of the granular particles (sand 20/30 mesh) of air velocity at 15 cm/s and the bed collapsing at a pressure drop higher than 14 inH_2O (approximately 3490 Pa). Figure 4.7 B and C show how Lee [74] solved this problem by introducing a dual bed with a dividing set of closely spaced louvers between the fine sand and coarse sand. Figure 4.7 C shows the inclined louver design, which gave a marked increase in the puffback spill at a given puffback intensity and increased the uniformity of the spill along the louver.

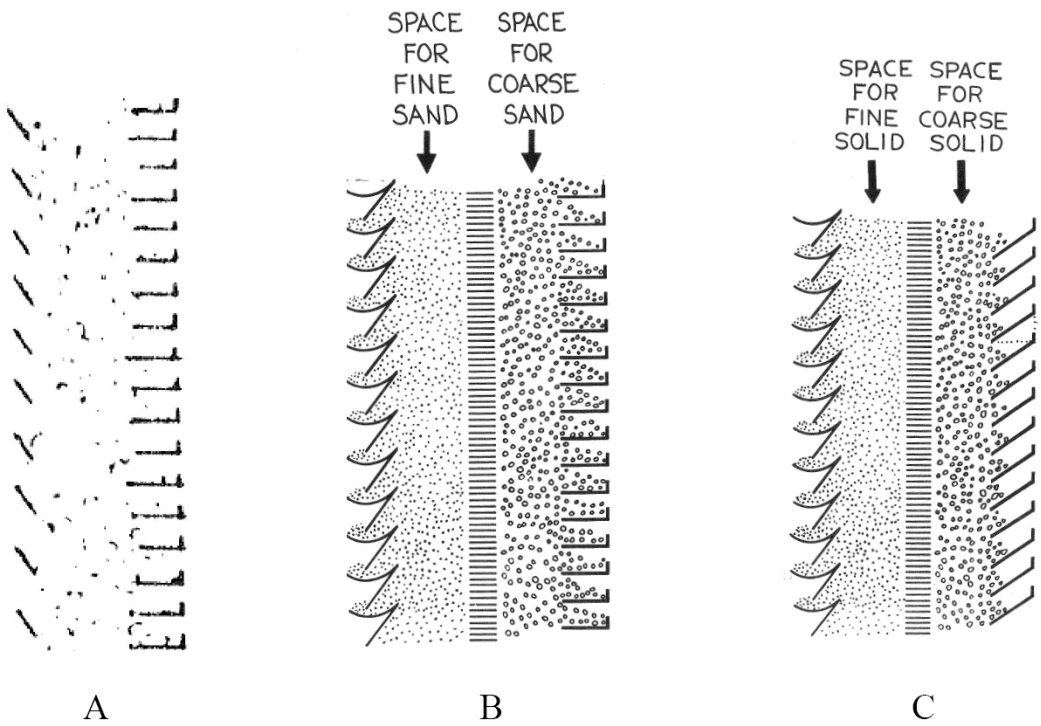

Figure 4.7: Back louver designs [73] [74]

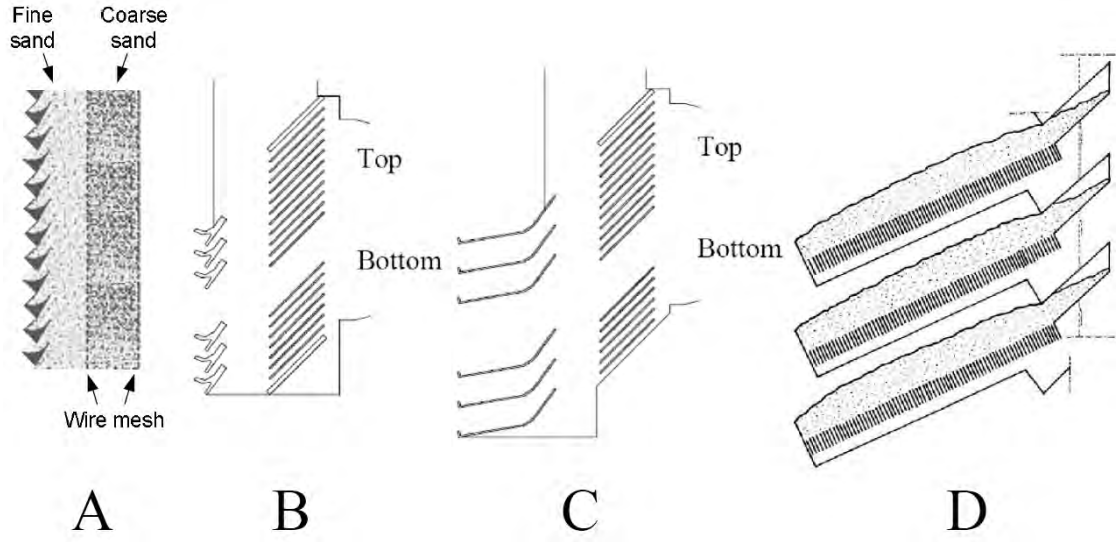

Figure 4.8: Back louver designs [93] [109] [110] [131]

Figure 4.8 A shows the usage of double wire mesh at the Folla plant [109]. Long time testing revealed problems of fine sand plugging the dividing sand wire mesh [137]. Risnes [110] removed the wire mesh and used inclined straight louvers as shown in figure 4.8 B. This eliminated the plugging problem but reintroduced the need to define a maximum filtration velocity, as velocity fluctuations and uneven velocity profiles can lead to local fluidization and entrainment of bed material as experienced by Lee [74]. Risnes [110] reports no granular particle fluidization and entrainment when using long inclined louver and filtration velocities up to 20 cm/s (superficial gas velocity). Furthermore, Risnes [110] achieved better uniformity by racing the back louvers as illustrated in figure 4.8 C. Figure 4.8 D illustrates the Filter Trays [131]. Squires suggests using perforated plates, sloping assembly of closely spaced flat plates, array of small bore tubes fused together or a fine honey comb structure as back louver boundaries [130].

Inclined and raised straight louvers (figure 4.8 C) have been used in the experimental part of this thesis, except for the Filter tray unit where a wire mesh in stainless steal was used. The Filter Tray unit is described in detail in chapter 5.2.

4.3 Cake removal from the panel bed filter

The removal of the filter cake depends on the dust cake properties (thickness, adhesion forces, porosity), the distribution of the puffback pulse in the clean gas volume and the propagation of the pressure pulse in the granular bed. Short filtration cycles might lead to higher particle penetration due to the reduced collection efficiency immediately after and during the puffback as illustrated in figure 4.9. Increased collection efficiency can therefore be achieved by controlling the puffback to only remove the filter cake without removing the filter roots. The filter will then always operate by surface filtration as discussed in chapter 3.4.

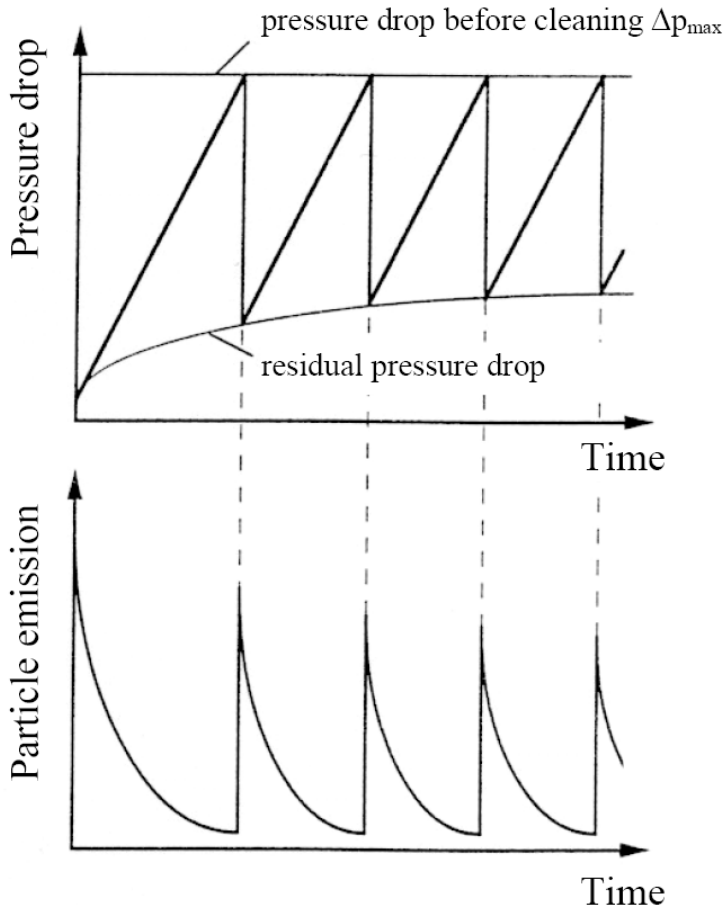

Figure 4.9: Filtration cycles and penetration values [110]

4.3.1 Soil failure during puffback

Squires' first patent is based on the knowledge that the filter cake can be removed by soil failure caused by a reverse surge of gas flow [127]. Studies done by Lee [73] [74] concluded that the mechanisms of the soil failure were caused by the transient aerodynamic drag forces. The spill was found to be closely related to the granular media characteristics. Lee [73] further identified four different bed stages during the puffback. Figure 4.10 A shows the start ($t = 0$) of the soil failure caused by the puffback when the first grains are thrown out. Figure 4.10 B shows the following local failure where grains jump from the inner edge of the gas entry surface. This local failure lasts from 10 to 100 ms. Figure 4.10 C shows the body failure where the whole bed moves forward and causes separation from the back louvers. Figure 4.10 D shows the de-separation and local failure as a small amount of sand falls from the outer edge as the bed is settling. Stage C and D last several times longer than stage B [110].

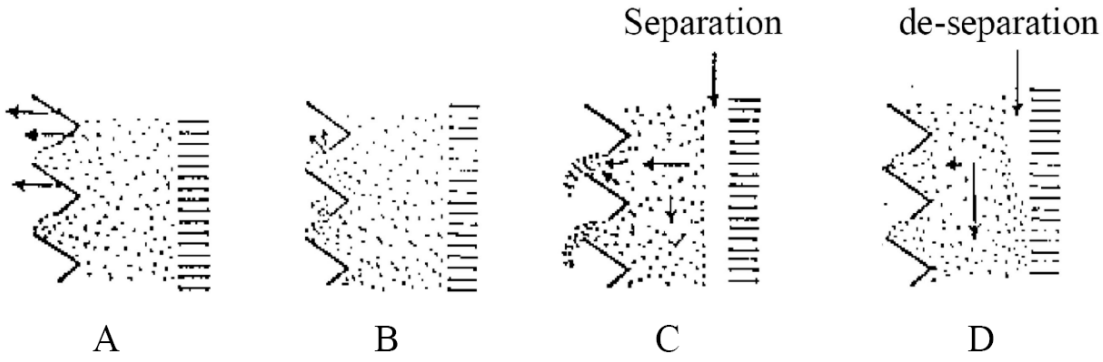

Figure 4.10: The different stages of bed failure during puffback [73]

4.3.2 Puffback theory

The puffback pulse can either be delivered by a vertical pulse (figure 4.11 A) or by a horizontal pulse (figure 4.11 B). Both setups are relatively spacious in order to uniformly spread the pressure pulse from the puffback within the clean gas volume.

During puffback, only the outermost layer of sand should be removed in order to maintain the cake roots (0.3 - 0.8 g/cm^2 for sand [110]). The desired body

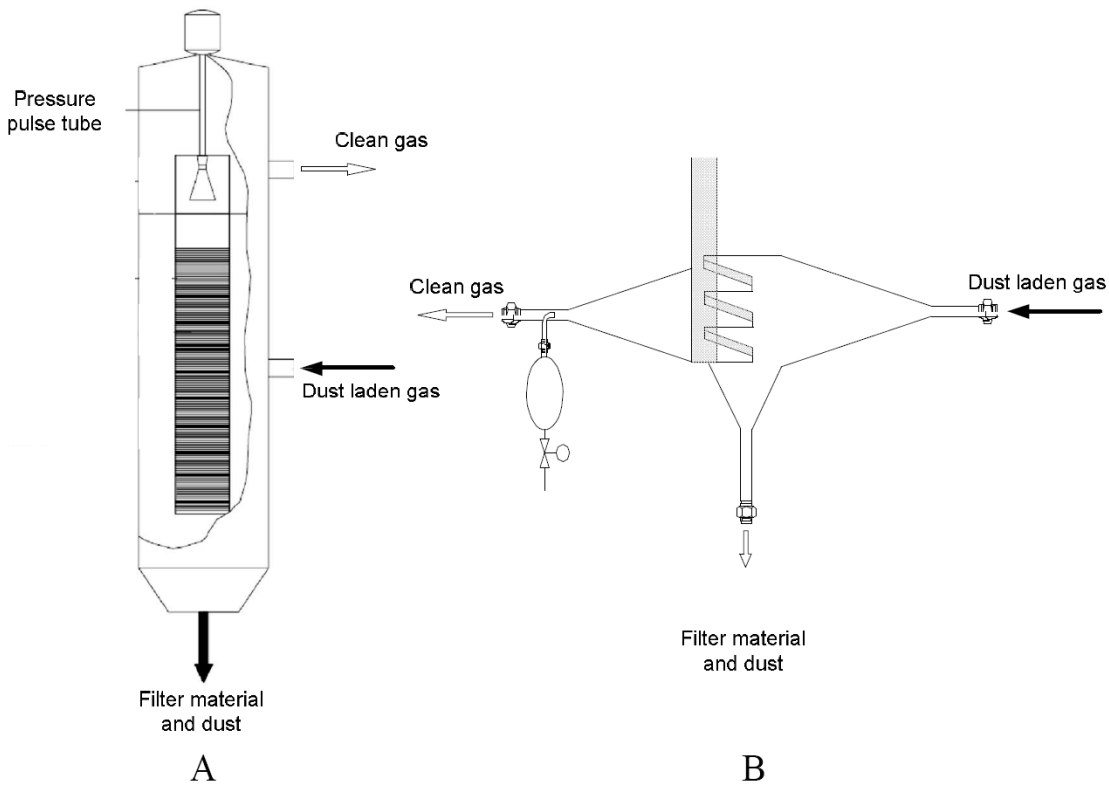

Figure 4.11: Vertical [93] and horizontal puffback setups

movement of the bed can only be caused by a pressure pulse, not a steady blow of air [73]. The pressure pulse has to surpass a minimum pressure value, ΔP_{min}, to obtain any spill of the granular material. The value of ΔP_{min} is in the range of 500-900 Pa depending on the granular material [73] [74] [110]. Lee [73] concluded that a fast rise time of the pressure curve resulted in more soil resistance that resulted in a higher ΔP_{min}. The active time theory and the specific impulse theory are two different theories explaining the spill from a puffback.

Active time theory

Lee [73] [74] defined the active time as the time the pulse exceeded ΔP_{min} as shown in figure 4.12 A. The theory states that the spill of granular material during a puffback is only dependent on the length of the active time, t_a. Equal active time is assumed to reveal equal spill, independent of peak pressure, ΔP_{peak}.

Figure 4.12 B shows how a vertical puffback pulse intensity is reduced as it moves downwards in the clean gas volume. The leakage through the bed will decrease the peak pressure and increase the total duration time of the pulse. At the bottom of the filter, the downwards pulse (red in figure 4.12 B) will be reflected (blue in figure 4.12 B) to give the total pressure (black in figure 4.12 B). Calibrating the reflection of the pressure pulse by regulating the distance of the reflecting

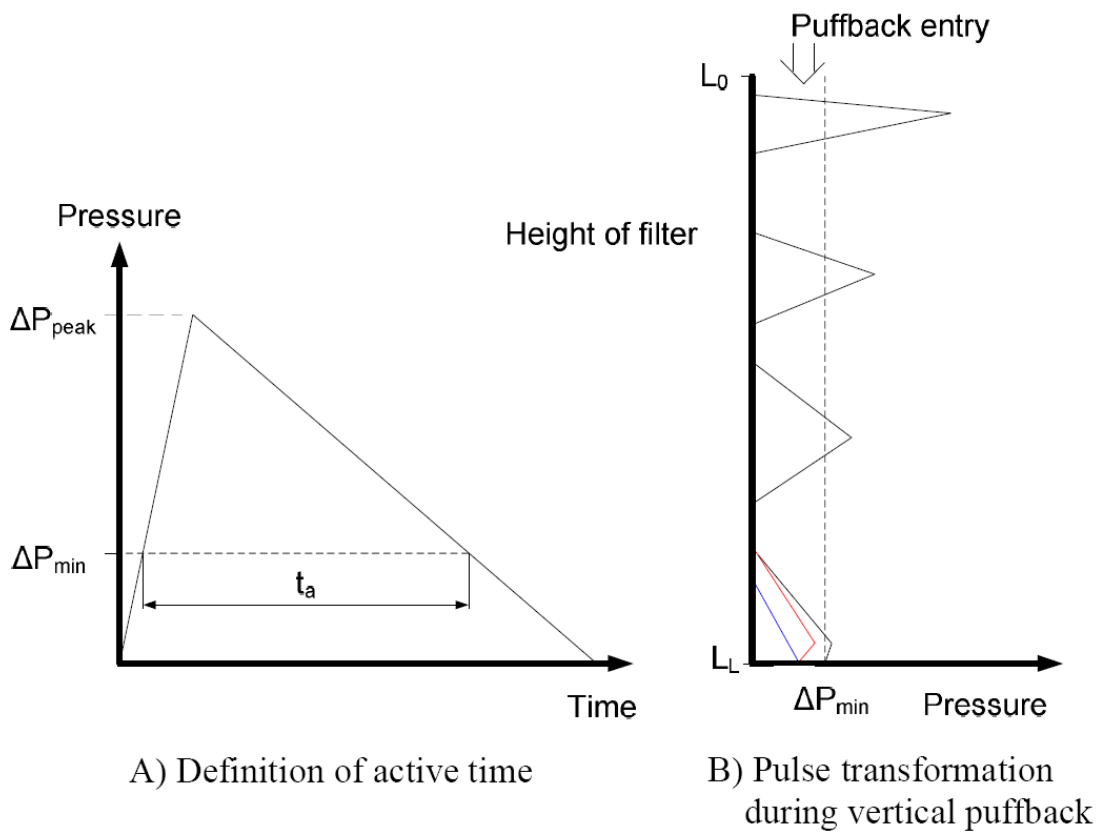

Figure 4.12: Active time definition [73] and vertical pulse behavior

surface will give equal active time throughout the length of the filter.

Specific impulse theory

Risnes [110] found a strong correlation between the average of the normalized spill and the the specific impulse, I_p, of the pressure pulse as shown in equation 4.1.

$$I_p = \int_{t_1}^{t_2} (\Delta P - \Delta P_{min})\, dt \tag{4.1}$$

Where t_1 and t_2 are the times in which the ΔP surpasses and drops below ΔP_{min}. Risnes' [110] theory claims that the specific impulse, not active time, is controlling the spill.

4.4 Current state of the panel bed filter

Experimental studies of the PBF have shown a behavior similar to permanently loaded bag filters [79] with the granular filters capability of filtration of high temperature gas [100]. The evolution of the PBF is a result of 40 years of ongoing research since Squires first patented it in 1967 [130].

Before the present work, Risnes'[110] L10-56 louvers with long inclined back louvers were the latest louvers that had been experimentally studied. Risnes ran over 85 hours of laboratory testing on a filter unit with a projected filtration area of 240 cm^2 (80mm x 300mm) and a collection efficiency of 99.83% and higher (superficial velocity 4.84 - 12.77 cm/s and inlet concentration 1.26-5.51 g/m^3).

The latest field studies were conducted on an industrial scale single filter element (1150 m^3/h) with the Folla louvers. The field studies were conducted on product gas from a bark boiler at 190°C and reported an average collection efficiency of 99.83% [93] [109]. The superficial velocity varied between 4 to 15 cm/s and the inlet dust concentration fluctuated from 0.6 -1.2 g/m^3.

The new filter tray design by Squires [130] is estimated to have a larger filtration surface and lower initial pressure drop compared to the L10-56 louvers [131]. Before this study, the collection efficiency of the filter tray design had not been confirmed by experimental studies.

Appendix B gives an overview of earlier publications related to the PBF.

4.4.1 PBF compared to other gas filtration equipment

Several gas cleaning technologies are available on the highly competitive commercial market. Multi cyclones are the most common gas cleaning device installed in Norwegian combustion facilities, often accompanied by other equipment to comply with new and stricter regulations for particle removal[110]. In dry systems, the electrostatic precipitators (ESP) and barrier filters (granular, metallic, ceramic and fibrous) have shown high collection efficiency [99]. The choice of which gas cleaning technology to use depends on the gas properties, emissions, reliability and cost (investment and operation). A detailed analysis of the different gas cleaning equipment is beyond the scope of this work.

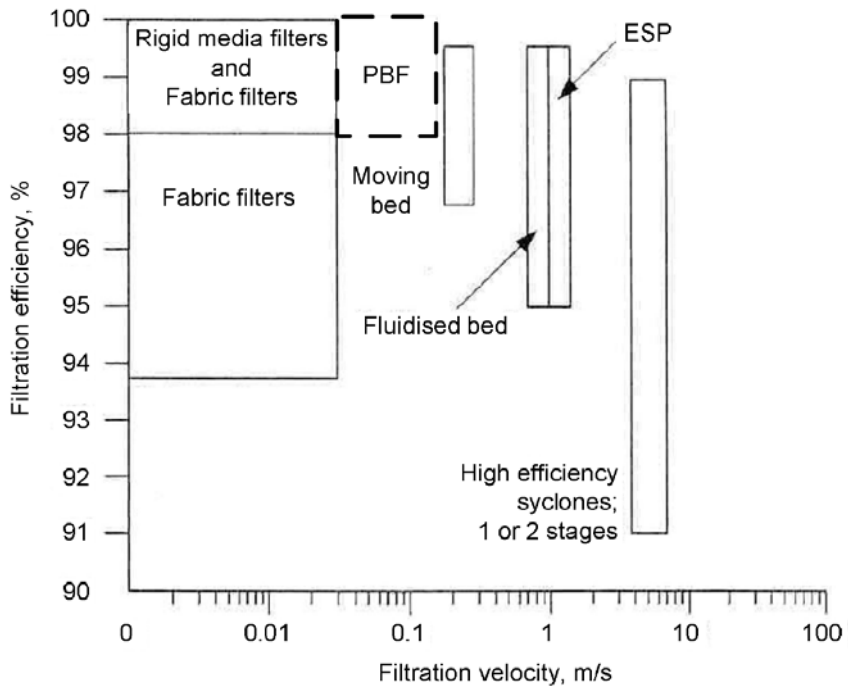

Figure 4.13: Comparison of gas velocity and collection efficiency [110] modified from [141]

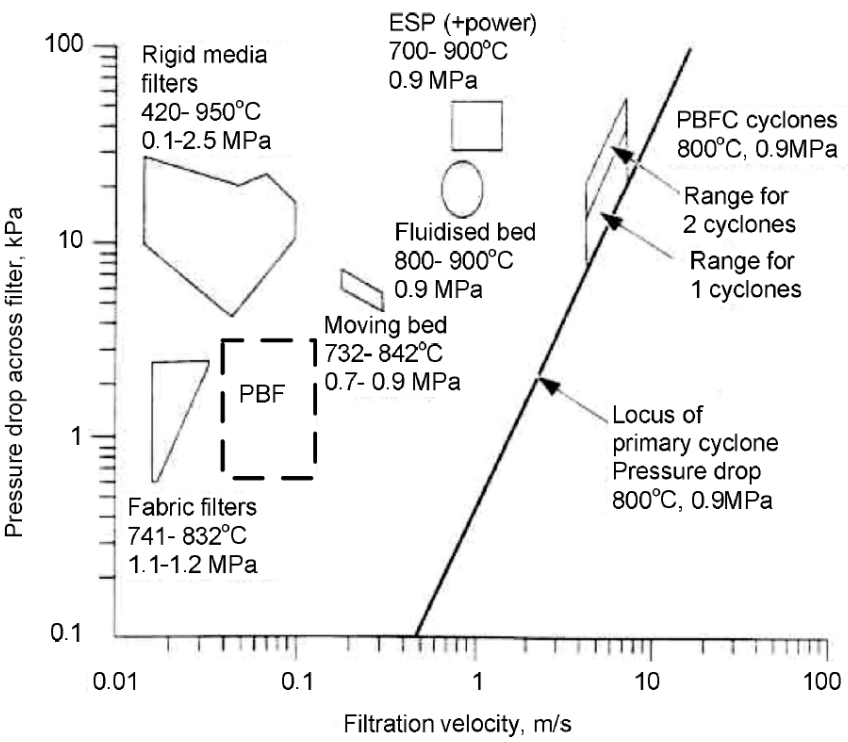

Figure 4.14: Comparison of gas velocity and pressure drop across filter [110] modified from [141]

Figure 4.13 compares the filtration velocity and filtration efficiency for different dry gas cleaning equipment. The figure shows that the PBF has a high filtration efficiency (collection efficiency) and a higher filtration velocity compared to fabric and rigid media filters. The filtration velocity is reversely proportional to the needed filter surface area (increasing the filtration velocity reduces the needed filtration surface). Reducing the filter surface area will reduce size and the investment cost of the filter.

Figure 4.14 shows that the pressure drop of the PBF corresponds to fabric filters and less to the reported values for rigid media filters. A comparison of the high temperature and high pressure (HTHP) data in figure 4.14 is done with the notification that the temperature rather than the pressure is the more significant variable influencing the pressure drop, dust separation and retention process in a filter [110]. The figure shows the low operational pressure drop across the PBF. The pressure drop can correlate the investment cost and operational cost of the fan. The PBF use of granular material allows for the possibility of high temperature filtration as long as cake filtration is achieved (the influence of temperature on cake filtration was discussed in chapter 3.4).

The choice of granules presents the possibility of filtrating a corrosive gas or a gas containing glowing or burning particles. The PBF can also provide chemical processing of the gas by using sorbents as granular material [128].

4.4.2 Entering the commercial market

The emission limits from Norwegian industry are regulated by the Norwegian Pollution Control Authority (SFT). The individually set emission limit can vary depending on location, size and type of industry. Several commercially available technologies might be suitable to an industry that has to invest in new gas cleaning equipment for particle removing. The choice of equipment is therefore also based on the economic cost (investment and operational costs), total size (cleaning equipment and support equipment) and the long time results of the filtration device in addition to the specific operational conditions described in the previous section.

- *Investment and operational cost*
  The production costs of the PBF are mainly determined by the steel prices and the labor costs. The cost of the granular filter medium comes on top of these costs and varies depending on the type of granular media used [133]. The operational costs are generally low since they depend on the wear-resistance of granular material.
  In addition, PBF systems with low capacity might have a relatively high investment cost when building a system of regeneration and re-usage of the granular material as described in chapter 5.4. The relative cost of the regeneration system ($/m^3) will decrease as the capacity goes up.

- *Total size of the filtration equipment*
  The high filtration velocity of the PBF reduces the filter surface needed compared to those of fabric and rigid media filters. The size of the housing

of PBFs with vertical cleaning is comparable to the housing of fabric and rigid media filters. The total size of the PBF will be larger than those of fabric and rigid media filters due to the support equipment (regeneration and re-usage of the granular material) and the relatively spacious geometry spreading the puffbak pressure pulse uniformly within the clean gas volume.

- *Long time results from continuous operation*
  The PBF lacks data from field tests of more than 1000 hours. The products reliability can be considered the most important advantage for products already on the commercial market.

It is believed that the potential future market for the PBF is within high temperature filtration.

Chapter 5

Experimental studies

"Stress is your body's way of saying you haven't worked enough unpaid overtime"

Scott Adams
Creator of the Dilbert comic strip

5.1 Introduction

The work presented in this thesis mainly consists of experimental studies of different filter designs. The purpose of the experimental studies was to improve the overall performance of the PBF with a focus on increasing the filter capacity, its high temperature applications and reducing the size of the puffback geometry.

- **Increase the filter capacity**
  Increasing the filter capacity will reduce the filter size and the production costs. This can be done by increasing the filtration velocity or by increasing the filtration surface.
  Laboratory studies using filter trays showed a collection efficiency of 99.78% with Sintered Bauxitte 20/40 (SB 20/40) as granular medium and filtration velocity of 14.9 cm/s. This is described further in chapter 5.2.

- **High temperature applications**
  High temperature filtration is a possible commercial market for the PBF.
  The development of a high temperature PBF prototype was built to clean the producer gas from the biomass gasifier in Güssing, Austria. The hydrogen rich producer gas had to be cleaned above 500°C to prevent the tar content from condensing. The gas could then be utilized in a Solid Oxide Fuel Cell. Field testing on the producer gas showed a collection efficiency above 99.98% and is further described in chapter 5.3.

- **Reduce the size of the puffback geometry**
  Reducing the size of the puffback geometry will reduce the total size of the PBF unit and make the filtration concept more commercially acceptable for applications with size constrains.

Filter size	**Laboratory**	**Prototype**	**Demonstration plant**
Publication	**Paper I**	**Paper II - III - IV**	**Paper V**
Purpose of investigation	Increase the filter surface area per louver and increase the filtration velocity	Develop a system to clean the producer gas from the biomass gasifier in Güssing, Austria at 500°C	Decrease the size of the puffback geometry and designing, building and testing the demonstration plant
Louver design	Filter trays	L10-56	Modified L10-56
Granular media	SB 20/40	SB 20/40	Olivine AFS30
Type of gas	Air	Producer gas from biomass gasification	Flue gas from biomass combustion
Type of dust	Standard dust	Ash	Ash
Temperature	Ambient	500-550°C	200°C
Filtration velocity	3.87-14.9 cm/s	2-8 cm/s	2-4 cm/s

Table 5.1: Overview of experimental work

A demonstration plant was built with regeneration and re-use of the granular material. The demonstration plant was built with a new compact puffback geometry that has been developed at NTNU as described in chapter 5.4.

Table 5.1 shows an overview of the experimental work done as part of this PhD.

5.2 Laboratory studies

The filter tray is a new louver design patented by Squires [130]. The patent claims to increase the ratio of gas entry surface to projected vertical area of the filter by 544% and to reduce the clean bed pressure drop by 25% compared to the wishbone louver [131]. The claim is based on calculated values and was not experimentally verified.

5.2.1 Setup

Figure 5.1 and figure 5.2 show the filter tray design modified for Sintered Bauxite 20/40. Figure 5.1 illustrates the borders of the Sintered Bauxite filling containers with thick solid lines, whereas black dots identify the volume occupied by the Sintered Bauxite in figure 5.2. An adjustable plate (gray in figure 5.1 and green in figure 5.2 (left)) were used to adjust the clean gas volume to get uniform spill during puffback.

The Sintered Bauxite spheres exited the refilling containers through two 18 mm holes shown in figure 5.2 (left). Gravity and the angle of repose transported the spheres down the tray where the bed was formed. During filtration the gas flowed

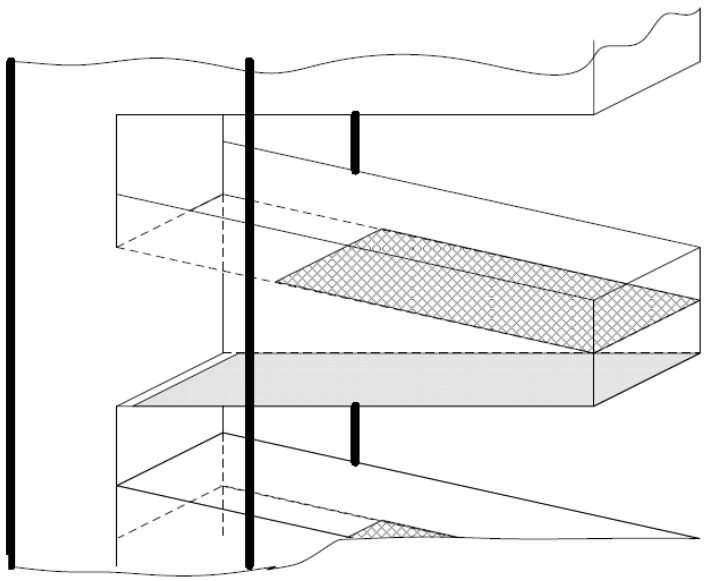

Figure 5.1: New louver designs

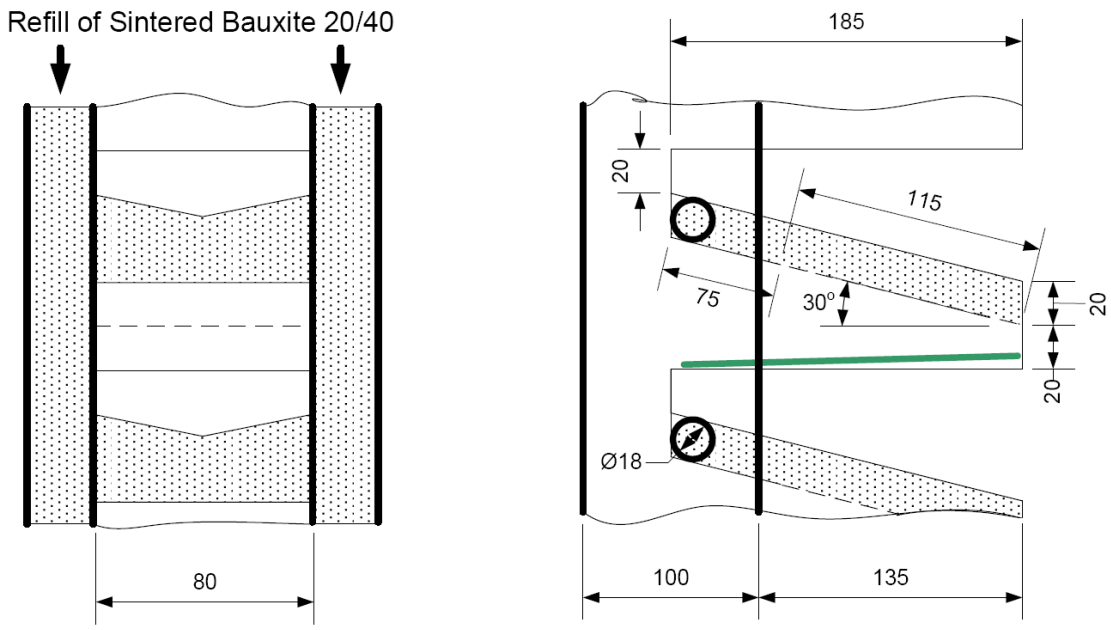

Figure 5.2: Filter Tray designed for Sintered Bauxite 20/40

through the bed and exited through the wire mesh placed at the lower part of the trays. The wired mesh was made of stainless steal with a mesh size of 300 μm.

The filter was constructed to study the new louver design. Easy access to modify the louvers was given priority. This reduced the total number of louvers and the ratio of gas entry surface to projected vertical area of the filter.

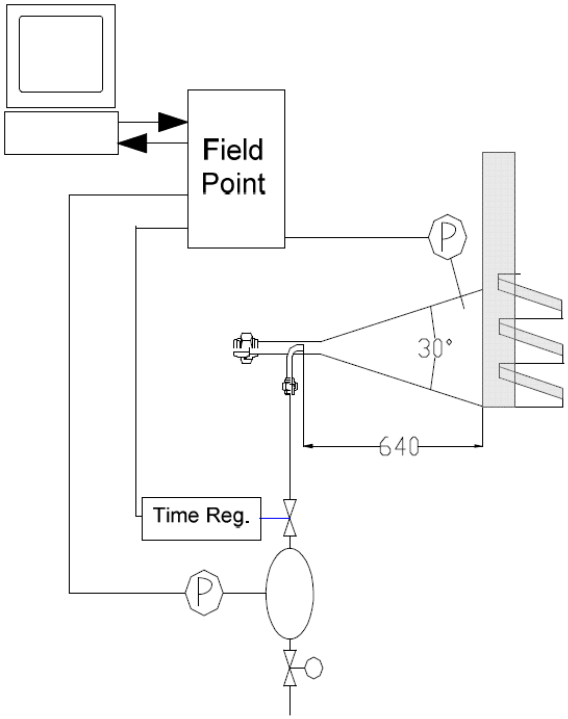

Figure 5.3: Setup of the puffback calibration

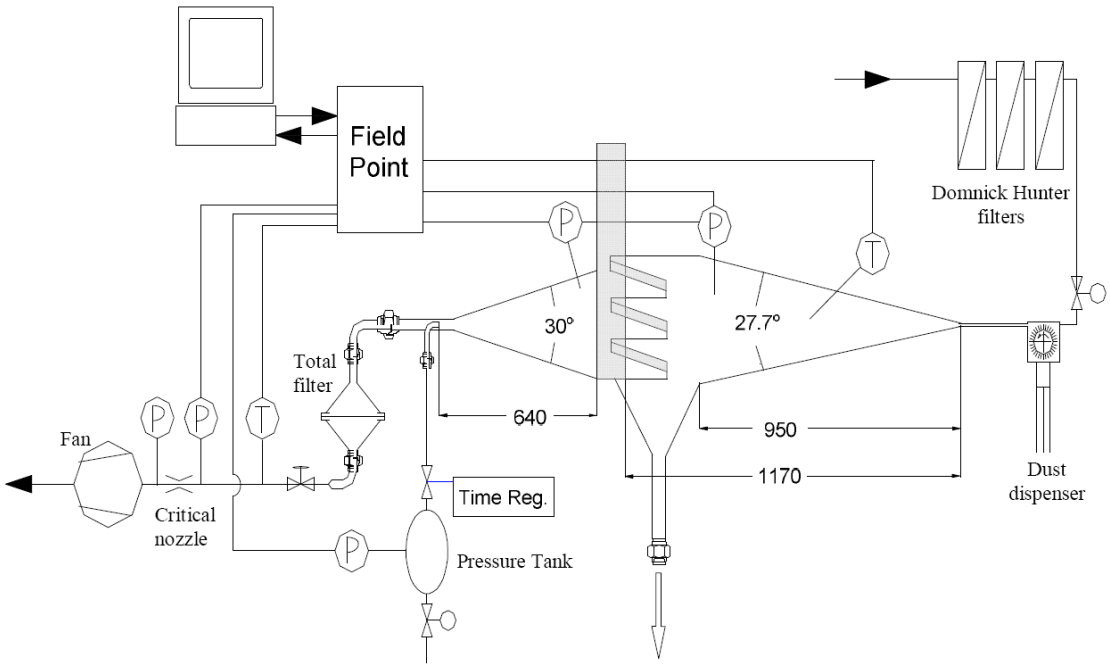

Figure 5.4: Setup of the filtration experiments

Puffback calibration

Figure 5.3 shows the setup during puffback calibration. Filtrated compressed air at approximately 7 bar was reduced to the desired pressure before entering the pressure tank. The puffback from the tank was controlled by a 3/4" Festo CPE 24 solenoid valve with manual regulating of the opening time. The opening time, tank pressure and the pressure in the clean gas volume were logged. The results from the puffback calibration are presented in Appendix C.

Experimental setup

Figure 5.4 shows the experimental setup. Compressed air at approximately 7 bar passes through three Domnick Hunter filters in which oil and moisture, coarse particles and fine particles are removed respectively. The pressure is reduced in a reduction valve before entering the particle dispenser (Palas gmbh, RBG 2000). Two types of dust were used for the experiments. The SAE-fine test dust ISO 12103-1 was also used by Risnes [110] and chosen for comparing the results. The second type of dust was collected from the filter bags of the local combustion plant in Marienborg Trondheim. This dust was used to investigate the dust penetration after several filtration cycles. Both dust types are described in more detail in Appendix C.

The filter inlet cone was built of 3 mm Lexan so the cake build up could be visible during the filtration of the dust laden gas. A total filter (Pall, Type A/E Glass Fiber) was placed after the PBF to gravimetrically determine the dust concentration in the cleaned gas. The gas flow was manually controlled by two parallel valves and measured with a calibrated critical nozzle [132] before going through the fan. A LabVIEW program was made to log the temperatures, pressures and flow rate.

5.2.2 Summary of laboratory studies

The optimal ratio of gas entry surface to projected vertical area of the filter was not prioritized in the experimental study which focused on the new louver design.

Table 5.2 shows a summary of the experiments conducted on the PBF. Relevant figures are included in Appendix C and the results were presented in Boston at the Clean Technology 2008 conference and published in the conference proceedings (chapter 7).

Overall, the results showed a high collection efficiency with filtration velocities up to 10 times higher than commonly used for fabric filters. The reduced collection efficiency obtained during Test #6 was due to a problem with the refilling of Sintered Bauxite.

Figure 5.5 shows the pressure drop for Test # 8 with a filtration velocity of 14.8 cm/s.

The clean bed pressure drop was approximately 10% of the reported pressure drop values of Wishbone louvers using sand as a granular medium as done by Risnes [110] and Lee [74].

Test #	Dust	Filtration velocity Actual [cm/s]	Filtration velocity Superficial [cm/s]	Concentration in [g/m^3]	Concentration out [mg/m^3]	Efficiency %
# 1	SAE	5.03	5.07	6.87	14.6^a	99.786^a
# 2	SAE	4.97	5.01	5.72	2.78	99.951
# 3	SAE	4.99	5.03	3.53	<0.05	>99.999
# 4	SAE	3.85	3.87	7.01	<0.05	>99.999
# 5	SAE	6.92	6.98	5.58	4.09	99.927
# 6	MB	5.76	5.81	4.86	45.15^b	99.071^b
# 7	MB	5.38	5.43	5.33	<0.05	>99.999
# 8	SAE	14.8	14.9	5.42	1.16	99.979

a) Started filtration without filter cake roots (clean bed)
b) Problem with the refilling of Sintered Bauxite

Table 5.2: Overview of laboratory studies

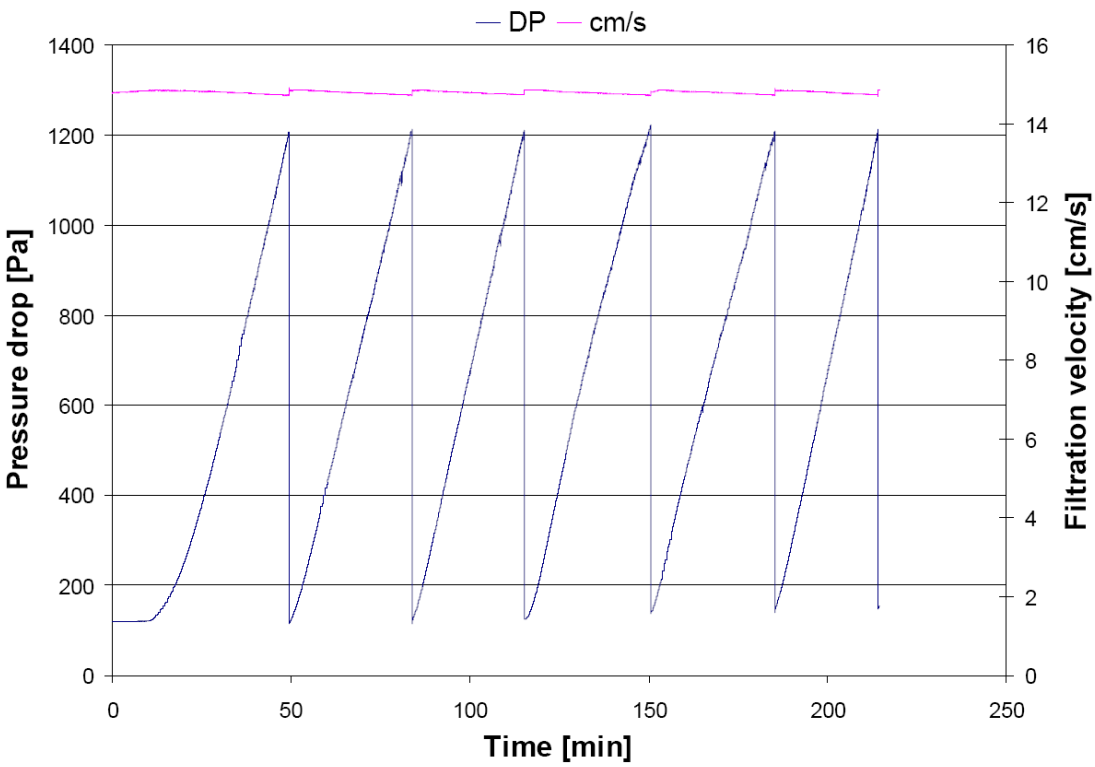

Figure 5.5: Filter testing of the filter trays.

5.3 BioSOFC

5.3.1 Project background

The BioSOFC research project started in the fall of 2003. The project is administrated by the Department of Energy and Process Engineering at the Norwegian

University of Science and Technology in cooperation with the Technical University of Vienna, Repotec and Biomassekraftwerk Güssing GmbH. The Norwegian companies Prototech, Vang Filter Technology, Vardar Energy, Trondheim Energy, Hadeland Energy and Agder Energy together with Agder University College are also part of the project. The project has been financially supported by the Research Council of Norway.

The project aimed to develop technology for commercialization of integrated high temperature fuel cell and gasification processes with high temperature gas cleaning. The research tasks include on-site testing of sub-systems already at a high level of development and their interaction, functionality and reliability in a complete system for high efficiency electricity production from biomass. The main project goal has been specified with the following sub-tasks:

- On-site testing of a high temperature gas filter and its capability to remove tars and particles from the gasification gas to such a level that stable long term operation of the fuel cell stack is achievable

- On-site testing of a 3-5 kW Solid Oxidize Fuel Cell stack using a slipstream from a commercial steam gasification unit at normal operation

- Study and testing of the influence of alkali metals and other trace compounds on the operation of a Solid Oxidize Fuel Cell

- System studies of the overall performance of the gasification - high temperature filter - Solid Oxidize Fuel Cell combination with respect to efficiencies, and optimisation of such a system

The gas cleaning of the producer gas before it enters the Solid Oxidize Fuel Cell has been studied with a focus on the particle removal. Details of the Solid Oxidize Fuel Cell and kinetics of the H_2S removal are outside the scope of this PhD thesis.

Project stages and solutions

Solving the problems in preparing the Güssing plant producer gas in order to be utilized in a Solid Oxidize Fuel Cell can be divided into three sub-tasks:

1. *Small scale granular filter experiments*
   The initial experiments on the Güssing producer gas were conducted on a small scale granular filter element. The results have been published in the Journal of Hazardous Materials (chapter 8).

2. *System design*
   The solution for cleaning and delivering the Güssing producer gas to the SOFC at 920°C has been built and tested in the laboratory at NTNU as well as the producer gas in Güssing. The results were presented at the 2007 ASME International Mechanical Engineering Congress Exposition (chapter 9).

3. *Up-scaled granular filter experiments*
   The granular filter experiments involve the design, building and testing of an up-scaled high temperature filter on the Güssing plant producer gas in Austria. The results were presented at the 10th World Filtration Congress (chapter 10).

5.3.2 The Biomassekraftwerk Güssing GmbH

The Biomassekraftwerk Güssing GmbH consists of a dual fluidized bed atmospheric steam gasifier, a low temperature gas cleaning system, a gas engine with an electricity generator, and a heat utilization system. The Fast Internally Circulating Fluidized Bed gasifier is an indirectly fired steam gasification unit using wood chips with a water content (wet basis) of 20 - 30% as fuel. The gasification zone consists of a bubbling fluidized bed steam gasifier and is physically separated from the combustion zone consisting of a circulating fluidized bed combustion reactor. Bed material is circulated between the zones while the gases remain separated, figure 5.6. Char is transported to the combustion zone together with the bed material and is combusted there, heating the bed material that is being recirculated to the gasification zone. Hence, the circulating bed material acts as a heat carrier from the combustion zone to the gasification zone. The thermal input to the plant is 8 MW and the electric efficiency is about 25% gross. The producer gases have a lower heating value of about 9 MJ/kg [51].

The producer gas

Producer gas used in the experiments is taken from the gasifier free-board. The gas temperature is approximately 900°C and lies just below atmospheric pressure (3-7 mbar). The producer gas, table 5.3, and the tar, figure 5.7, are highly dependent upon the fuel and the gasifier operation. The tar components in the producer gas are in gaseous form and might condense in temperatures below 500°C.

The Biomassekraftwerk Güssing GmbH is described in further detail by Bolhár-Nordenkampf [13][14][15], Hofbauer [48][49][50][51][52], Kaiser [60][61] and Rauch [105] [106].

Hydrogen	30-45	Vol%
Carbon monoxide	20-30	Vol%
Carbon dioxide	15-25	Vol%
Methane	8-12	Vol%
Nitrogen	1-3	Vol%
Hydrogen sulfide	100-200	ppm
Ammonia	1000-2000	ppm
Particles	40-100	g/Nm^3
Tar	1-2	g/Nm^3

Table 5.3: Güssing plant producer gas composition on dry basis

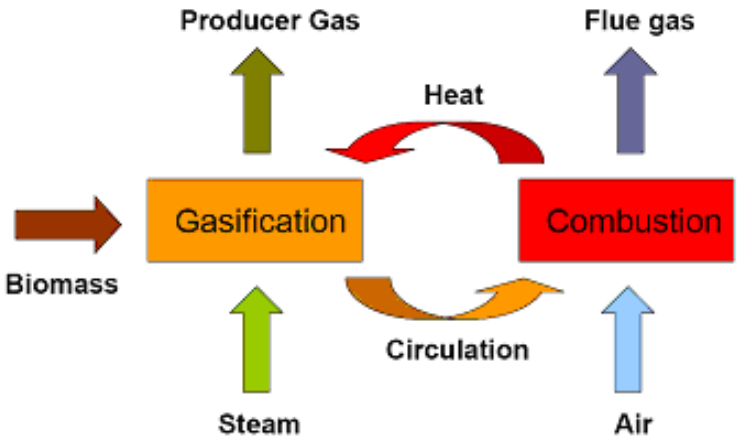

Figure 5.6: Principle of the FICFB-gasification process[51]

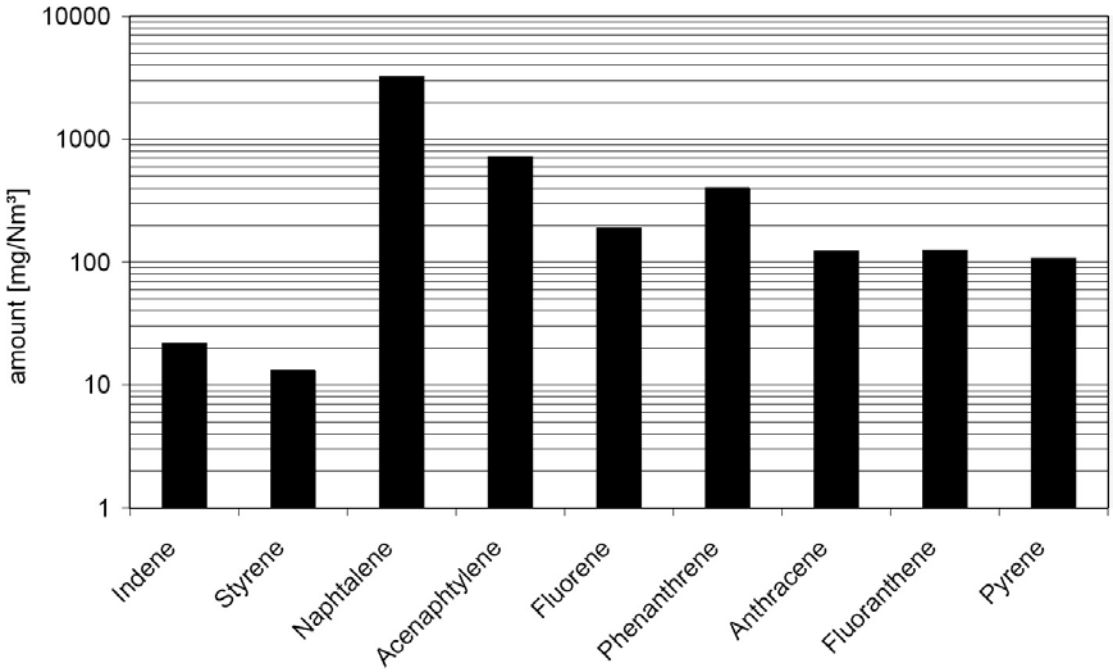

Figure 5.7: Güssing plant producer gas tar composition

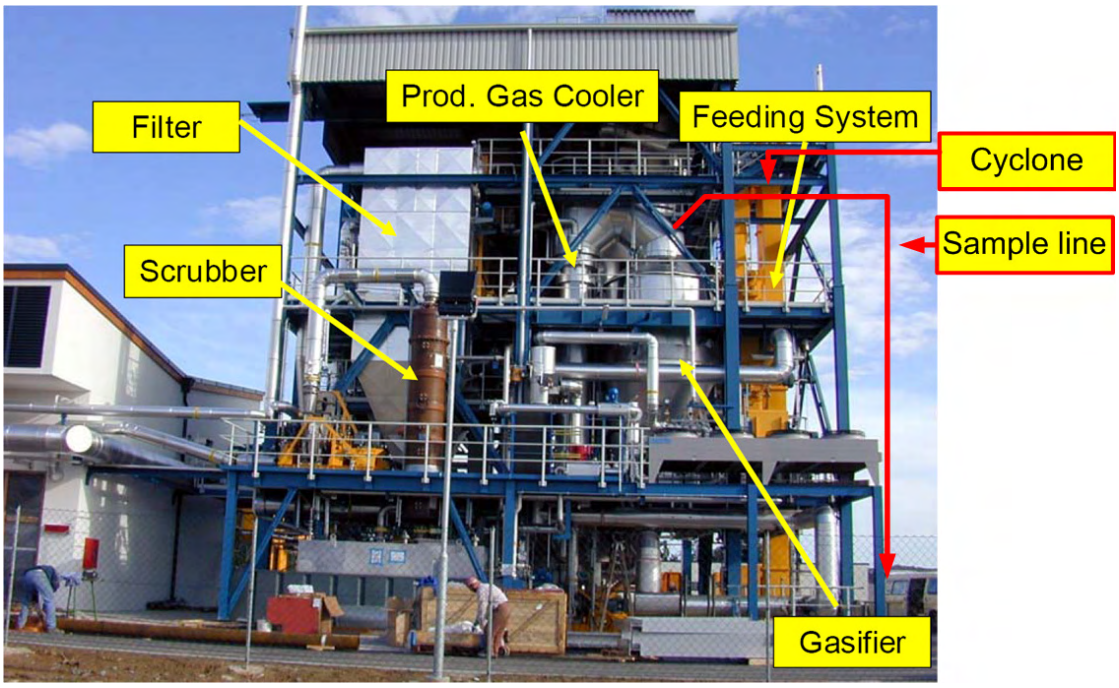

Figure 5.8: Güssing sampling line

5.3.3 Small scale granular filter experiments

The purpose of the small scale experiments was to investigate if the PBF in combination with a cyclone could remove the particles from the producer gas sufficiently enough to utilize the gas in a SOFC. The lower temperature limit during filtration was set to 500°C to avoid tar condensation. The upper temperature limit was set to 550°C due to kinetic limitations of the H_2S sorbent.

Setup

Figure 5.8 shows the location of the cyclone and the sampling line during the small scale experiments at the Güssing plant. The sampling line also functioned as a gas cooler and operated with a constant wall temperature of 550°C. The cyclone was designed for 1 Nm^3/hour. The dust concentration in the cyclone was reduced from 40-60 g/Nm^3 down to 2-3 g/Nm^3.

Alumina Oxide spheres, Sintered Bauxite 20/40 (Appendix A), were used as granular material in the electrically heated PBF. Nitrogen was used for on-line pulsing to remove the dust cake. Figure 5.9 shows the setup downstream from the PBF. The tar was removed with a water cooled acetone container which the producer gas was bubbling through. The flow was measured by a calibrated orifues nozzle. Temperatures, pressures and filter pressure drop build-up were logged, and the mass flow and filtration velocity were calculated in real time.

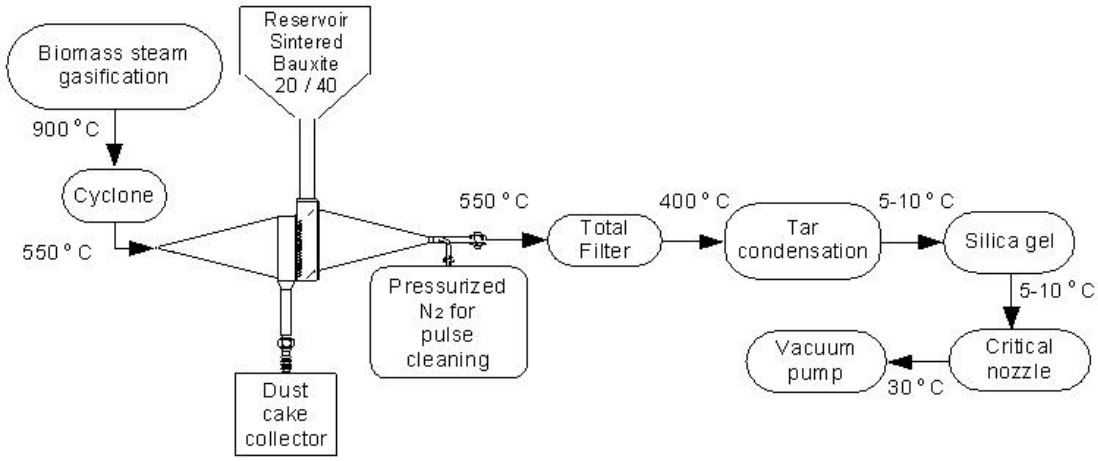

Figure 5.9: Setup

Summary of small scale results

Field tests performed at about 525°C showed dust cake formation on the granular surfaces. The 1-2 g/m^3 tar in the producer gas did not condense, and did not influence the dust filtration, or the filter cleaning. No detectable weight increase on the total filter (in mg) was measured after the tests so the dust concentration after the filter could not be calculated. The results showed a filter efficiency above 99.995% from the biomass gasification producer gas with a relatively low pressure drop over the filter. The pressure drop over the PBF is competitive with those of bag filters even with considerable higher filtration velocities. Furthermore, the tars in the producer gas did not condense in the filter or influence the particle removal in any way.

The good results from the small scale tests were considered to be sufficient for a continuation of the project.

5.3.4 System design

The purpose of the system design was to build a system capable of running a 5 kW$_{el}$ SOFC on the Güssing producer gas. This included the designing, building and testing of every component that would be used in the final setup in Austria.

Setup

The components in the system has been divided into:

- *Gas cooler*
  The gas cooling was done by keeping the pipe wall at a constant temperature from the gasifier to the filter during the small scale tests.

- *Gas cleaning*
  The gas cleaning components consisted of a cyclone, a PBF and a bed of H_2S

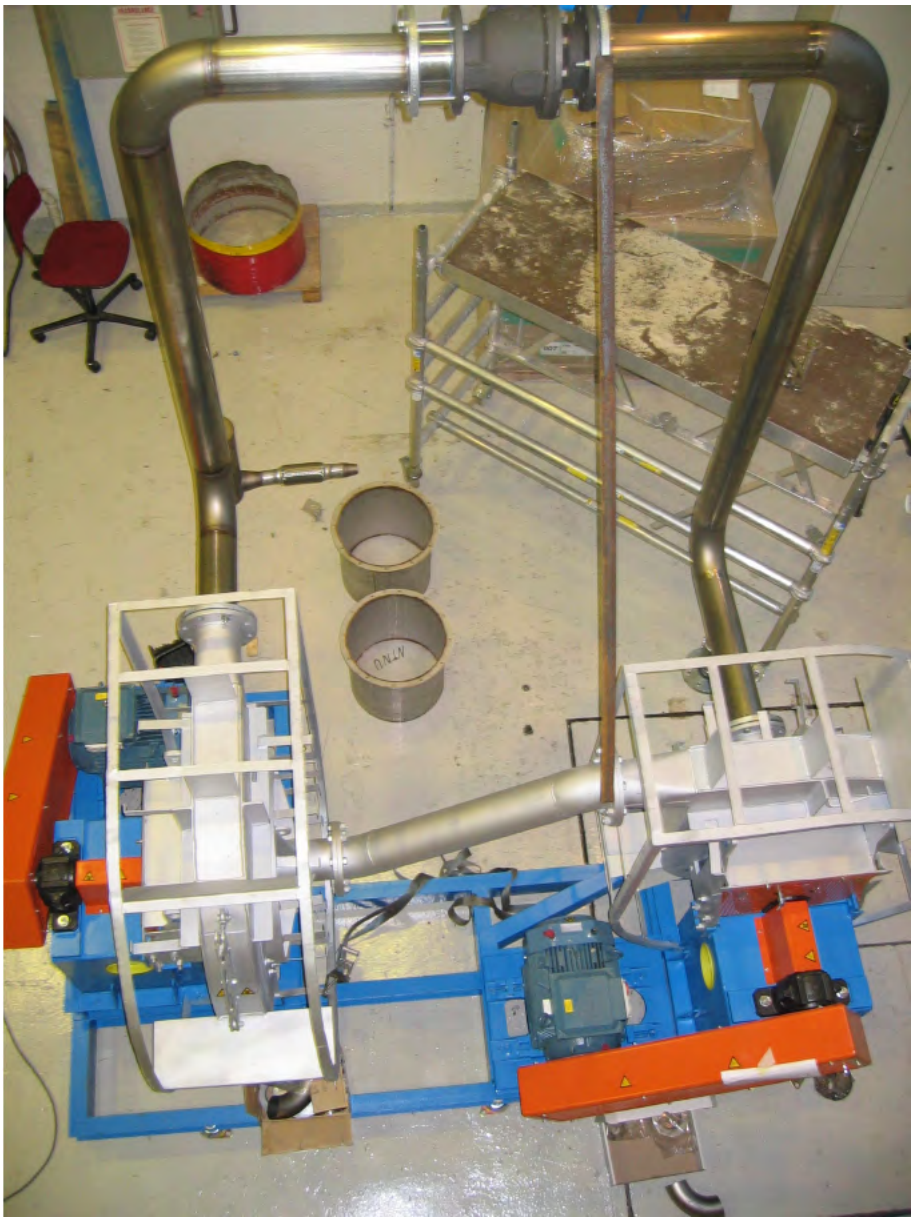

Figure 5.10: Pressure control loop

sorbents. The construction and calibration of the upscaled PBF is further described in Appendix D. The construction input to the H_2S bed will not be a part of this thesis due to the confidentiality agreement with the sorbet supplier.

- *Pressure control loop (PCL)*
  The Güssing gasifier operates at a pressure slightly below atmospheric pressure (3-7 mbar), while the Solid Oxide Fuel Cell requires the cleaned producer gas at a pressure slightly above atmospheric pressure (1-3 mbar). The PCL was constructed to increase the pressure in the hydrogen rich producer gas by 0.1 bar. The designed operation temperature was between 500°C to 525°C

due to the tar content. Figure 5.10 shows the two 11 kW fans and the 7 m loop that had to be electrically heated in order to not have initial tar condensation. Secound, the loop had to emit heat supplied by the fans in order to achieve steady conditions.

- *Gas heater*
  The gas heater was designed to heat the producer gas to 920°C.

- *SOFC*
  The production and operation of the SOFC in Austria was controlled by Prototech.

The temperatures, pressures and volume flows were monitored and logged in a LabVIEW program through Field Point. Appendix D shows the design drawings and describes the LabVIEW program.

Summary system results

The system designed for running a 5 kW_{el} SOFC was individually tested in the laboratory before being assembled in Güssing, Austria. The system performed well when assembled during the field tests.

5.3.5 Up-scaled granular filter experiments

The purpose of the experiments was to design, build and test a new scaled-up filter module on the Güssing gasification producer gas and to compare the efficiency of the scaled-up filter to the small filter. The new filter unit was designed for a continuous volume flow 10 times larger than that of the small scale filter. The filter was designed to operate at the same conditions as the small scale filter.

Setup

The experiments on the Güssing producer gas were conducted between 500°C to 550°C. The first sampling line was replaced before starting the scaled-up filtration tests. The new sampling line also operated with a constant wall temperature of 550°C, but the cyclone was moved to ground level. The cyclone was designed for 8 Nm^3/hour and the dust concentration in the new cyclone was reduced from 80-100 g/Nm^3 down to 10-13 g/Nm^3.

Like the small PBF, the filter was electrically heated and alumina spheres were used as the granular material. Nitrogen was used to remove the dust cake. The tar condensation was done with a water cooled acetone container that the producer gas was bubbling through. The flow was measured by an orifues nozzle. Temperatures, pressures and filter pressure drop build-up were logged. The mass flow and filtration velocity were calculated in real time.

Summary of the up-scaled results

The results from the Güssing gasifier showed a filter efficiency above 99.98% while operating at 525°C. The results were in the same range compared to the small scale experiments and with other granular and ceramic high temperature filters.

The filter tests were conducted with a volume flow of 8 m^3/h (S.T.P) due to the needs of the SOFC-stack.

5.3.6 BioSOFC in hindsight

The complete setup was assembled in Güssing in the fall of 2007. The system design, including the gas cleaning, worked perfectly. Unfortunately an internal short-circuit in the SOFC made it impossible to reach the overall project goal.

5.4 Demonstration plant

Bjertnæs Sag AS is a company making wood panels. The company is located in Jevnaker in southern Norway. Wood chips from the production process are burned in a furnace. The heat from the furnace is sent through a district heating network and used on the plant and sold to nearby industry.

The 450 kW furnace has a fully automated controll system and was delivered by the danish company Danstoker in 2003. The furnace burns dried wood chips of Norwegian spruce or pine with heating values of 19839 kJ/kg and 19280 kJ/kg respectively. The wood chips are fed into the furnace through a screw feeder. The flue gas passes the heat exchanger in the top of the furnace before it enters the flue gas canal at 130^oC. Particles from the furnace are removed in a cyclone before the gas goes through a fan and out the chimney, as illustrated in figure 5.11.

The furnace is in operation throughout the year with the exception of a few weeks during the summer when the plant closes. The furnace operates on part load of between 30-40% during normal daytime operation in the winter months and between 10-15% during nights and weekends. The water temperatures for the district heating are controlling the furnace operation and the furnace enters sleeping mode when the yield drops below 20%. The variation in the furnace load influences the particle emission. The particle concentration between the fan and the chimney was between 0.15-0.17 g/m^3.

A summary of key parameters is given in table 5.4.

5.4.1 Purpose

The main purpose of the work done at Bjertnæs Sag AS was to reduce the particle emission out of the chimney. The particle reduction was achieved by designing, building and testing an upscaled PBF at NTNU. This included developing a new geometry for the release of the puffback pulse.

One PBF module was installed at Bjertnæs Sag in 2007. The results from the field tests were presented at the American Filtration and Separation Society

Furnace manefactoror	Danstoker
Fuel	Norwegian spurce and pine
Fuel water content	20-40%-vol
Output heat	450 kW
Maximum gas flow	750 Nm^3/hr
Temperature out	120-140 ^oC
Particle emmision during startup	0.3-0.35 g/m^3
Particle emmision during steady operation	0.15-0.17 g/m^3
Yearly operation	Approximate 300 days/year

Table 5.4: Technical data Bjertnæs Sag AS

conference, 19-22 May, 2008, Valley Forge, USA, and published in the conference proceedings (Chapter 11).

5.4.2 Setup

An isokinetic slipstream was taken from the flue gas duct between the fan and the chimney. One PBF module was placed in the filter housing and heated to 190 ^oC. The module consists of two gas entry surfaces, each with a frontal area of 0.75 m^2 (0.5 x 1.5 m). Each gas entry surface consists of 85 louvers giving the module a total frontal gas entry surface of 1.5 m^2 and 170 louvers.

Figure 5.12 illustrates the new geometry for puffback used on this module. The geometry is inspired from the pulse cleaning setup of fabric filter bags [79] and the final geometry design is the result of iterations through laboratory testing [97]. The final configuration is much less spacious compared to previous se-

Figure 5.11: Original flue gas layout from 2005

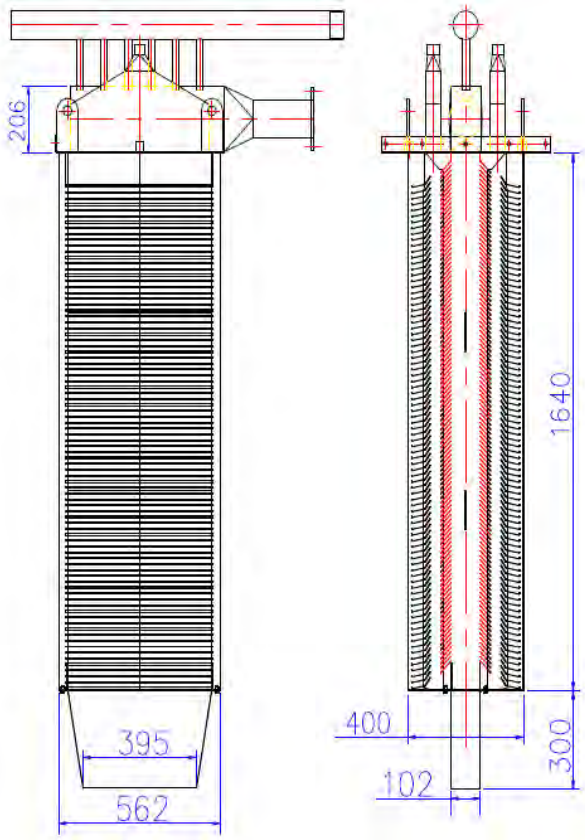

Figure 5.12: Bjertnæs filter module

tups [93] [109] [110].

After the filter, the gas flow was measured by a Micatrone MFS-C-100 flow sensor and regulated by a pneumatic valve controlled via LabVIEW. The gas was then sucked in through the fan and out through the chimney.

The filter cake was removed off-line. The filter cake and the granular material were fed through a star valve at the bottom of the filter house. The fly ash was then separated from the granular material in a drum sieve. The granular material was then pneumatically sent up to a reservoir over the filter as shown in figure 5.13. Figure 5.13 also shows the cyclone (1), pulse valve (2), star valve (3), sieve (4), pneumatic sender (5) and the furnace (6). The dust concentration was measured gravimetrically in the flue gas canal from the furnace, before the filter as well as in the clean gas duct after the filter.

Quartz sand was used in the demonstration plant in order to reduce the wear and tear of the star valve. the star valve was used to extract the bed material from the filter house and was made of cast iron. Using quartz significantly reduced the degradation of the star valve, but grinded a small fraction of the quartz sand that had to be extracted in the sieve.

The temperatures, the pressures, the volume flow and all the supporting equipment were logged and controlled using Compact FieldPoint. The interface was programmed in LabVIEW. Appendix E gives an overview of auxiliary components

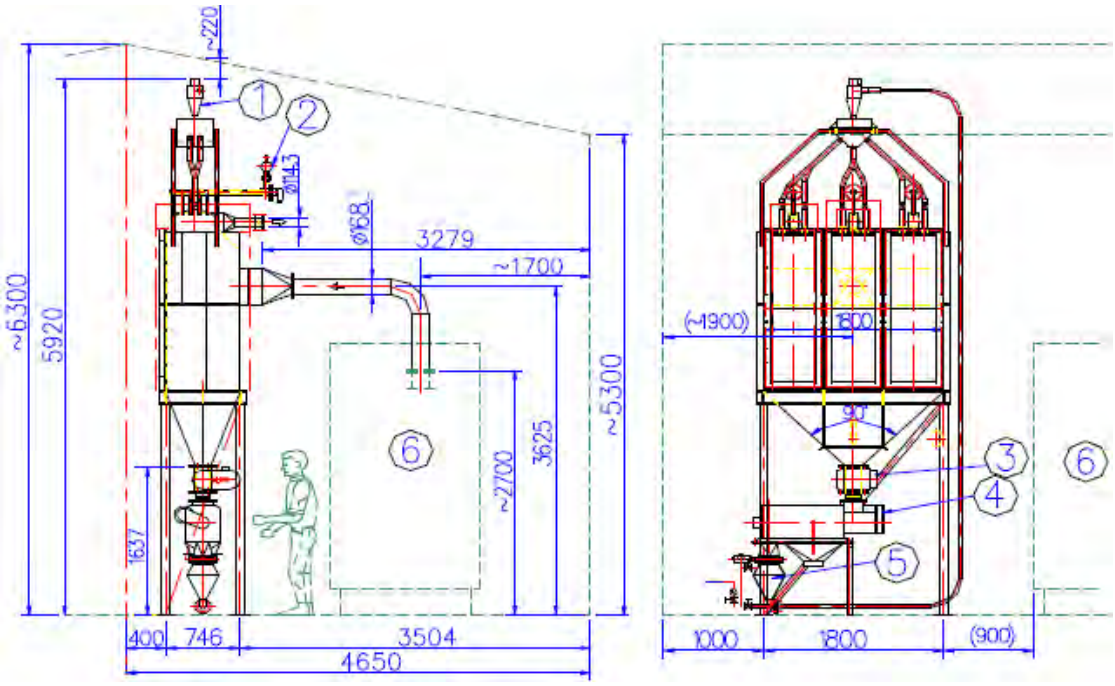

Figure 5.13: Sand return setup

and equipment.

5.4.3 Summary of demonstration plant results

Results from the field studies showed a reduction in the dust concentration from approximatly 170 mg/m^3 at the filter inlet to 3 mg/m^3 at the filter outlet, giving a filtration efficiency of 98.23%. The filtration experiments were done with a superficial face velocity of 7.85 cm/s. The operation of the furnace gave fluctuating gas conditions. Additional shutdowns due to fuel feeding problems eliminated the posibility of long time tests with steady gas conditions during these initial tests.

Further experiments are planned which include the implementation of three filter modules filtrating the entire gas flow from the furnace. The LabVIEW control program has to then be modified in order to regulate the fan according to the furnace conditions.

5.5 Summary of experimental studies

The experimental studies were part of the ongoing filter development done at NTNU in cooperation with professor Squires of the University if Technology in Virginia. This work has contributed to the experimental verification of the patented clames regarding the new filter tray louver design as well as the building and testing of two high temperature filters for particle removal from biomass gasification producer gas and the startup of a demonstration plant with a new compact puff-back geometry. The design fundamentals presented by Lee [73] [74], Risnes [110]

and Squires [131] were implemented in the construction of the new filters.

Several hours of testing have been done on the different experimental setups, both in the laboratory and on site at the final locations. The results show an overall high collection efficiency for each of the different Panel Bed Filter setups and have been presented individually in five papers.

- **Paper I** presents the setup and results of the laboratory study using the new filter tray louvers. The paper compares the results to those achieved by Risnes using L10-56 louvers and Wishbone louvers. The paper was presented at Cleantech 2008, 1 - 5 of June 2008 in Boston, USA, and reprinted in Chapter 7.

- **Paper II** presents the setup of the small scale high temperature experiments done in Güssing, Austria. The results are presented and the specific cake resistance values are compared to high temperature results found in the literature. The paper is published in the Journal of Hazardous materials and reprinted in Chapter 8.

- **Paper III** describes the setup and laboratory testing of the equipment used in the BioSOFC project. The paper was presented at the 2007 ASME International Mechanical Engineering Congress and Exposition, 11-15 November in Seattle, USA, and reprinted in Chapter 9

- **Paper IV** presents the setup of the scaled-up high temperature experiments done in Güssing, Austria. The results including a comparison of the results from the two high temperature filters and to results from high temperature filtration experiments found in the literature are presented. The paper was presented at the 10th World Filtration Congress in Leipzig, Germany, 14 - 18 of April, 2008 and reprinted in Chapter 10.

- **Paper V** describes the demonstration plant setup and full scale experimental results. The paper was presented at the American Filtration and Separation Annual Conference in Valley Forge, USA, 19-22 May, 2008 and reprinted in Chapter 11

5.5.1 Comparison of results

Table 5.5 gives an overview of the design criteria of the different filters used in the experimental work. The filter modules were designed for Sintered Bauxite alumina spheres which have a narrower particle size distribution and a lower angle of repose than the quartz sand. The vertical distance between the L10-56 louvers was reduced with 2 mm from the design of Risnes in the scaled up filter in order to compensate for the reduced angle of repose of the alumina spheres.

The small filter modules did not have any size constrains and horizontal puffbacks were therefore used. The results from the horizontal puffback calibration were congruent with Risnes' impulse theory [110] (Chapter 4.3.2). Vertical puffbacks were used for the large filter modules and the results from from the vertical puffback calibration supported Lees' active time theory [73] (Chapter 4.3.2). The

	Laboratory	**Prototype**		**Demonstration plant**
		Small scale	**Up scaled**	
Flow rate				
- design		1 m^3/h	8.5 m^3/h [a]	250 m^3/h
- maximum	12 m^3/h	2 m^3/h	20 m^3/h [b]	375 m^3/h
Granular material	SB 20/40	SB 20/40	SB 20/40	Olivin ASF30 [c]
Louver design	Filter trays	L10-56	L10-56	L10-56
Puffback direction	Horizontal	Horizontal	Vertical [d]	Vertical [d]

a Continuous operation
b Discontinuous operation
c Tested with SB 20/40 and AFS30 in the laboratory
d Compact puffback geometry

Table 5.5: Overview of filter design parameters

filter module used in the demonstration plant was tested with both alumina spheres and quartz sand in the laboratory [97].

Figure 5.14 compares the results from the high temperature filtration on biomass gasification gas with the L10-56 louver to those obtained by Risnes [110] and Nos [93]. The experiments have been conducted with different gas composition, bed materials, dust materials, dust concentration and temperatures. The figure

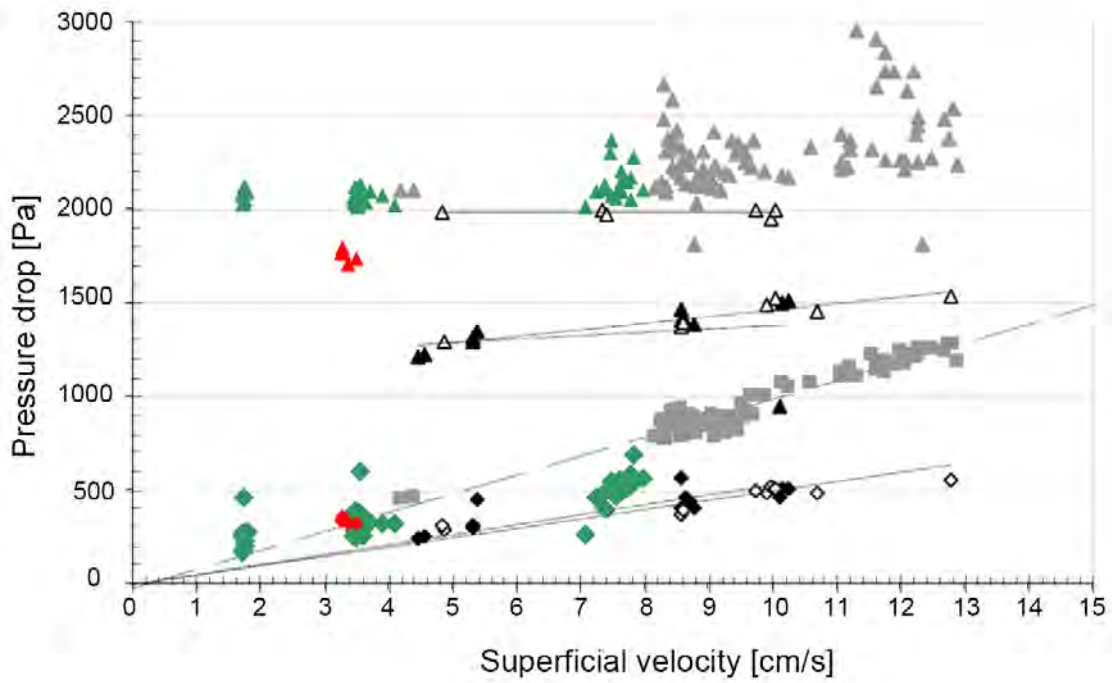

Figure 5.14: Maximum pressure drop (triangles) and residual pressure drop (rectangular) vs superficial velocity; Results from the present study (Green - small HT PBF and red - up scaled HT PBF) compared to those obtained by Rinsnes [110] (black - Wishbone. open - L10-56, gray - Folla [109])

illustrates the residual pressure reduction of the L10-56 louvers compared to the R2 louvers used at Folla. The reduction in residual pressure can allow for longer filtration cycles as described in chapter 4.2. The figure further show that the residual pressure from the high temperature filtration with the L10-56 louvers are in the same range as those obtained from Risnes [110] with the same louvers.

The results from the high temperature filtration of biomass gasification gas further showed that the tar in the producer gas did not condense, influence the dust filtration, or the filter cleaning. Furthermore, the low residual pressure drop and high collection efficiency above 99.98% make the Panel Bed Filter competitive to the rigid media filters that are comercially available for the high temperature applications as described in chapter 4.4. The differences in the K_2^* values in the small scale filter are assumed to be due to the change in cyclone efficiency with the velocity. The cyclone has a cut size of 1.72 μm with an efficiency of 96% with 1 m^3/h. The inlet dust concentration to the filter was measured before installing the filter and was fluctuating between 2-3 g/m^3 depending on the gasifier operation with an average of 2.71 g/m^3. The gas composition with the high temperature and vaporous tar concentration made particle sizing difficult. The inlet dust concentration is therefore assumed to constantly be 2.71 g/m^3 throughout the experiments. This assumption does not take into consideration the lower cyclone efficiency at lower flow rates. The reduction in velocity at a flow rate of 0.5 m^3/h and the reduced cyclone efficiency will increase the K_2^* as can be seen in figure 5.15. The specific cake resistance values are in the upper range compared to those obtained from literature as described in **Paper II**.

The new cyclone and sampling line built for the scaled-up high temperature filtration tests gave a specific cake resistance value of 0.9 - 2.1 $\cdot$ 10^{-6} s^{-1}. This lower value is assumed to be due to settling of core particles in the filter housing

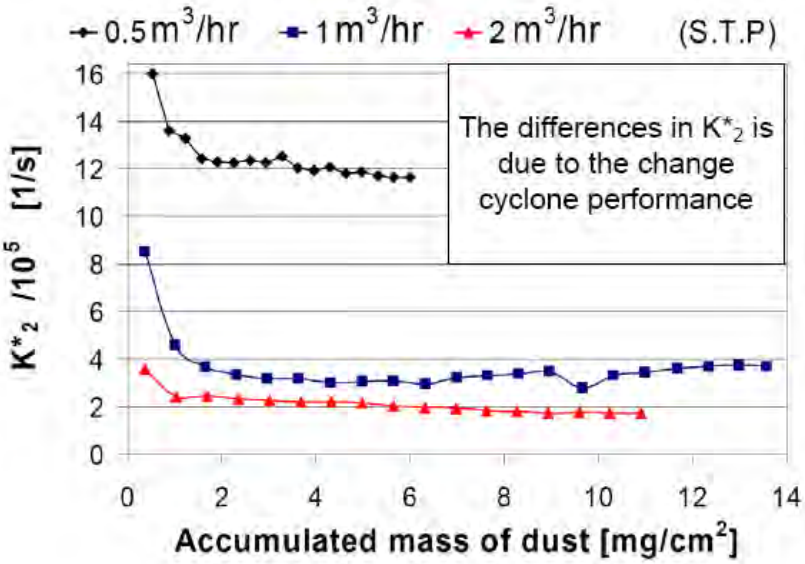

Figure 5.15: Specific cake values obtained for the small scale filter

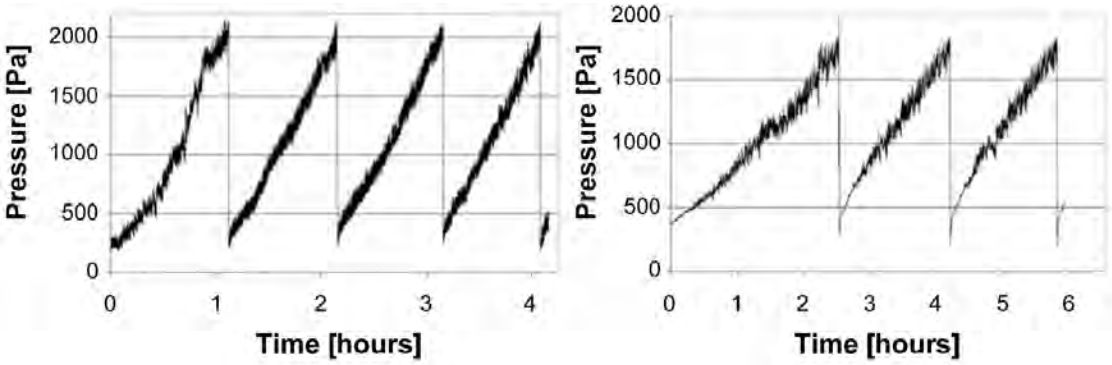

Figure 5.16: Pressure buildup; Left: small scale filter with an average filtration velocity of 3.72 cm/s, Right: scaled-up filter with an average filtration velocity of 3.56 cm/s

before entering the filter.

The average dust concentration where measured gravimetrically for both high temperature filters. The measurements were done with a heated total filter to avoid tar condensation. The average concentration does not count for the fluctuating conditions in the gasifier during the experiments.

Figure 5.16 compares the pressure buildup from the small scale and the scaled-up filters. The figure shows the classical linear pressure buildup as a function of superficial flow velocity associated with cake filtration. The longer time interval between cleaning cycles for the scaled-up filter is assumed to be due to particle settling in the filter housing.

Figure 5.17 compares the residual pressure from the experimental study of the

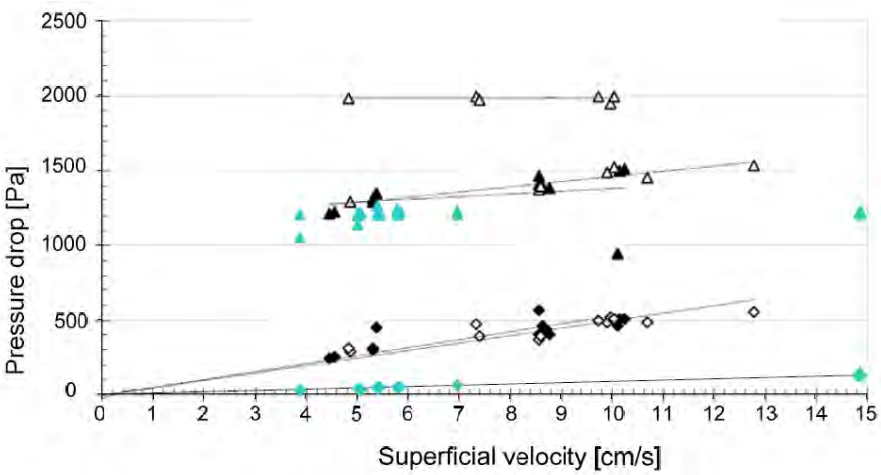

Figure 5.17: Maximum pressure drop (triangles) and residual pressure drop (rectangular) vs superficial velocity; Results from the present study (blue - filter trays) compared to those obtained by Rinsnes [110] (black - Wishbone, open - L10-56)

filter tray design to the results obtained by Risnes using the wishbone and L10-56 louver design [110]. The shallow bed of the filter tray design significantly reduces the residual pressure. The cycle time of the new filter trays was approximately doubled compared to those of the L10-56 louvers and further six times longer than the wishbone louver as described in **paper I**. The increased cycle time will increase the overall efficiency since the panel bed filter has the highest particle penetration immediately after the puffback as described in chapter 4.3.

Alumina spheres were used instead of quartz sand as granular material in the filter tray experiments which allowed for using a meshed grid without the clogging problem experienced in earlier designs [137]. The meshed grid acted as a fixed boundary of the bed which allowed higher filtration velocities of up to 14.8 cm/s with a collection efficiency of 99.979%.

Figure 5.18 compares the specific cake resistance from the experimental testing of the new filter tray design to the results of Risnes using the L10-56 lovers [110]. The figure shows that specific cake resistance values are in the lower range of those obtained by Risnes [110] using the same test dust (SAE-fine, appendix A).

The experimental study of the filter tray louver focused on the louver design. The emphasis on louver design made us prioritize easy access to the louvers over optimizing the louver setup for maximizing the ratio of gas entry surface to projected vertical area of the filter. The ratio of gas entry surface to projected vertical

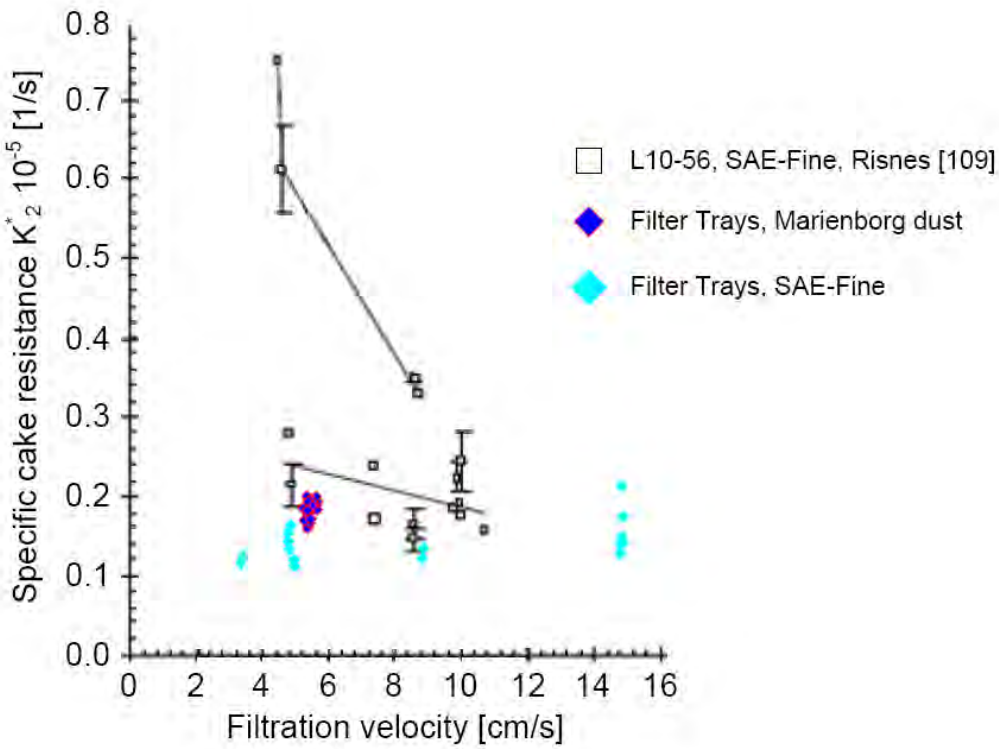

Figure 5.18: Comparison of specific cake values obtained in the laboratory to those of Risnes [110]

area of the experimental setup was 0.99, or an increase compared to the Wishbone louvers of 186.8%. The ratio of gas entry surface to projected vertical area of the experimental setup can be increased by approximately a factor of 2 by removing the adjustable plate in the clean gas volume and optimizing the distance between the louvers. The ratio of gas entry surface to projected vertical area would then be approximately equal to the L10-56 louver [131], but with a significantly lower residual pressure drop.

The demonstration plant visualized the possibility of continuous operation with regeneration and recirculation of the bed material as described in **paper V**. The new geometry of the puffback cleaning pulse were built and tested in the laboratory at NTNU [97]. Figure 5.19 shows the new compact puffback design which reduces the filters total height with approximately 1000 mm (a reduction of the puffback geometry hight of approximately 70%) compared to the Folla design [114].

The furnace was operated on part load during the test period which significantly reduced the volume flow from the furnace. Low dust concentration and shutdowns both at night and several unexpected shutdowns due to ice blocking in the biomass feeding system made continuous testing impossible. Additional vibration problems from the compressor caused initial stability problems in the filter bed. The compressor problems were minimized by moving the compressor and the vibration were reduced by use of insulation. The plant was operated with quartz sand. The fine fraction of the quartz sand was sieved out before being pneumatically transported into the filter reservoir. The pneumatic transport might have broken some of the quartz particles into smaller size pieces, which again could be fluidized in the back louver and go out with the gas. This might have lead to the lower collection efficiency of 98.23% compared to the other panel bed filters tested.

Table 5.6 summarizes the results from the experimental study.

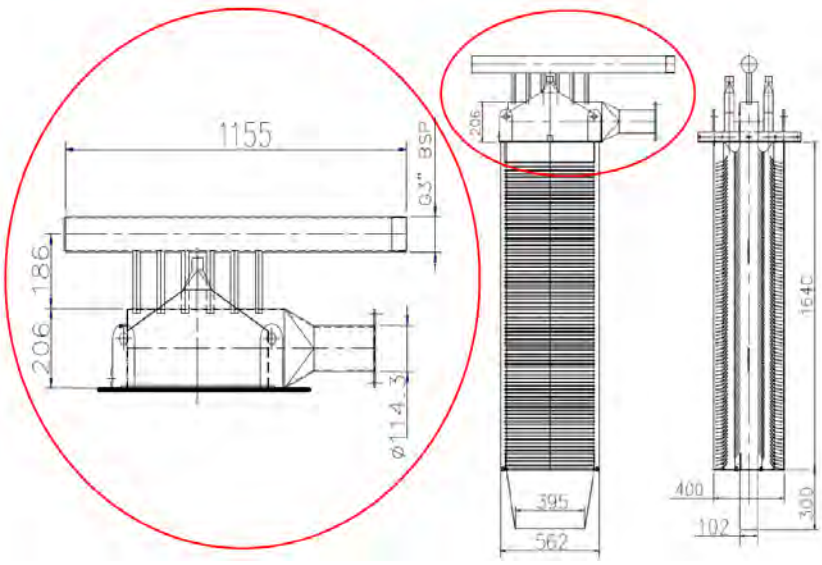

Figure 5.19: New puffback geometry used at the demonstration plant

Filter size	**Laboratory**	**Prototype**	**Demonstration plant**
Publication	**Paper I**	**Paper II - III - IV**	**Paper V**
Purpose of investigation	Increase the filter surface area per louver and increase the filtration velocity	Develop a system to clean the producer gas from the biomass gasifier in Güssing, Austria at 500°C	Decrease the size of the puffback geometry and designing, building and testing the demonstration plant
Type of gas	Air	Producer gas from biomass gasification	Flue gas from biomass combustion
Type of dust	Standard dust	Ash	Ash
Temperature	Ambient	500-550°C	190°C
Filtration velocity	3.85-14.8 cm/s	2-8 cm/s	2-4 cm/s
Collection efficiency	> 99.071	> 99.98	> 98.23

Table 5.6: Summary of results

Chapter 6

Conclusions and further work

"We cannot solve our problems with the same thinking we used when we created them"

Albert Einstein (1879-1955)
Scientist

6.1 Conclusions

The work described in this thesis has been focused on the evaluation and further development of the panel bed filter. A review of earlier work performed on the panel bed filter has been done as part of defining the status of the panel bed filter. In addition, the classification and thermo chemical conversion of biomass has been briefly reviewed since the field experiments were conducted on slipstreams from biomass gasification and combustion plants. The experimental section covers laboratory studies, prototype studies as well as industrial scale experiments. The laboratory study covers a new louver design, the prototype study cover high temperature filtration and the demonstration plant study cover a new puffback geometry as well as the startup and the running of the first experimental series of a commercial plant.

Laboratory study

A panel bed filter with filter tray louvers was built and tested in the laboratory using Sintered Bauxite as bed material. The filter was tested with different filtration velocities (3.85 - 14.8 cm/s) and dust concentrations (3.53 - 7.01 g/m^3). The experimental study showed a high collection efficiency (99.78%) with a significantly reduced residual pressure after puffback compared the results of L10-56 louvers obtained by Risnes [110]. The lowered residual pressure allows the filter tray design to operate with filtration cycles which are twice as long compared to the L10-56 louvers using the identical dust material and concentrations.
The potential for optimizing the clean gas louver design is an increase of the ratio of the surface area to the projected frontal area from 0.99 to 2, thereby doubling

the time between the filtration cycles.

Prototype study

The two filters in the prototype study used Sintered Bauxite to remove the particles at above 500°C from a slipstream of the biomass gasification plant in Güssing, Austria. The small filter was tested with a filtration velocity of 2 - 8 cm/s (0.5 to 2 Nm^3/h) with a collection efficiency above 99.995%. The upscaled filter was tested with a filtration velocity of 3.3 - 3.7 cm/s (8 Nm^3/h) with a collection efficiency above 99.98%.
Both filters showed dust cake formation on the granular surfaces. The filters were exposed to a high tar concentration of 1-2 g/m^3 in the producer gas. The results showed a high filter efficiency with a relatively low pressure drop over the filter competitive with those of bag filters even with the considerably higher filtration velocities achieved with the panel bed filter. Furthermore, the tars in the producer gas did not condense in the filter or influence the dust removal in any way.

Demonstration plant study

The panel bed filter for the demonstration plant was designed for three parallel filter modules in one housing, each designed for a normal load of 250 Nm^3/h (maximum flow of 375 Nm^3/h). A new puffback geometry was developed through experimental iteration in the laboratory. The new puffback geometry was implemented in the demonstration plant together with the possibility for regeneration and recirculation of the quartz sand used as bed material.
The experimental on-site testing at Jevnaker, Norway, gave an average collection efficiency of 98.23%. The new puffback geometry worked as expected and reduced the total height of the filter with approximately 1 meter (a reduction of the puffback geometry hight of approximately 70%) compared to the earlier designs. The on-site testing showed that the control system programmed in LabVIEW worked as expected and allowed for long time continuous testing. Unfortunately, low dust concentrations from the furnace, fuel icing problems and part loading due to the mild winter made long time testing impossible.
The demonstration plant shows an example of a complete panel bed filter setup. Comparing this setup to Folla [93] shows a reduction in total volume due to the new puffback geometry and the use of L10-56 louvers instead of the Folla-louvers (chapter 4.2).

Overall conclusions

Through extensive experimental testing and optimization, the panel bed filter have shown an overall high collection efficiency for the different working conditions. The capacity to handle velocity changes in the impinging gas combined with the possibility of high temperature gas cleaning make the panel bed filter a promising alternative to the current commercial high temperature filters. An implementation of the new filter tray louver design as well as new puffback geometry both

increase the filtration speed and decrease the total size of the panel bed filter which would make the panel bed filter more compact and cost effective and thus more attractive to the commercial market.

6.2 Recommendations for further work

The longest test done as part of this work lasted less than 45 hours. More experimental data is therefore needed in order to evaluate the long term efficiency of the panel bed filter. A continuation of the experimental investigation should therefore aim for continuous sampling for preferably more than 1000 cycles in order to see the long time particle penetration.

New louver design

The filter tray design has shown the capability to operate with velocities up to 14.8 cm/s with a low residual pressure. However, the filter trays have not been optimized with the intention of maximizing the bed surface area to projected frontal area. An optimization study should include a numerical investigation with an experimental verification. The optimization study should also aim for a vertical puffback in order to further reduce the footprint of the filter. The new and improved louver design should then be used in future rigs for high temperature applications and in future demonstration plants.

High temperature applications

The operation temperature of the H_2S sorbent reactor was the limiting factor during the high temperature study. Removing the H_2S sorbent reactor will allow the filter to operate at higher temperatures. A combined theoretical and experimental investigation could be focusing on the potential for using the panel bed filter to remove the dust from the flue gas before the heat exchanger in a commercial fluidized bed gasifier. Theoretically, the filter would then strongly reduce the fowling of the heat exchanger which would improve the efficiency and reduce the maintenance cost of the plant.

Demonstration plant

A natural continuation of this work would be to install all three filter modules. Bypassing the existing as well as modifying the LabVIEW control program to regulate the filter fan according to the furnace conditions would allow for filtration of the entire volume flow of the flue gas.

Chapter 7

Paper I

Experimental Investigation of a New Granular Filter Design

Presented and published in proceedings of:

Clean Technology 2008
Boston, USA, June 1-5, 2008

Daniel Stanghelle, Johan Hustad and Otto K. Sønju

Department of Energy and Process Engineering
Norwegian University of Science and Technology, Trondheim, Norway

Is not included due to copyright

Chapter 8

Paper II

Granular Bed Filtration of High Temperature Biomass Gasification Gas

Published in:

Journal of Hazardous Materials
2007, Vol 144, pp 668-672

Daniel Stanghelle[a], Torbjørn Slungaard[b], and Otto K. Sønju[a]

[a] *Department of Energy and Process Engineering*
Norwegian University of Science and Technology, Trondheim, Norway
[b] *Vetco Aibel A/S, Stjørdal, Norway*

Is not included due to copyright

Chapter 9

Paper III

A 5 kW$_{el}$ Solid Oxide Fuel Cell stack operating on biomass gasification producer gas system design and results

Presented and published in proceedings of:

2007 ASME International Mechanical Engineering Congress Exposition
Seattle, USA, November 11-15, 2007

Daniel Stanghelle, Arnstein Norheim, Øyvind Skreiberg,
Johan Hustad and Otto K. Sønju

Department of Energy and Process Engineering
Norwegian University of Science and Technology, Trondheim, Norway

Is not included due to copyright

Chapter 10

Paper IV

High temperature granular bed filtration of biomass gasification gas

Presented and published in proceedings of:

10th World Filtration Congress
Leipzig, Germany, April 14-18, 2008

Daniel Stanghelle, Arnstein Norheim, Johan Hustad and Otto K. Sønju

Department of Energy and Process Engineering
Norwegian University of Science and Technology, Trondheim, Norway

Is not included due to copyright

Chapter 11

Paper V

Granular filtration of biomass combustion flue gases

Presented and published in proceedings of:

American Filtration and Separation Society
Valley Forge, USA, May 19-22, 2008

Daniel Stanghelle, Johan Hustad and Otto K. Sønju

Department of Energy and Process Engineering
Norwegian University of Science and Technology, Trondheim, Norway

Is not included due to copyright

Appendix A

Filter material and test dust

A.1 Filter material

A.1.1 Sintered Bauxite 20/40

The Sintered Bauxite was purchased from Saint-Globain Proppants, Fort Smith, Arkansas, USA.
Median particle diameter = 0.662 mm
Shape/Spericicity (Krubein & Sloss) = 0.9

Chemical name	**Common name**	**% By weight**
Aluminum silicate	Mullite	15 - 35
Aluminum oxide	Corundum	65 - 85

Physical properties

Bulk density	2.04 g/cc 127 lbs/ft^3	
Specific gravity	3.5 g/cc	
Absolute volume	0.0347 gal/ib	
Acid solubility, %	1.9	
Crush Resistance @ Stress %	7 500 psi 10 000 psi 12 500 psi 15 000 psi	0.5 1.2 2.2 4.0

Size

Sieve No.	% Retained
20	5
30	75
40	20
<40	Trace

A.1.2 Olivin AFS30

Olivin quarts sand was purchased from North Cape Minerals.

CHEMICAL COMPOSITION

MgO	49,9	%
SiO_2	41,5	%
Fe_2O_3	7,2	%
Cr_2O_3	0,32	%
Al_2O_3	0,44	%
NiO	0,32	%
MnO	0,09	%
CaO	0,09	%
Na_2O	0,01	%
K_2O	0,02	%

PHYSICAL PROPERTIES

Bulk density	1700 - 1900 kg/m³
Specific gravity	3200 - 3300 kg/m³
Hardness	6,5 - 7,0 Moh's scale
Colour	Greenish grey
Melting point	Approx. 1760 °C
Initial sintering	Approx. 1450 °C
Angle of repose	Approx. 45 °
Stowage factor	0,54 m³/t (19 ft³/t)

MINERALOGICAL COMPOSITION

Forsterite	Mg_2SiO_4	93 %
Fayalite	Fe_2SiO_4	7 %

The chemical and physical data are expected average figures at loading at the company port. They are given in good faith but without guarantee. All chemical analyses are in dry state. Oxides are not indication of the phases present, only conventional representation of elements.

PARTICLE SIZE DISTRIBUTION

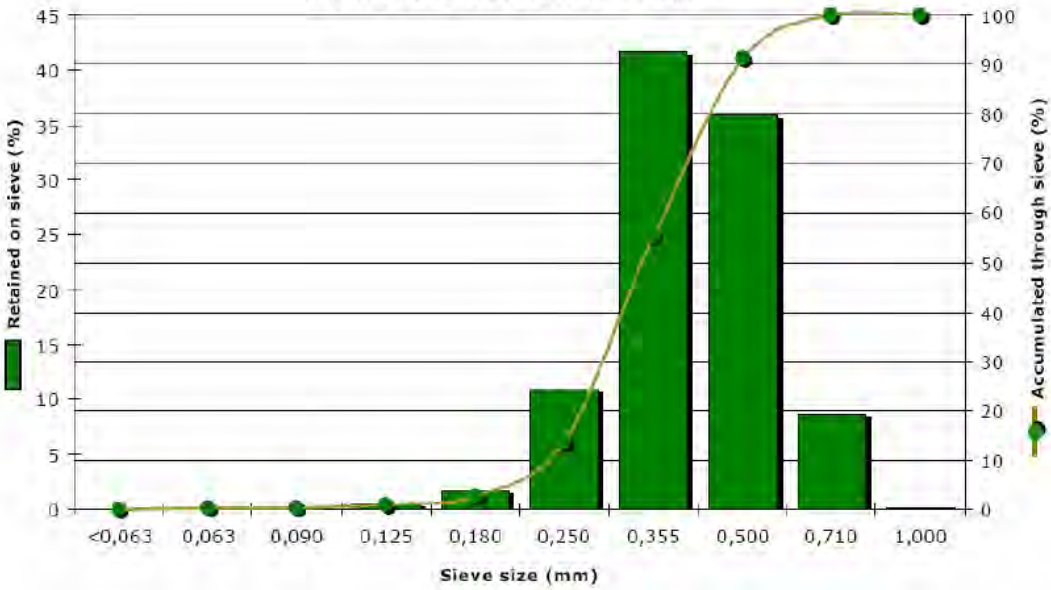

A.2 Test dust

A.2.1 SAE-fine test dust

The SAE-fine test dust was bought from Ellis Components, Derbyshire, England. Product name = ISO 12103-1

Component	% By weight
SiO_2	68 - 76
Al_2O_3	10-15

Size and physical properties[a]

Particle size measurements[b]	
$dp_{50,3}$	12.6 μm
$dp_{95,3}$	41.1 μm
Particle size information from supplier [c]	
$dp_{50,3}$	9 μm
Loose bulk density, dry	677 kg/m^3
Compact bulk density, dry	1053 kg/m^3

a Measurements completed and reported by Risnes [110]
b Malvern analysis, particles suspended in water
c Coulter(R) Multisizer

A.2.2 Marienborg dust

The Marienborg test dust was sampled from the bag filters at the Marienborg combustion plant in Trondheim. The plant burns woody materials to provide heat to the district heating system in Trondheim. The sampled dust was taken from the last bag filters used to remove the fine dust located downstream from the cyclone and core bag filters. The fly ash particles mainly consist of carbon and a Malvern analyzer was used to get the particle size distribution. The dust size analysis was done by SINTEF Materials and Chemistry.

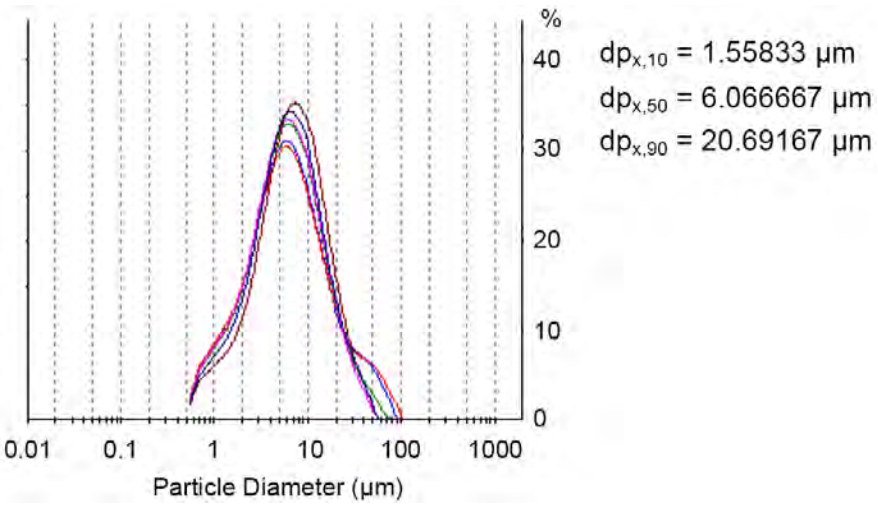

Figure A.1: Marienborg dust size distribution

Appendix B

Overview of work done at NTNU

Name	**Year**	**Title**
Claus Heen	Spring 1980	Sandfilter for røykgassrensing
S. Berg	Fall 1980	Utvikling av sand-filter for rensing av avgass ved høy temperatur
Njål Dvergsdal Einar Høydal	Spring 1982	Rensing av høytemperatur røykgass
Njål Dvergsdal Einar Høydal	Fall 1982	Høytemperatur sandfilter - Utprøving av modul II
Arnfinn Øverås	Spring 1983	Partikkelbevegelser i røykgass
Karstein Fallmyr Arild Haugene Terje Skog	Spring 1983	Utvikling av et sandfilter for rensing av høytemperatur røykgass
Karstein Fallmyr Arild Haugene Terje Skog	Fall 1983	Sandfilter for rensing av høytemperatur røykgass - Forsøk med FeSi-støv
Tom Engebretsen	Spring 1984	Sandfilter for rensing av høytemperatur røykgass -Laboratorieforsøk med FeSi-støv
Claus Heen	Fall 1984	Panel bed filter development for high temperature gas cleaning
Tom Engebretsen	Fall 1984	Sandfilter for rensing av høytemperatur røykgass - feltforsøk med FeSi støv og flyveaske fra kullforbrenning

Name	**Year**	**Title**
Olav R. Stadaas	Spring 1985	Videreutvikling av sandfilter for rensing av høytemperatur røykgass
Olav Stadaas	Fall 1985	Sandfilter for rensing av høytemperatur røykgass laboratorieforsøk og simulering
Espen Hope Kverna	Fall 1986	Sandfilter for rensing av høytemperatur røykgass - Design og planlegging av modul 4
Terje Rafdal	Fall 1991	Videreutvikling av panelbedfilter for rensing av høytemperatur røykgass
Terje Rafdal	Fall 1992	Panelbedfilter - Klargjøring modul 4
Hilde Pettersen	Spring 1993	Panelbedfilter - Forsøk med varm gass
Øivin Saanum	Spring 1996	Videreutvikling av panelbedfilter for rensing av høytemperatur røykgass
Nils Vang	Fall 1996	Utvikling av panel bed filter Delrapport 1
Torbjørn Selanger	Summer 1997	Utprøving av nye louvergeometrier på panel bed filter
Andew Stronach	Summer 1998	Panel Bed Filter - Industrial gas cleaning
Øyvind Rudberg	Summer 1999	Delrapport 1 og 2
Håvar Risnes	Fall 1999	Status report - The panel bed filter
Håvar Risnes	Fall 1999	Evaluering av ovn til PBF
Håvar Risnes	Fall 1999	Delrapport 3
Håvar Risnes	Fall 1999	Delrapport 4
Øyvind Rudberg	Fall 2000	Theoretical and experimental investigation of a granular filter coupled to a biomass gasifier
Roar Botnevik	Spring 2002	Theoretical and experimental investigation of gas cleaning with a granular filter. Emphasis on the removal of particle and gaseous impurities from combustion and gasification processes
Håvar Risnes	Fall 2002	High temperature filtration in biomass combustion and gasification processes
Daniel Stanghelle	Fall 2003	Gassrensing med granulært filter for høytemperatur anvendelser
Daniel Stanghelle	Spring 2004	Gassrensing med granulært filter for høytemperatur anvendelser
Magnus Paulsen	Fall 2005	Gassrensing med granulært filter
Magnus Paulsen	Spring 2006	Gassrensing med granulært filter
Ingunn Roald Natvig	Fall 2006	Gassrensing med granulært filter for høytemperatur anvendelser
Ingunn Roald Natvig	Spring 2007	Gassrensing med granulært filter
Ronny Schimpke	Spring 2008	Experimental development of louver designs for Panel Bed Filtration

Appendix C

New louver design

C.1 Equipment and setup

The filter trays in the laboratory scale panel bed filter are shown in figure C.1 and figure C.2. The filter trays upper angle of 30° was experimentally found to be working for Sintered Bauxite 20/40. Figure C.3 shows the inlet cone that was built of Lexan to allow the louvers to be visually observed during operation. Figure C.4 shows the outlet cone as well as the double pipe used for the puffback (the puffback pulse comes from below as shown in figure C.5). Figure C.5 shows the puffback calibration setup and figure C.6 shows the correlation between spill, tank pressure and valve opening time. The calibration showed a uniform spill and a tank pressure and valve opening time of 1 bar and 148 ms was chosen for the experiments. Figure C.7 shows the experimental setup.

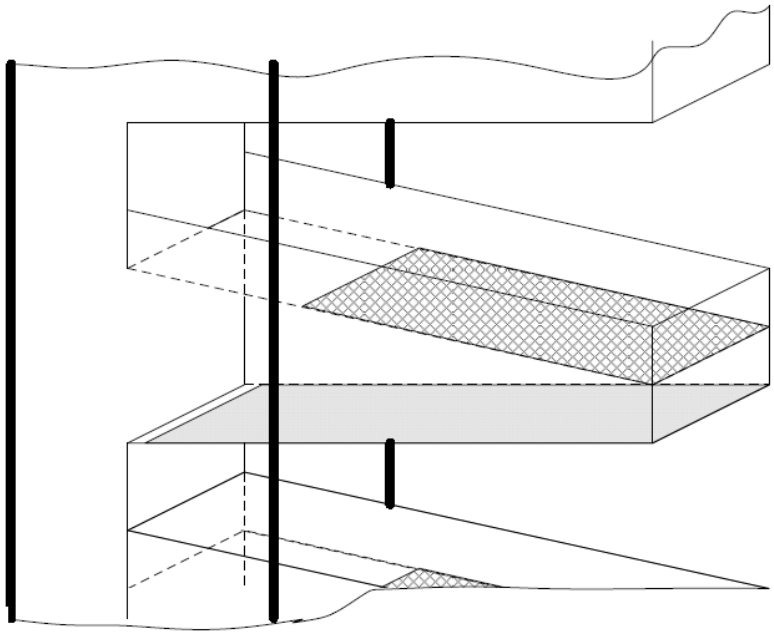

Figure C.1: Filter tray design

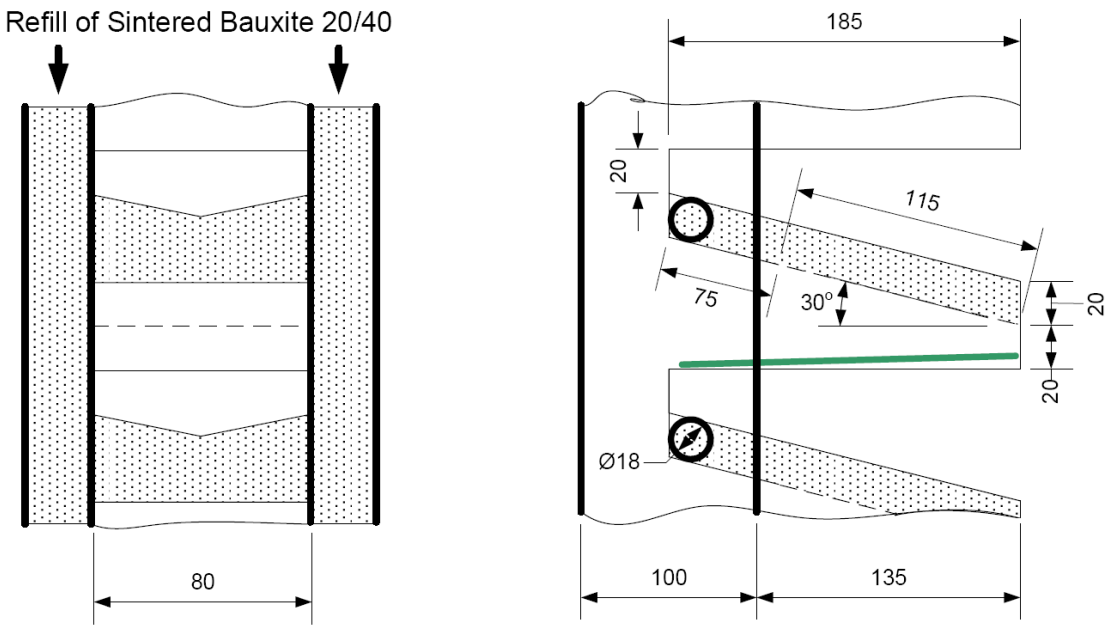

Figure C.2: Filter tray design

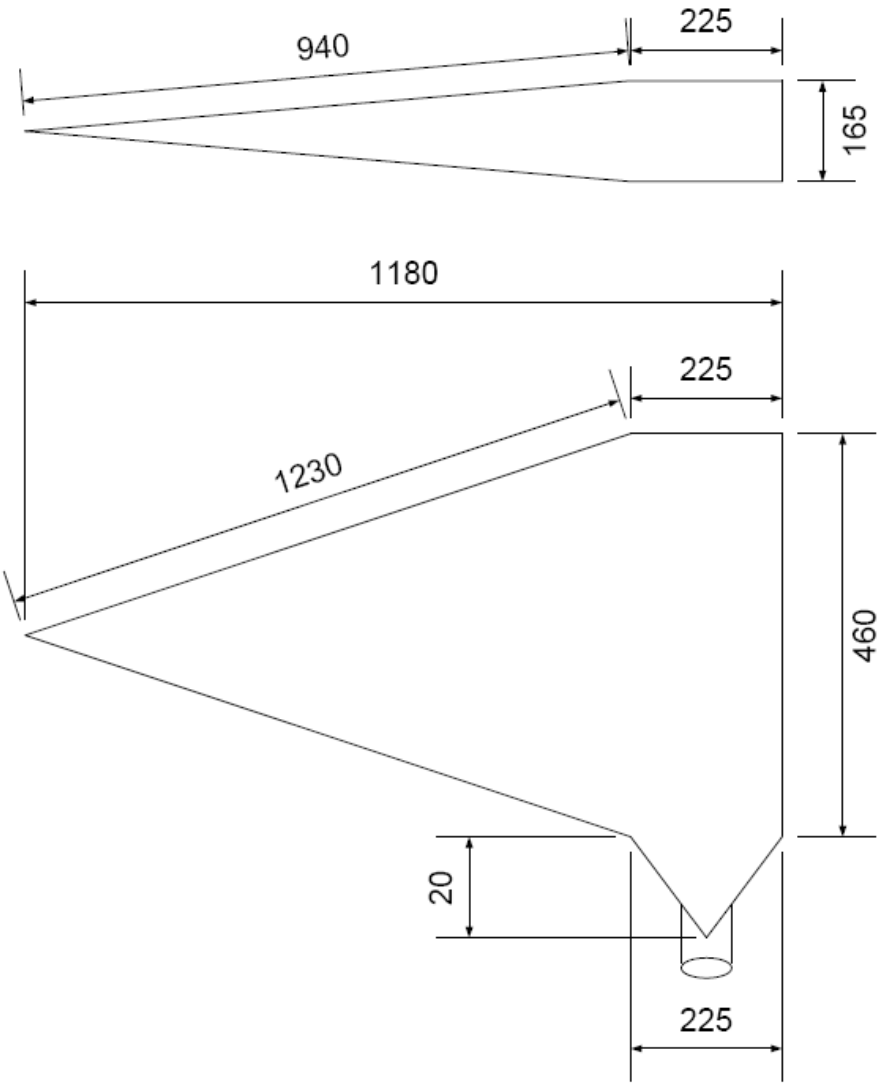

Figure C.3: Filter inlet cone

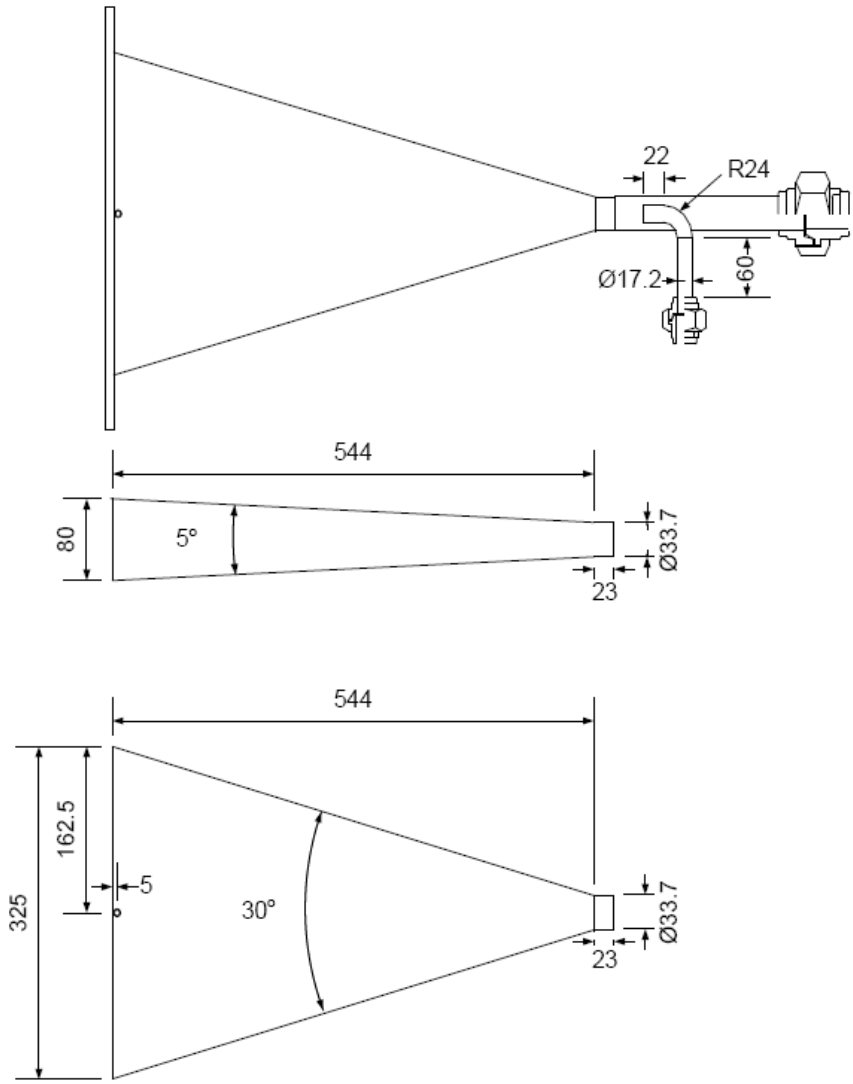

Figure C.4: Filter outlet cone

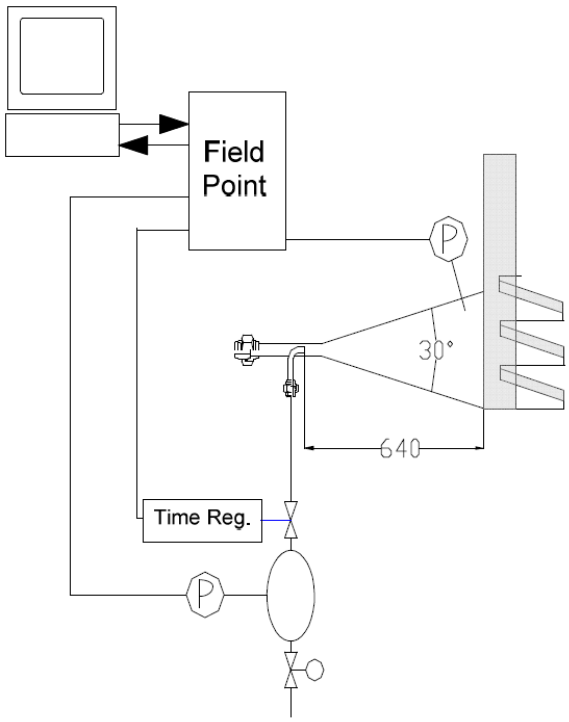

Figure C.5: Puffback calibration setup

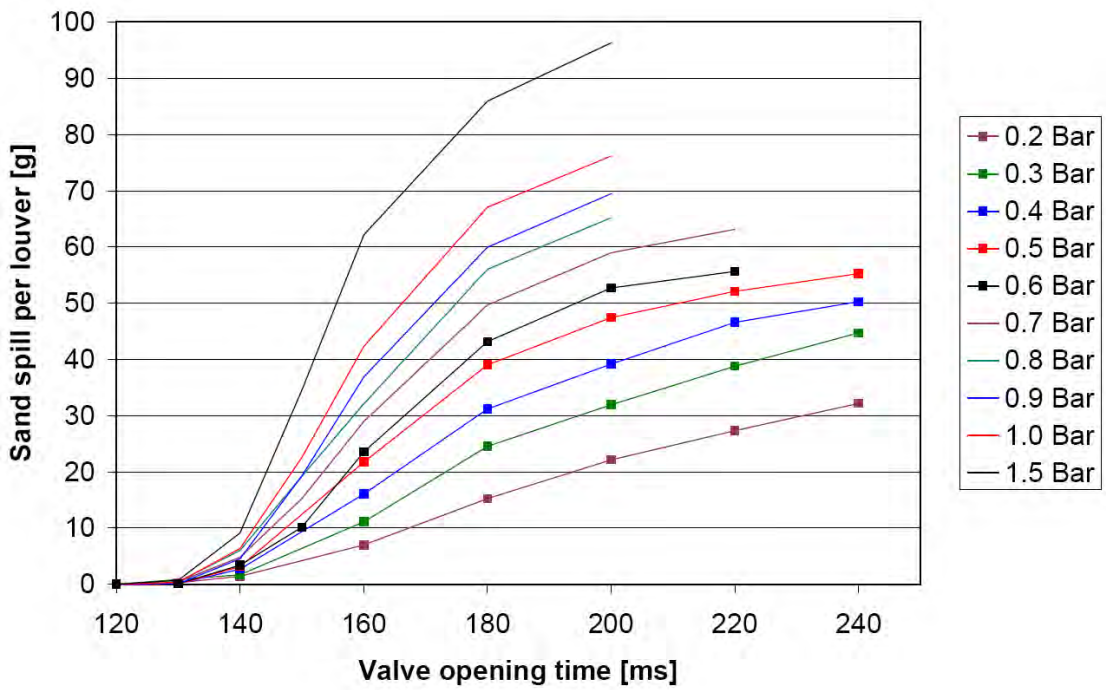

Figure C.6: Filter tray calibration curve

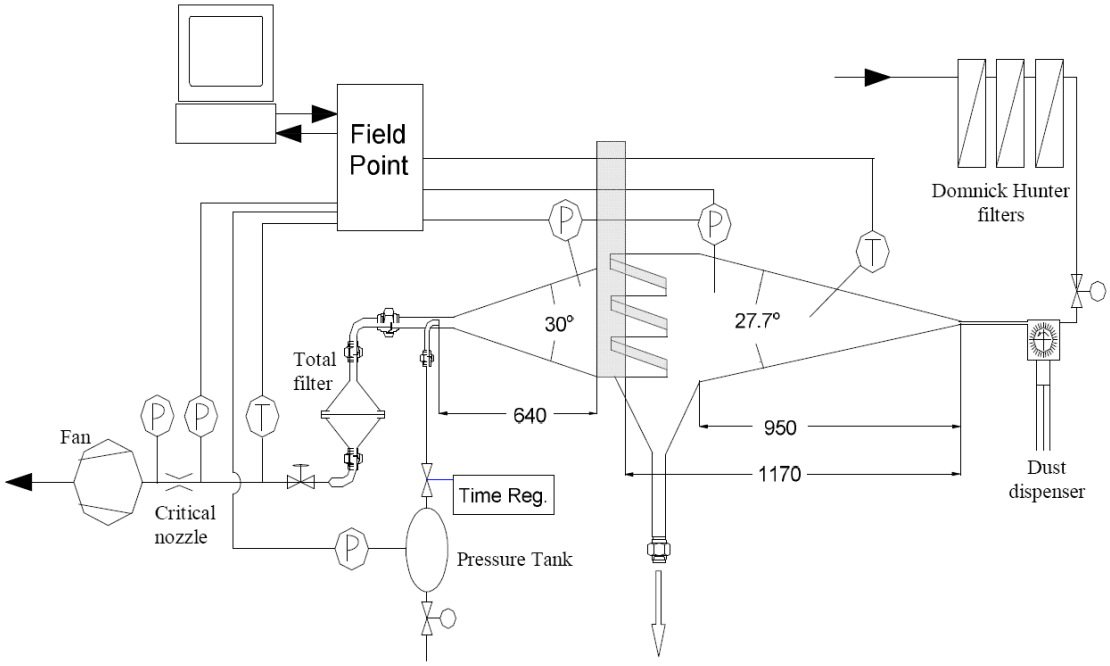

Figure C.7: Filter tray experimental setup

C.2 Results

Test #	Dust	Filtration velocity Actual [cm/s]	Filtration velocity Superficial [cm/s]	Concentration in [g/m^3]	Concentration out [mg/m^3]	Efficiency	Figure
# 1	SAE	5.03	5.07	6.87	14.6[a]	99.786[a]	C.8
# 2	SAE	4.97	5.01	5.72	2.78	99.951	C.9
# 3	SAE	4.99	5.03	3.53	<0.05	>99.999	C.10
# 4	SAE	3.85	3.87	7.01	<0.05	>99.999	C.11
# 5	SAE	6.92	6.98	5.58	4.09	99.927	C.12
# 6	MB	5.76	5.81	4.86	45.15[b]	99.071[b]	C.13
# 7	MB	5.38	5.43	5.33	<0.05	>99.999	C.14
# 8	SAE	14.8	14.9	5.42	1.16	99.979	C.15

a) Started filtration without filter cake roots (clean bed)
b) Problem with the refilling of Sintered Bauxite

Table C.1: Overview of laboratory studies

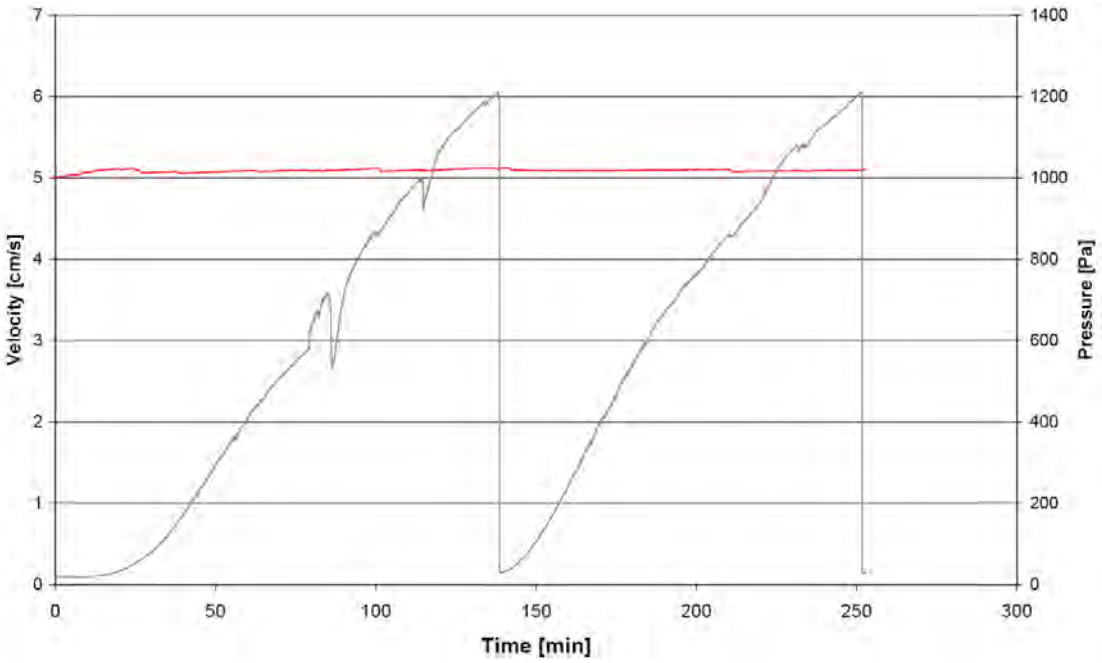

Figure C.8: Filter tray test #1

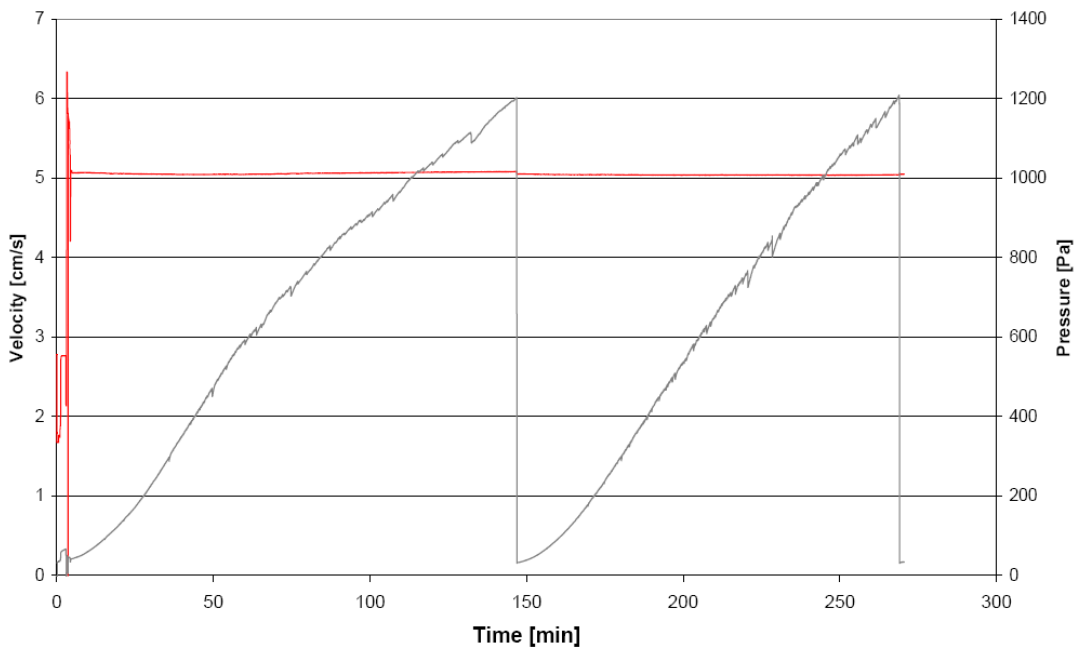

Figure C.9: Filter tray test #2

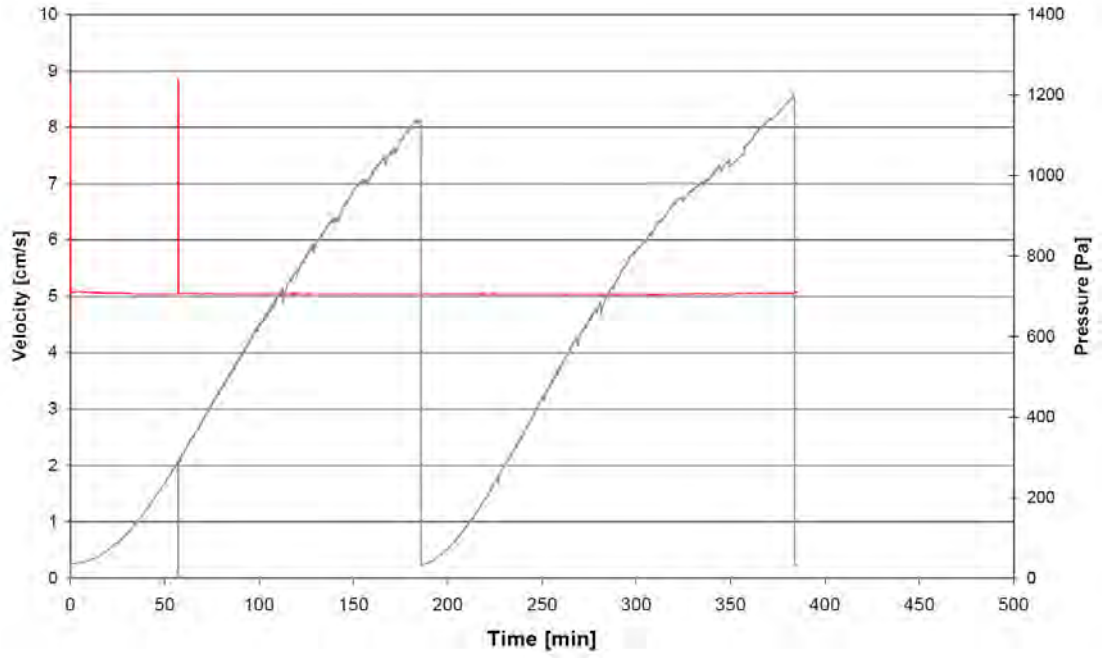

Figure C.10: Filter tray test #3

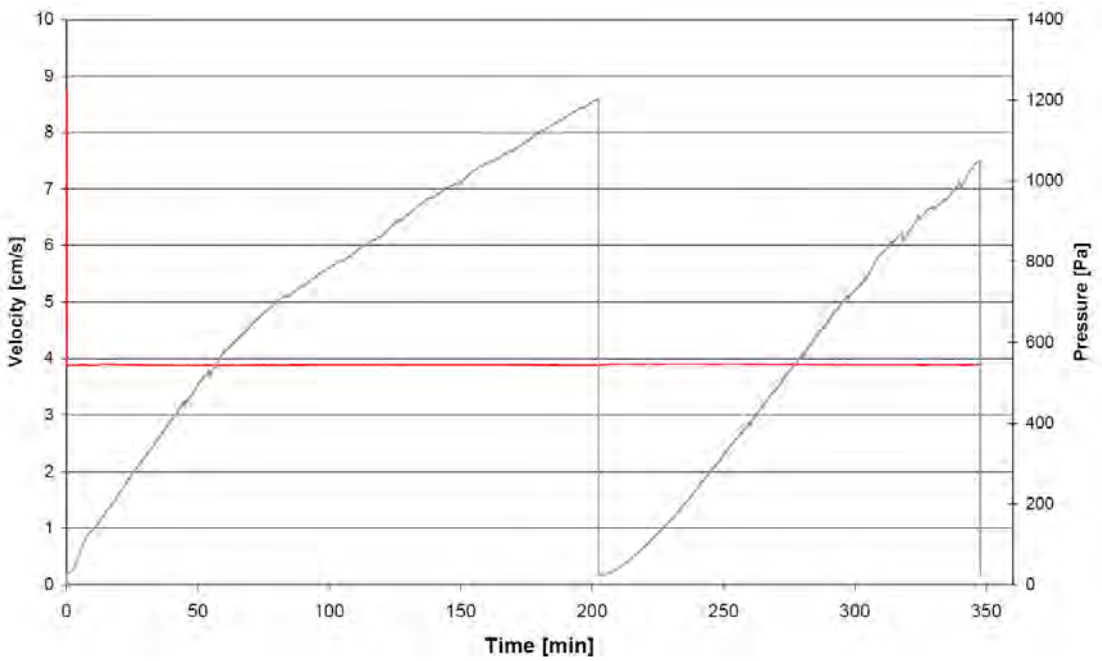

Figure C.11: Filter tray test #4

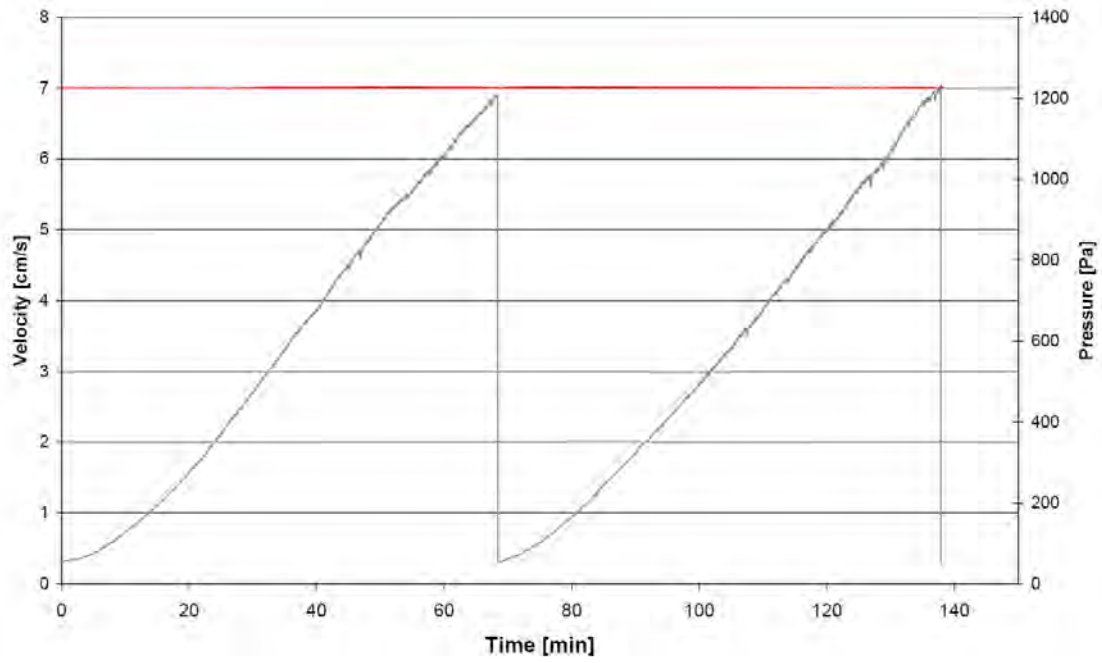

Figure C.12: Filter tray test #5

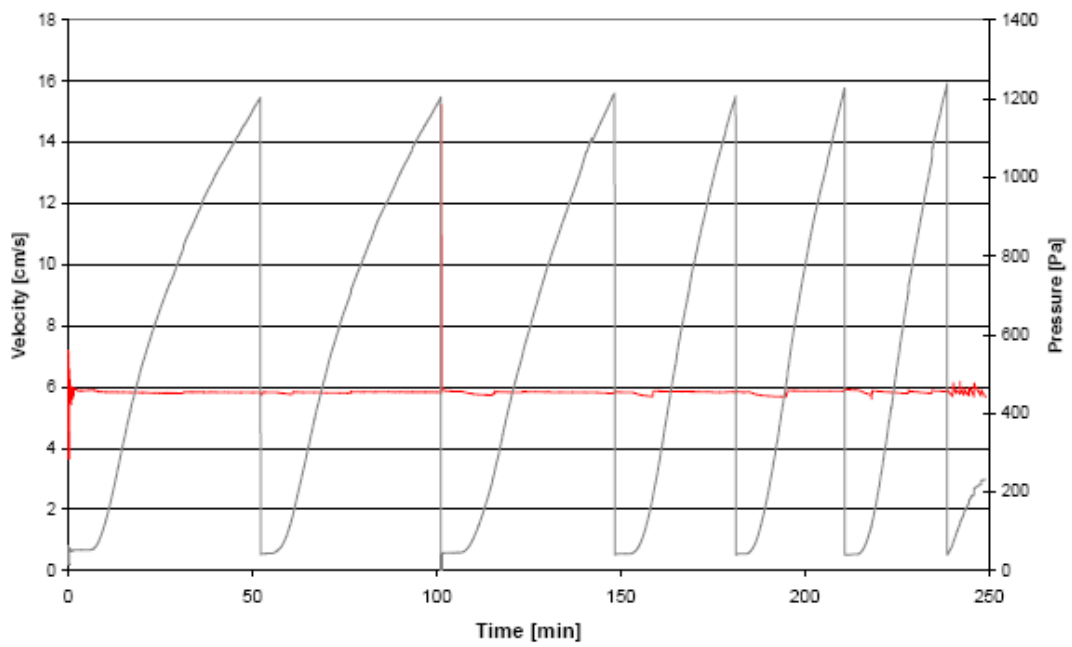

Figure C.13: Filter tray test #6

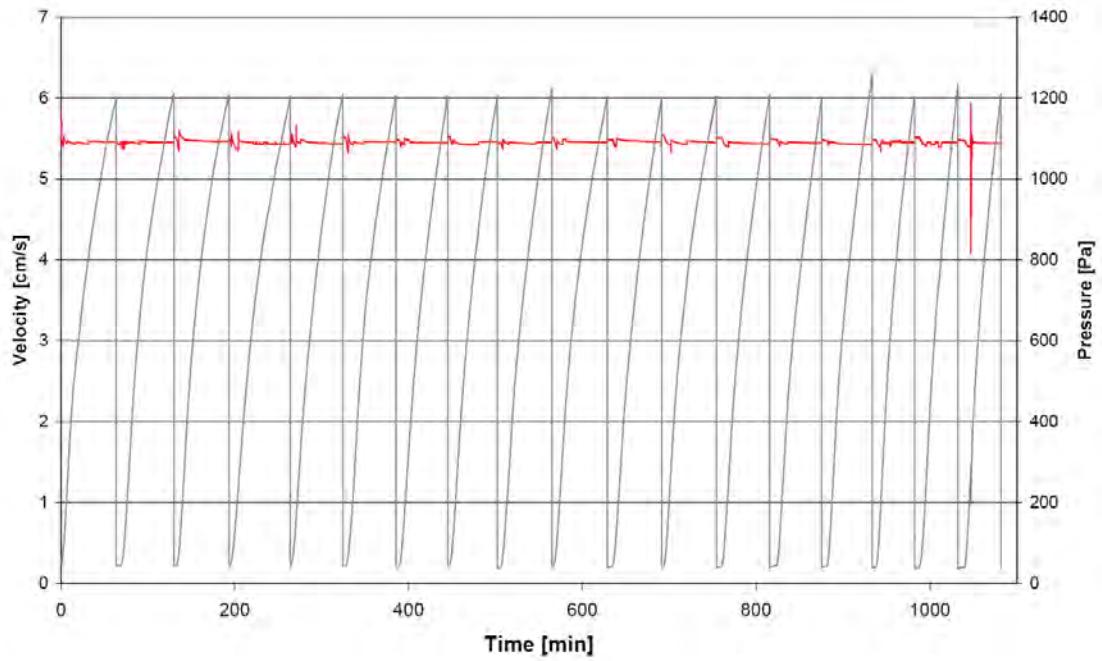

Figure C.14: Filter tray test #7

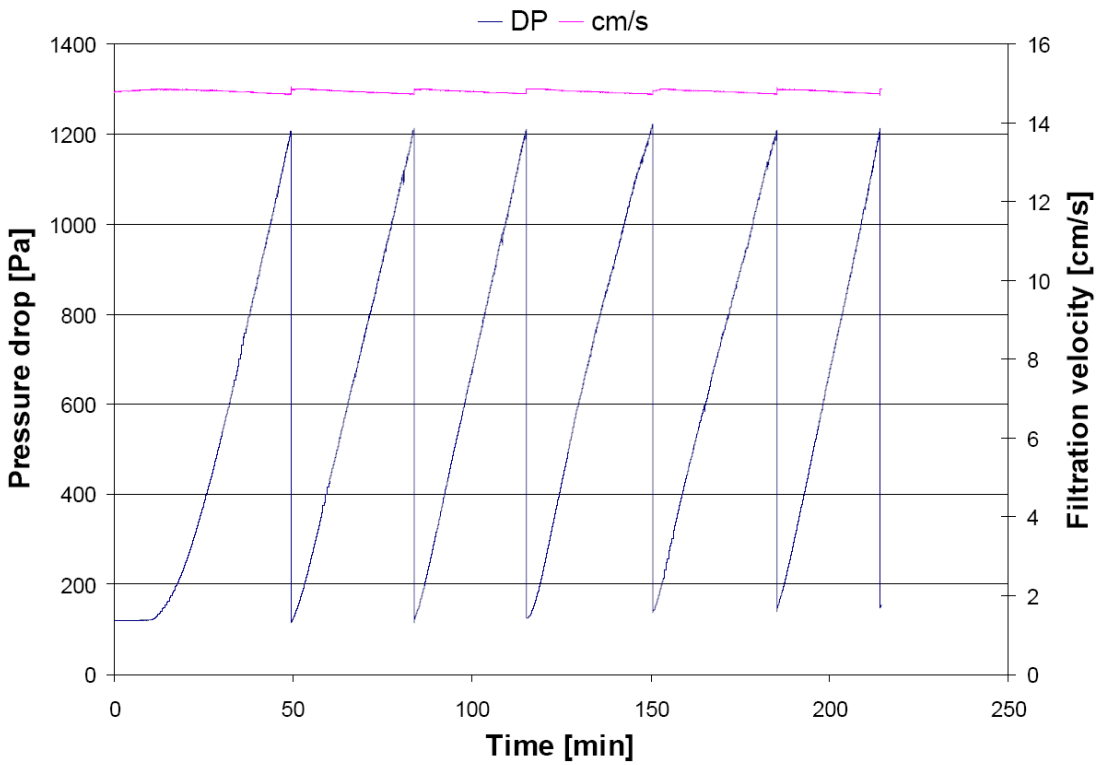

Figure C.15: Filter tray test #8

C.3 Axillary equipment and data handling

The temperature was measured with K-termoelements and the pressure was measured with Keller PAA-S23S (0-2 bar abs) and Keller PD-41X (0-50 mbar). Field point were used to transform the analog signals from the temperature and pressure transducers to a digital input signal for the PC. A LabVIEW program was made to monitor the experiments and save the data.

The volume flow through the filter was measured with a calibrated nozzle before entering the Becker KVT 3.80 vacuum pump. Figure C.16 shows the nozzle setup. The nozzle calibration is valid for chocked flow. The criteria for chocked flow can be calculated with equation C.1.

$$\frac{P_2}{P_1} = \left(\frac{2}{k+1}\right)^{\frac{k}{k-1}} \tag{C.1}$$

k is the specific heat ratio and P_1 and P_2 is the pressure before and after the nozzle. For air with $k = 1.4$ will the chocking pressure ratio be 0.528. The chocked mass flow can then be found with equation C.2:

$$\dot{m} = P_1 C_D A' \sqrt{\frac{k}{RT}\left(\frac{2}{K+1}\right)^{\frac{k+1}{k-1}}} \tag{C.2}$$

C_D is a correction factor of the flow separation from the walls and A' the critical flow area of the nozzle. Five nozzles was made and calibrated to find the C_D correction factor. The differences in the critical flow area from the nozzle area was included in the C_D during the calibration. The C_D calibration curves was implemented in the LabVIEW program with an iterative solution to calculate the flow in real time.

The system was also used in Güssing after changing the specific heat ratio input to 1.37 for the producer gas (dry basis).

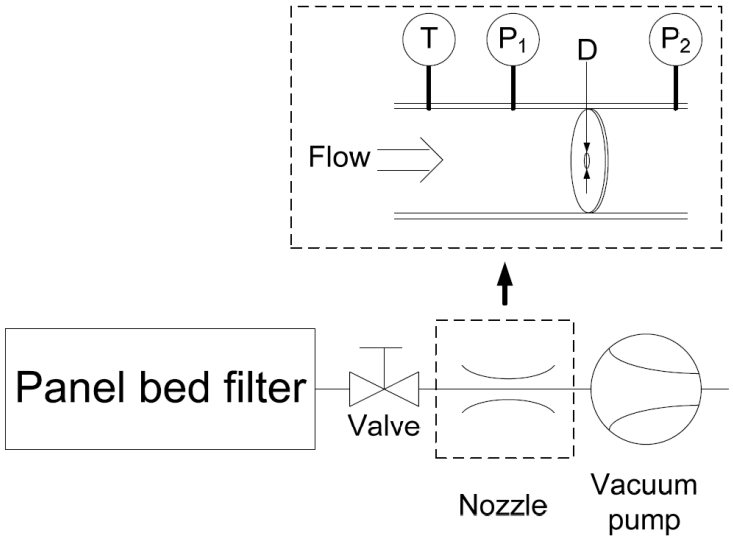

Figure C.16: Calibrated nozzle for calculating the flow rate

Appendix D

BioSOFC

D.1 Small scale panel bed filter

The small scale panel bed filter was designed and tested with quartz sand (AFS30) during Risnes' [110] work. In this work, quartz sand has been switched with alumina and the filter has been tested with higher temperatures. Figure D.1 shows the design principle for the small panel bed filter. Figure D.2 shows design details and figure D.3 shows the inlet cone (the outlet cone was used for the filter trays test and is described in Appendix C). Figure D.4 shows mounting of the louver part of the filter.

Figure D.5 shows the calibration setup. During the calibration the inlet cone was removed. The pressure tank was filled with air through the reduction valve and the puffback was released through the manually controlled solenoid valve. During the puffback, the pressure in the outlet cone was logged with a Kulite XTE 190 pressure transducer and logged together with the tank pressure, solenoid valve opening time and the spilled mass. Figure D.6 shows the calibration results.

The filter was heated with ICA135 heating cables that were tread in ceramic elements as shown in figure D.7. The heating was controlled by PID-regulators (the cable resistance was between 0.46-0.49 Ω/m with standard 230 V). The filter was insulated with 10 cm Superwool and 20cm Rockwool. The temperature was measured with K-termoelements and the pressure was measured with Keller PAA-S23S (0-2 bar abs) and Keller PD-41X (0-50 mbar). A heated glass fiber filter (Pall Type A/E) was used to measure dust input and penetration during the field tests.

After the filter, the cleaned producer gas was cooled down and the tar from the cleaned producer gas was removed by bubbling through acetone. The water was then removed with silica gel. The volume flow was measured with a critical flow nozzle before being sucked through the vacuum pump. The nozzle and pump is described in Appendix C. The control system was programmed in LabVIEW and was based on the program described in Appendix C.

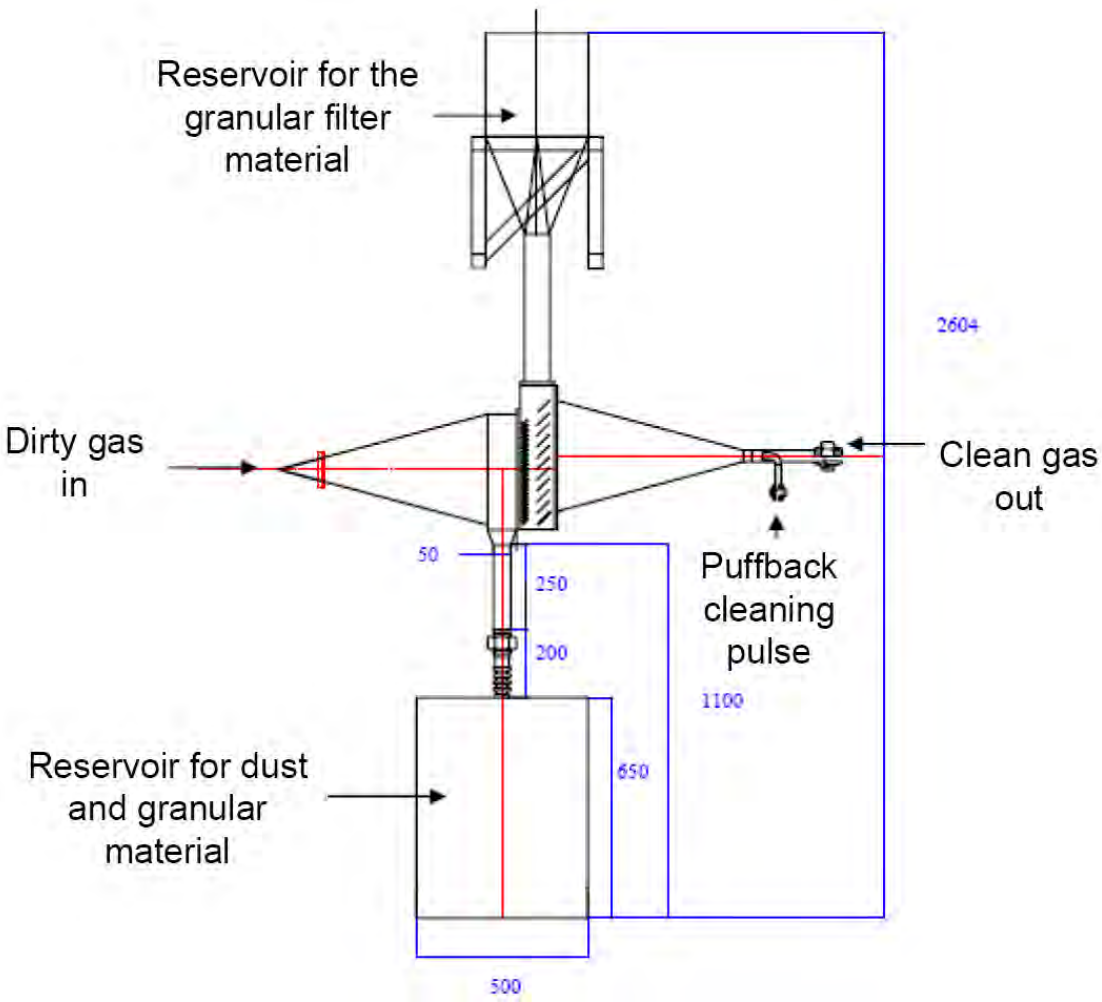

Figure D.1: Small scale panel bed filter [mm]

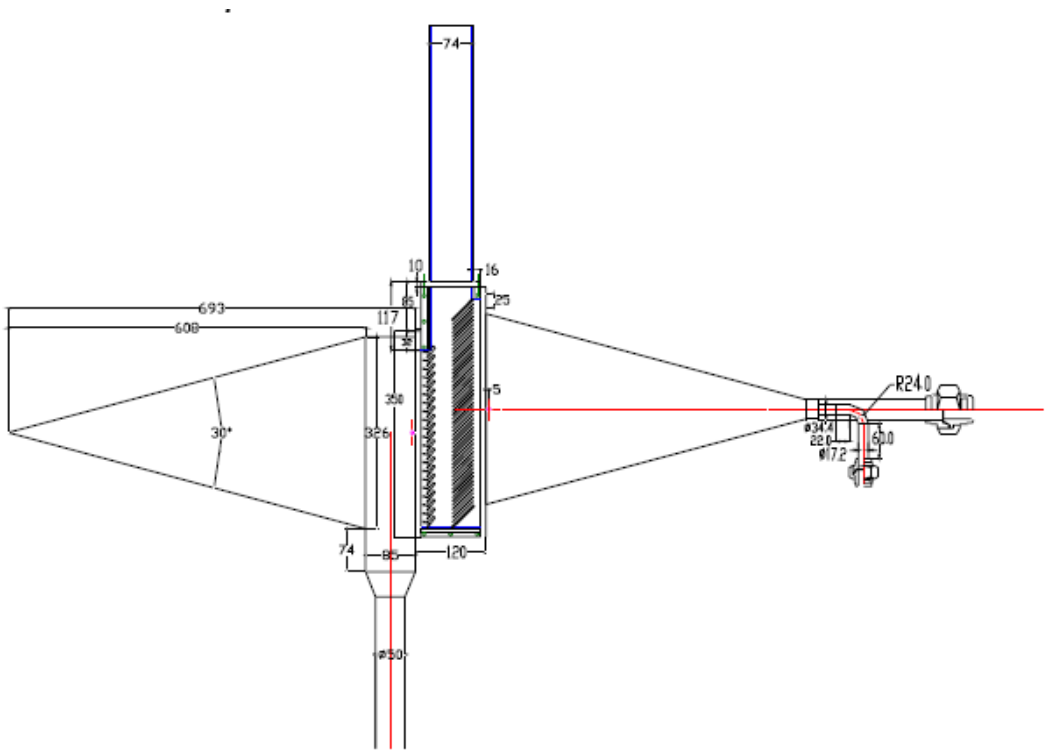

Figure D.2: Small scale panel bed filter [mm]

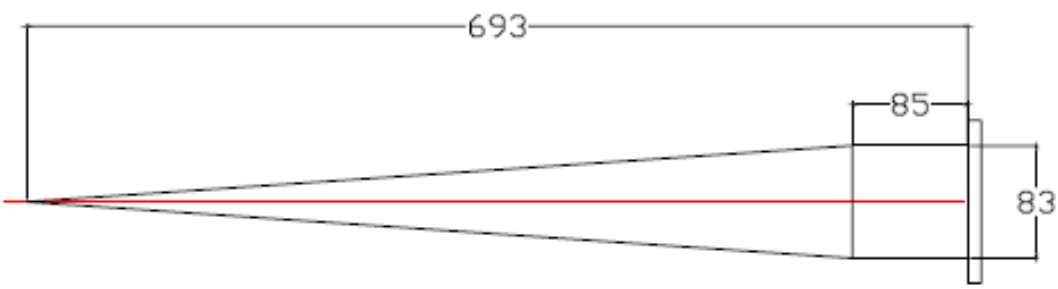

Figure D.3: Inlet cone for the small scale panel bed filter [mm]

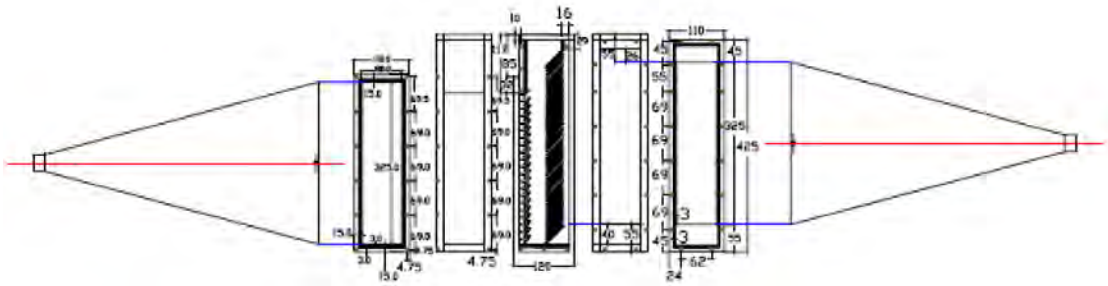

Figure D.4: Small scale panel bed filter louver mounting [mm]

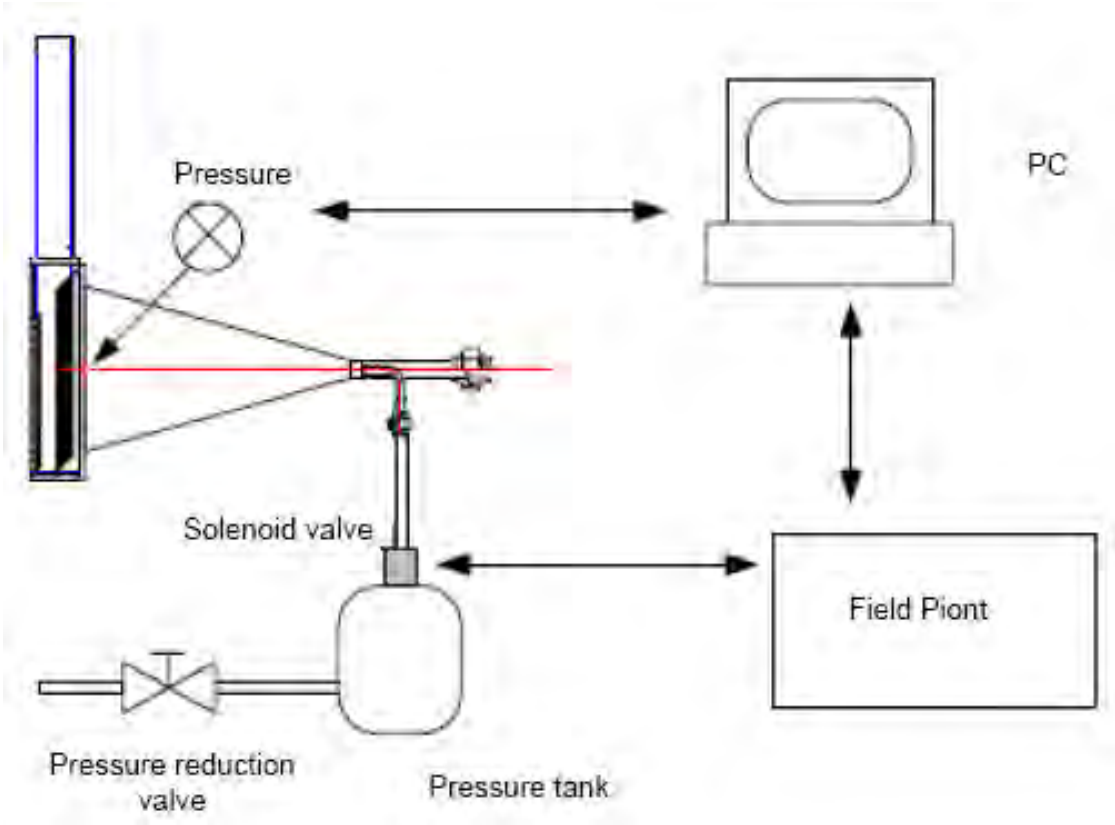

Figure D.5: Small scale panel bed filter calibration setup

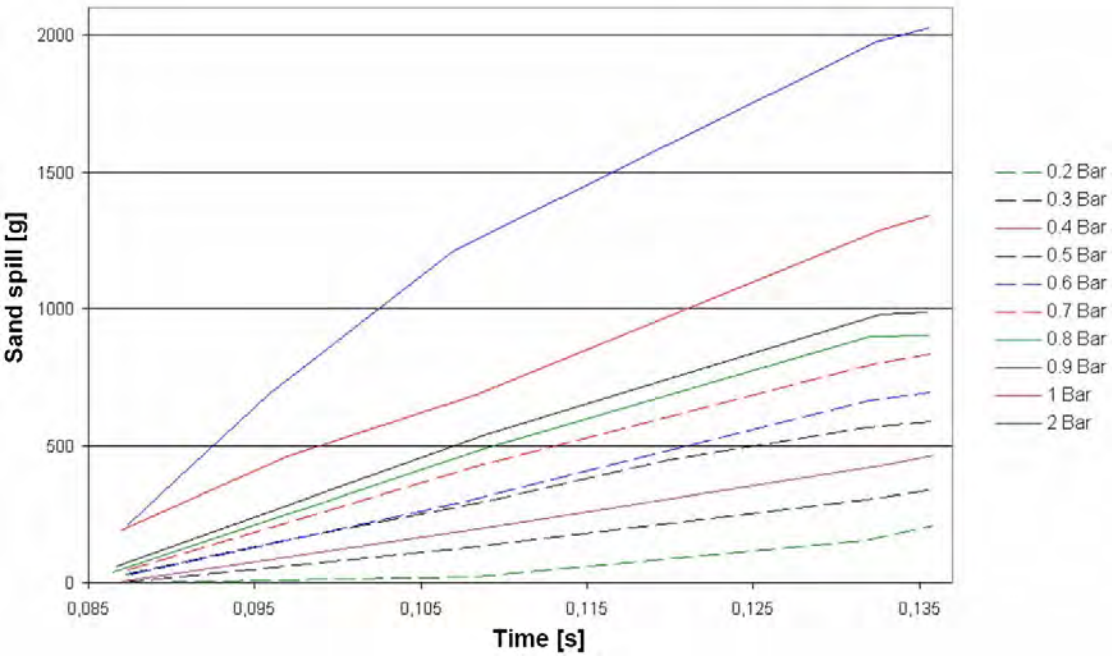

Figure D.6: Small scale panel bed filter calibration results

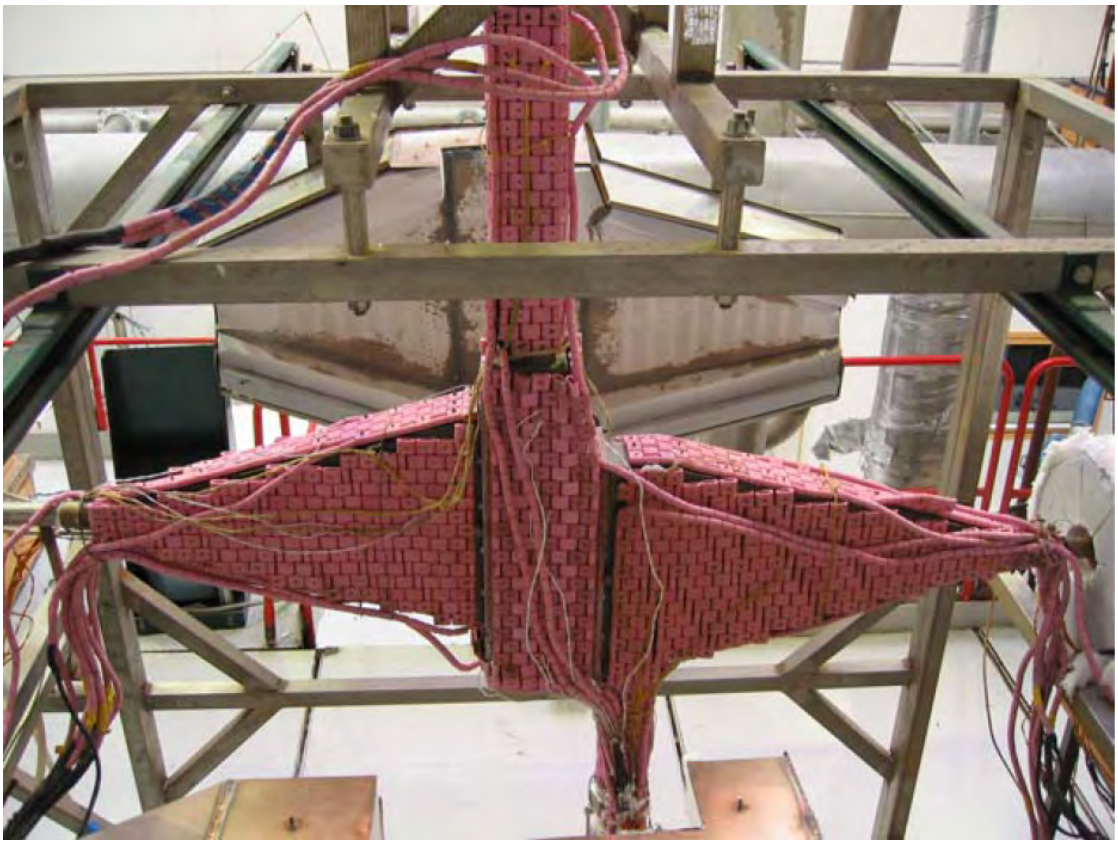

Figure D.7: Small scale panel bed filter heating cables

D.1.1 Small scale results

Test #	Temperature	Concentration
Laboratory test #1	100-120°C	4.08 g/m^3 [a]
Laboratory test #2	100-120°C	3.87 g/m^3 [a]
Laboratory test #3	100-120°C	3.68 g/m^3 [a]

a SAE - standard dust

Test #	Temperature	Volume flow	
Güssing test #1	500-550°C	1 Nm^3/h	
Güssing test #2	500-550°C	1 Nm^3/h	
Güssing test #3	500-550°C	1 Nm^3/h	[a]
Güssing test #4	500-550°C	2 Nm^3/h	[b]
Güssing test #5	500-550°C	0.5 Nm^3/h	[c]
Güssing test #6	500-550°C	0.5 Nm^3/h	[d]
Güssing test #7	500-550°C	2 Nm^3/h	[c] [d]
Güssing test #8	500-550°C	2 Nm^3/h	
Güssing test #9	500-550°C	1 Nm^3/h	
Güssing test #11	500-550°C	2 Nm^3/h	

a plastic tube breakage due to acetone (9 hours)
b problem with the gasification plant (shutdown)
c cyclone breakage, needed to be welded
d noise due to H_2S measurements
Test #10 was stopped due to leakage

The inlet dust concentration in Güssing was measured before the tests with a volume flow of 1 Nm^3/h. The dust concentration fluctuated between 2-3 g/m^3 with an average of 2.71 g/m^3.

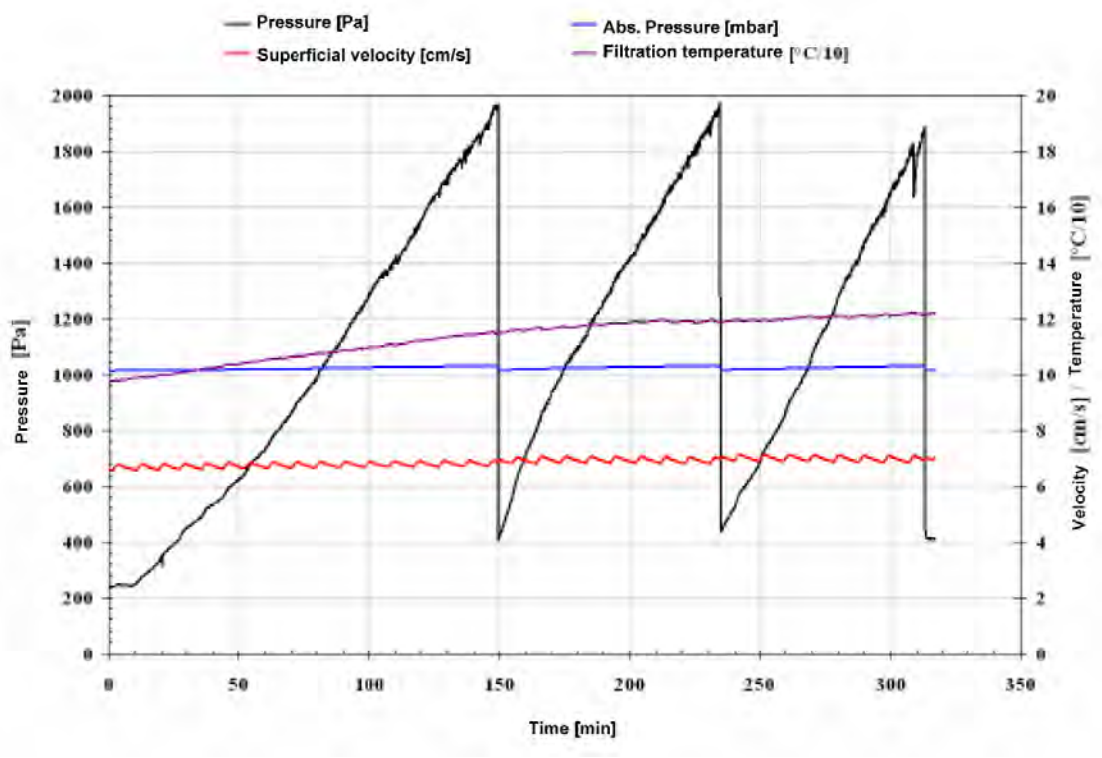

Figure D.8: Small scale panel bed filter laboratory test #1

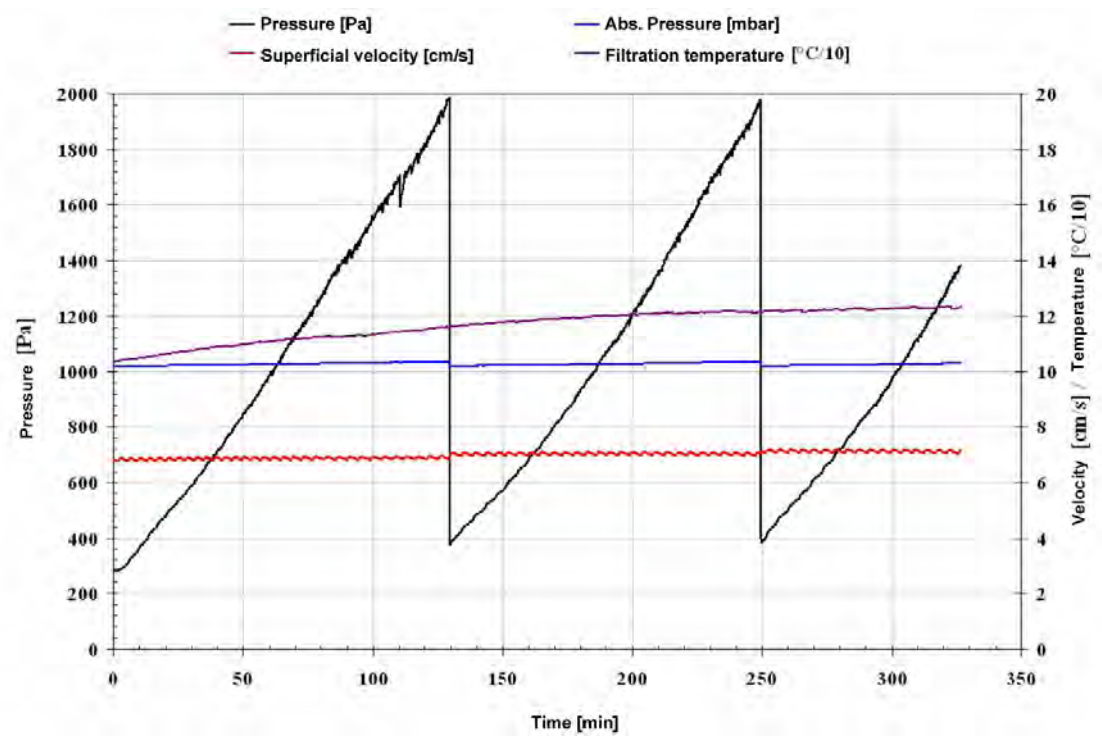

Figure D.9: Small scale panel bed filter laboratory test #2

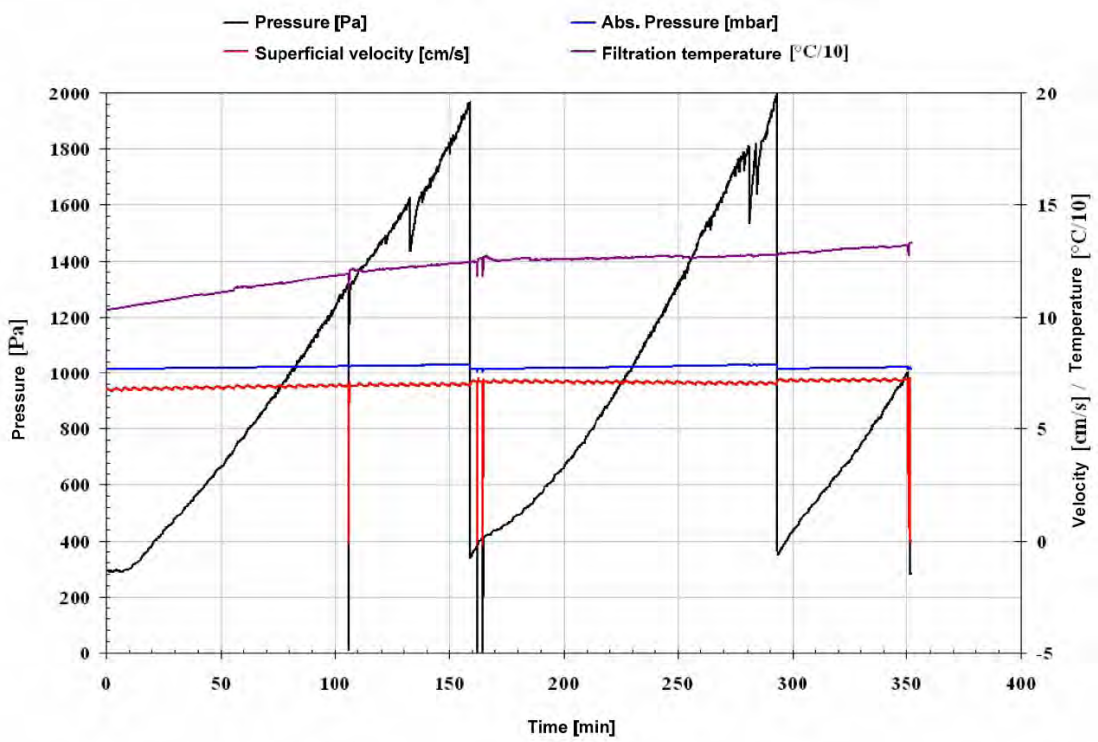

Figure D.10: Small scale panel bed filter laboratory test #3

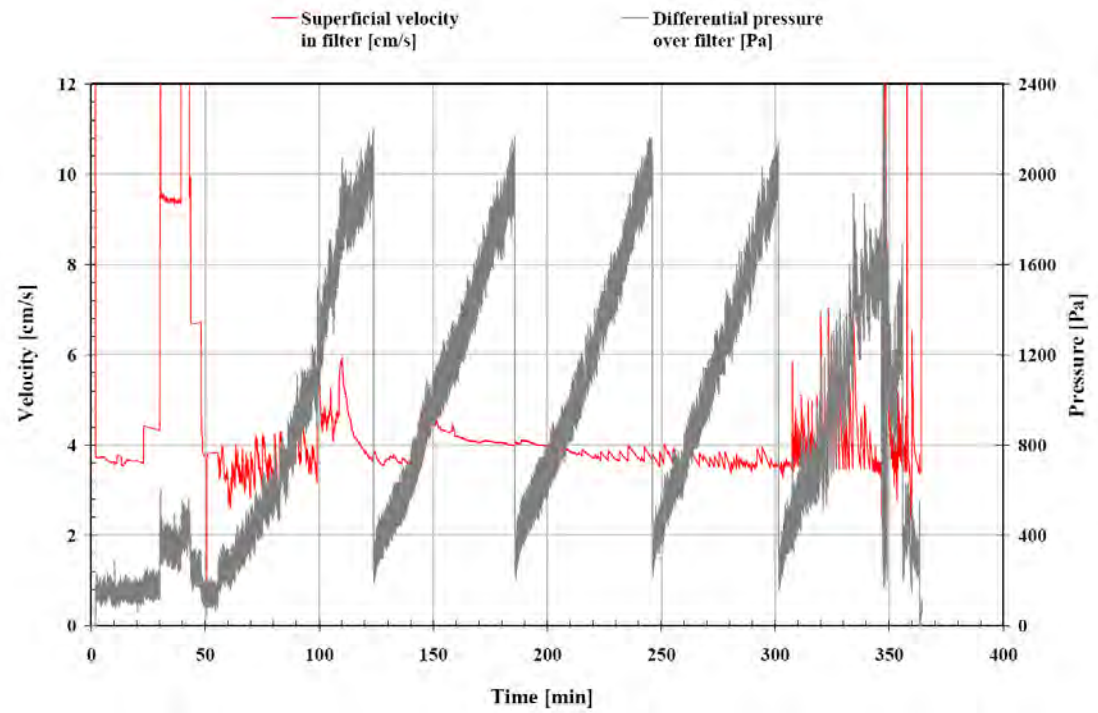

Figure D.11: Small scale panel bed filter test #1

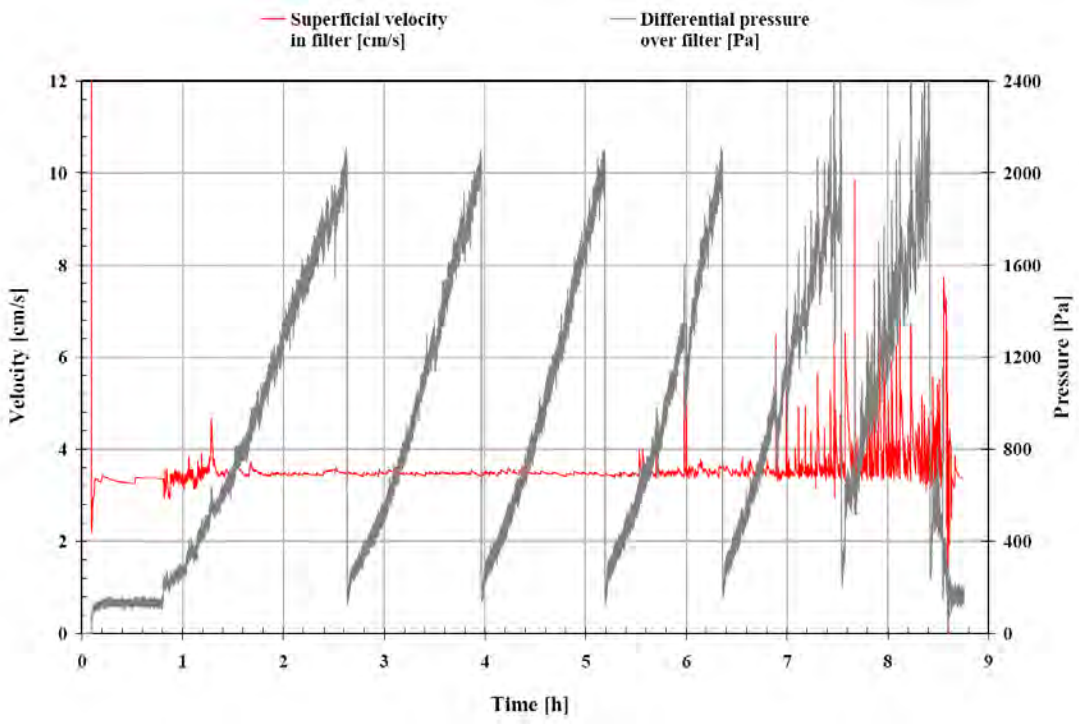

Figure D.12: Small scale panel bed filter test #2

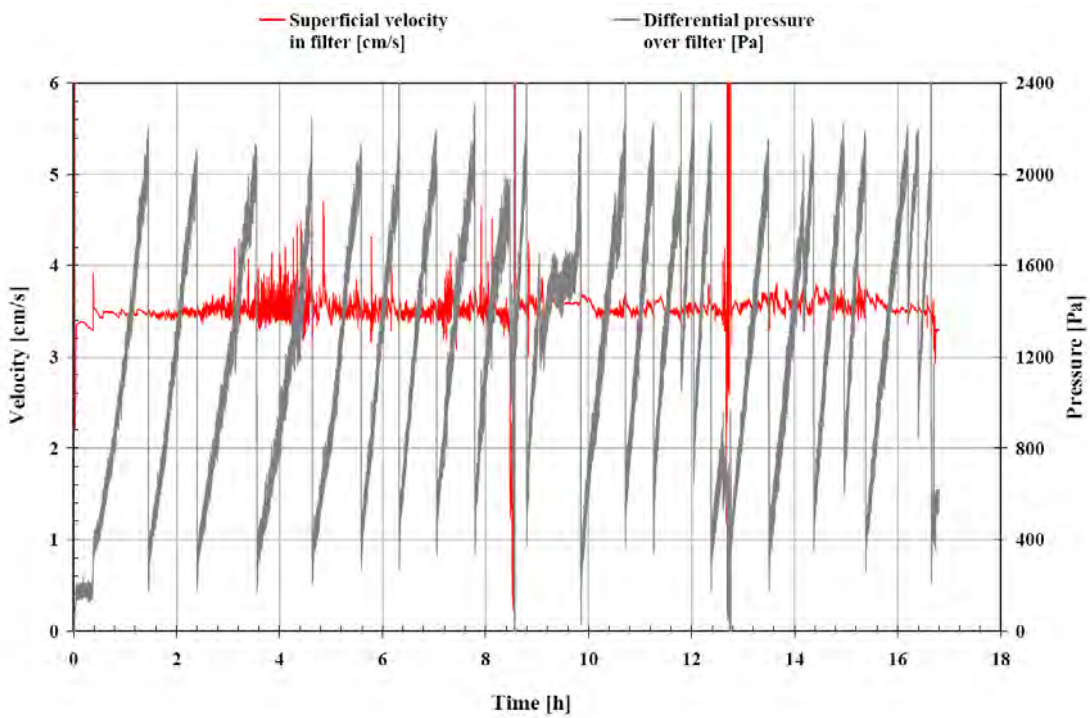

Figure D.13: Small scale panel bed filter test #3

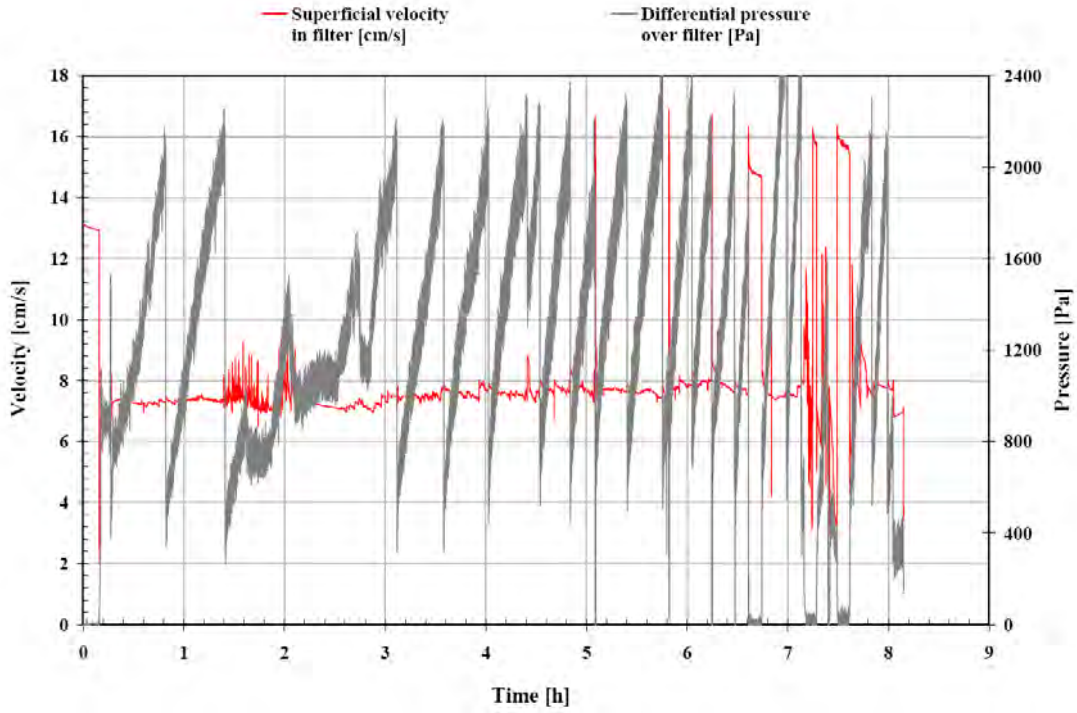

Figure D.14: Small scale panel bed filter test #4

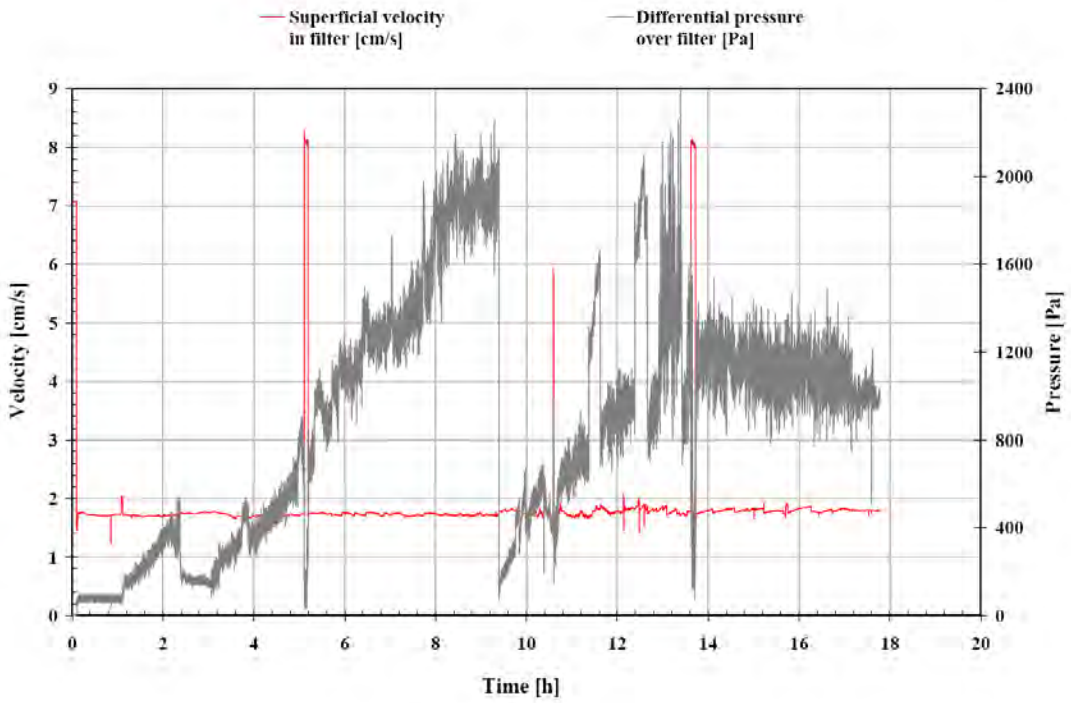

Figure D.15: Small scale panel bed filter test #5

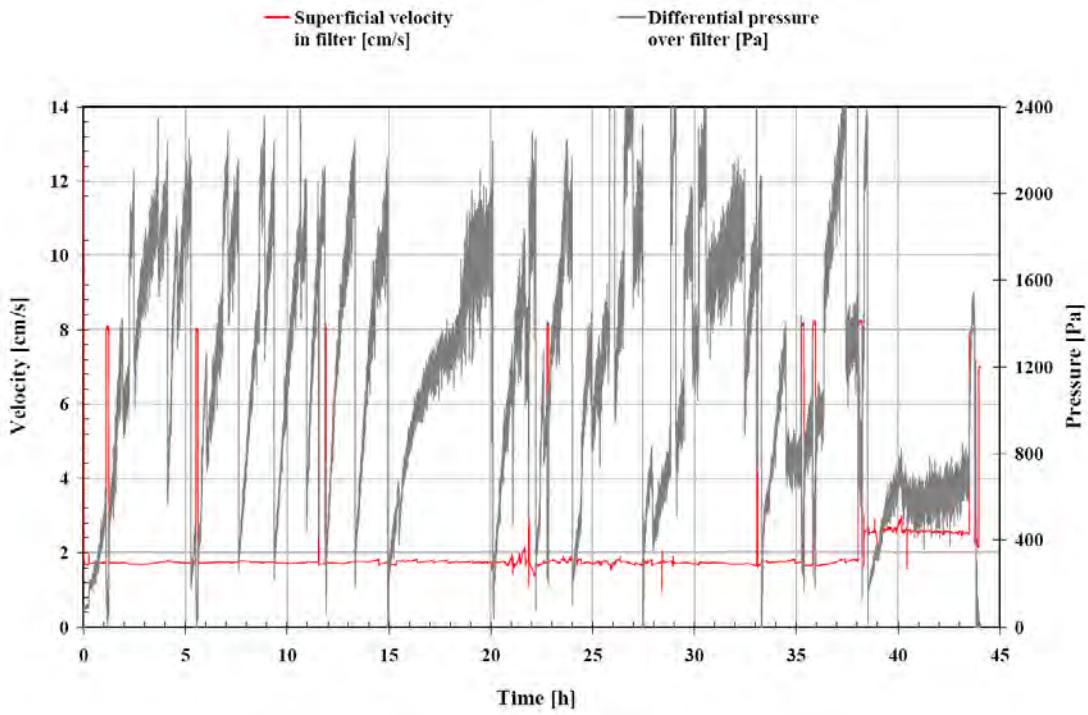

Figure D.16: Small scale panel bed filter test #6

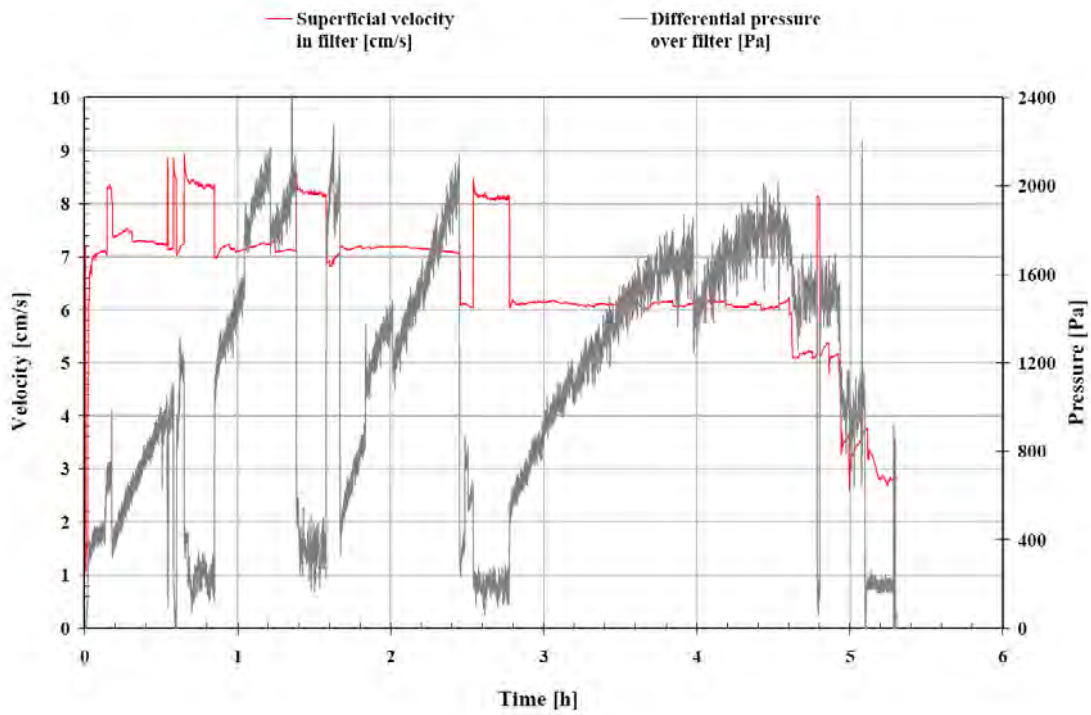

Figure D.17: Small scale panel bed filter test #7

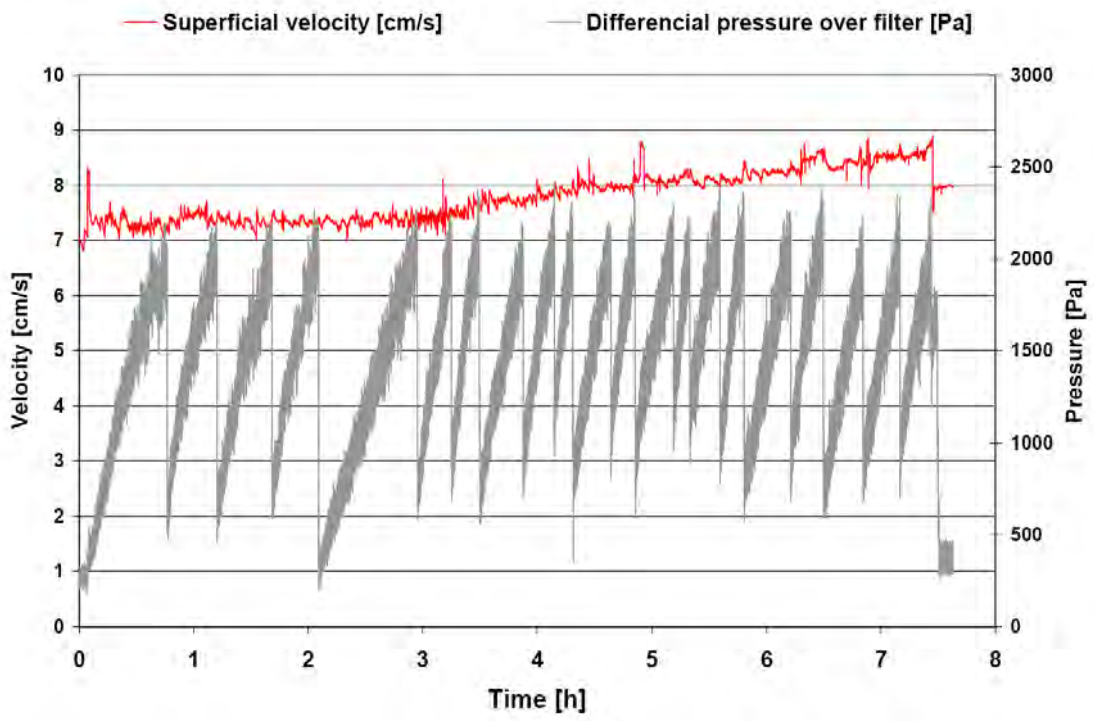

Figure D.18: Small scale panel bed filter test #8

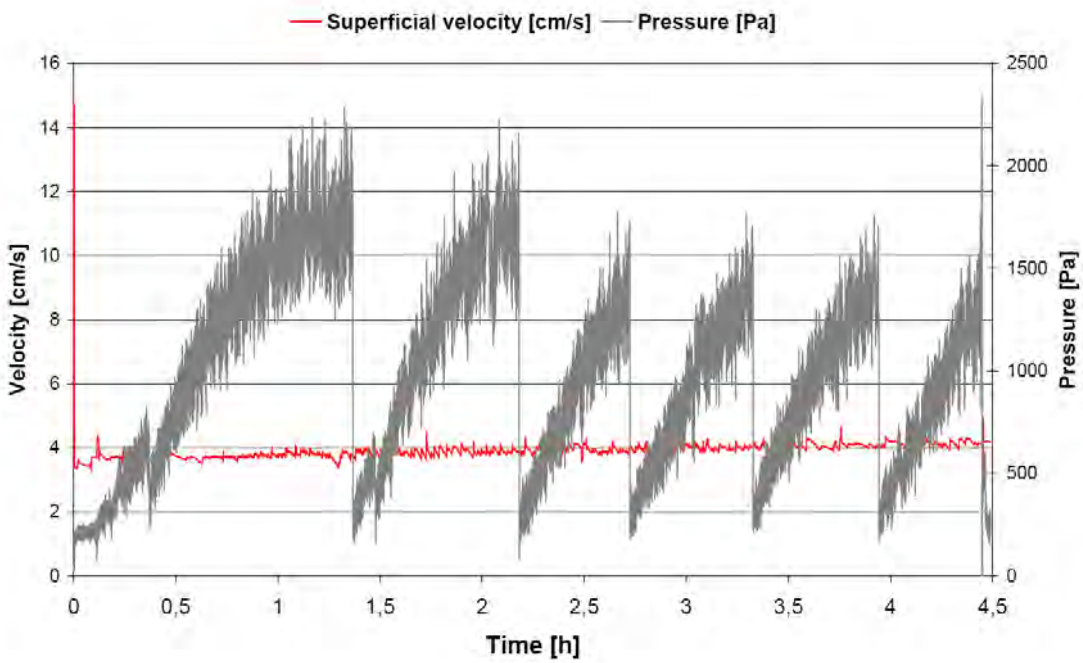

Figure D.19: Small scale panel bed filter test #9

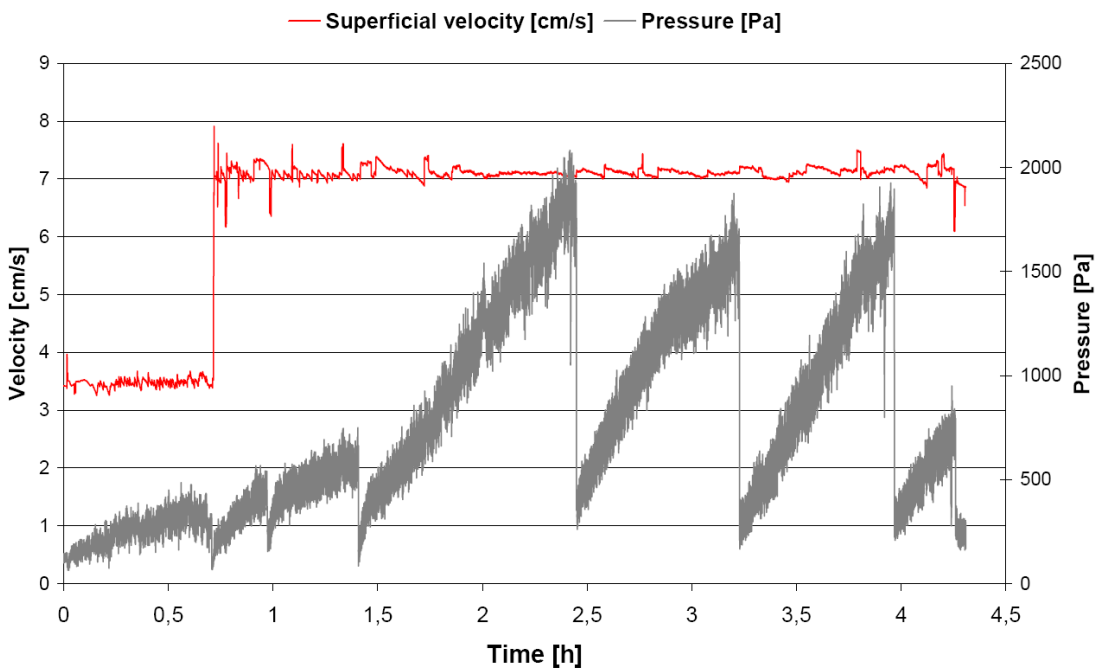

Figure D.20: Small scale panel bed filter test #11

D.2 Scaled up panel bed filter

Figure D.21 and figure D.22 show the design of the up-scaled panel bed filter. The volume flow through the filter can be closed by two valves behind each of the gas exits before they come together so the filter filter can operate each of the two sides independently. Figure D.23 shows the filter housing without insulation and figure D.24 shows the filter module. Figure D.25 shows the filter installation in Güssing.

The equipment for heating, insulation and instrumentation of the up-scaled filter was done in the same way as it was done for the for small scale filter (explained in Appendix D.1). A heated glass fiber filter (Pall Type A/E) was used to measure dust input and penetration during the field tests.

After the filter, the cleaned producer gas was cooled down and the tar from the cleaned producer gas was removed by bubbling through acetone. The water was then removed with silica gel. The volume flow was measured with a critical flow nozzle before being sucked through the vacuum pump. The nozzle and pump are described in Appendix C. The control system was programmed in LabVIEW and was based on the program described in Appendix C.

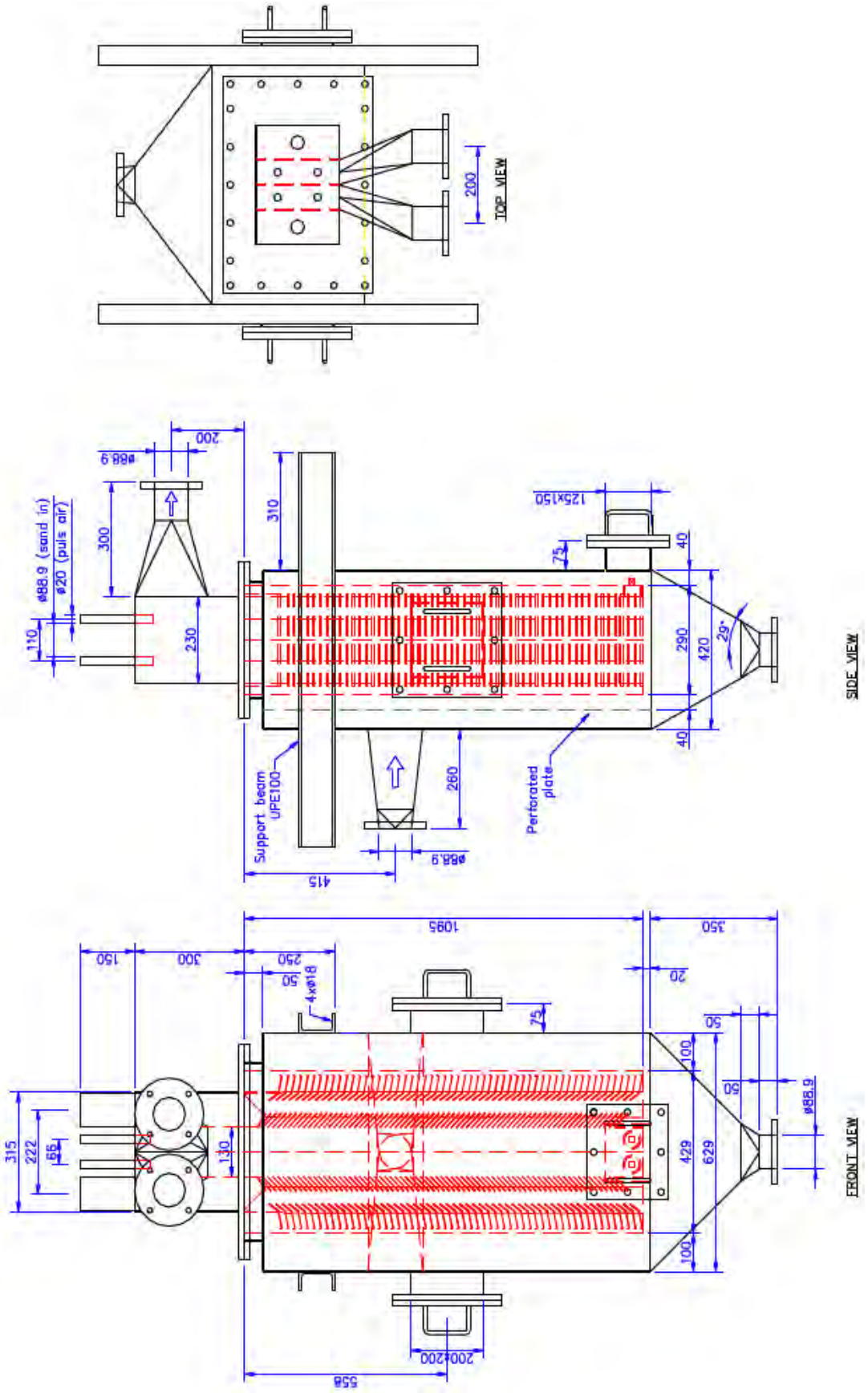

Figure D.21: Scaled up panel bed filter [mm]

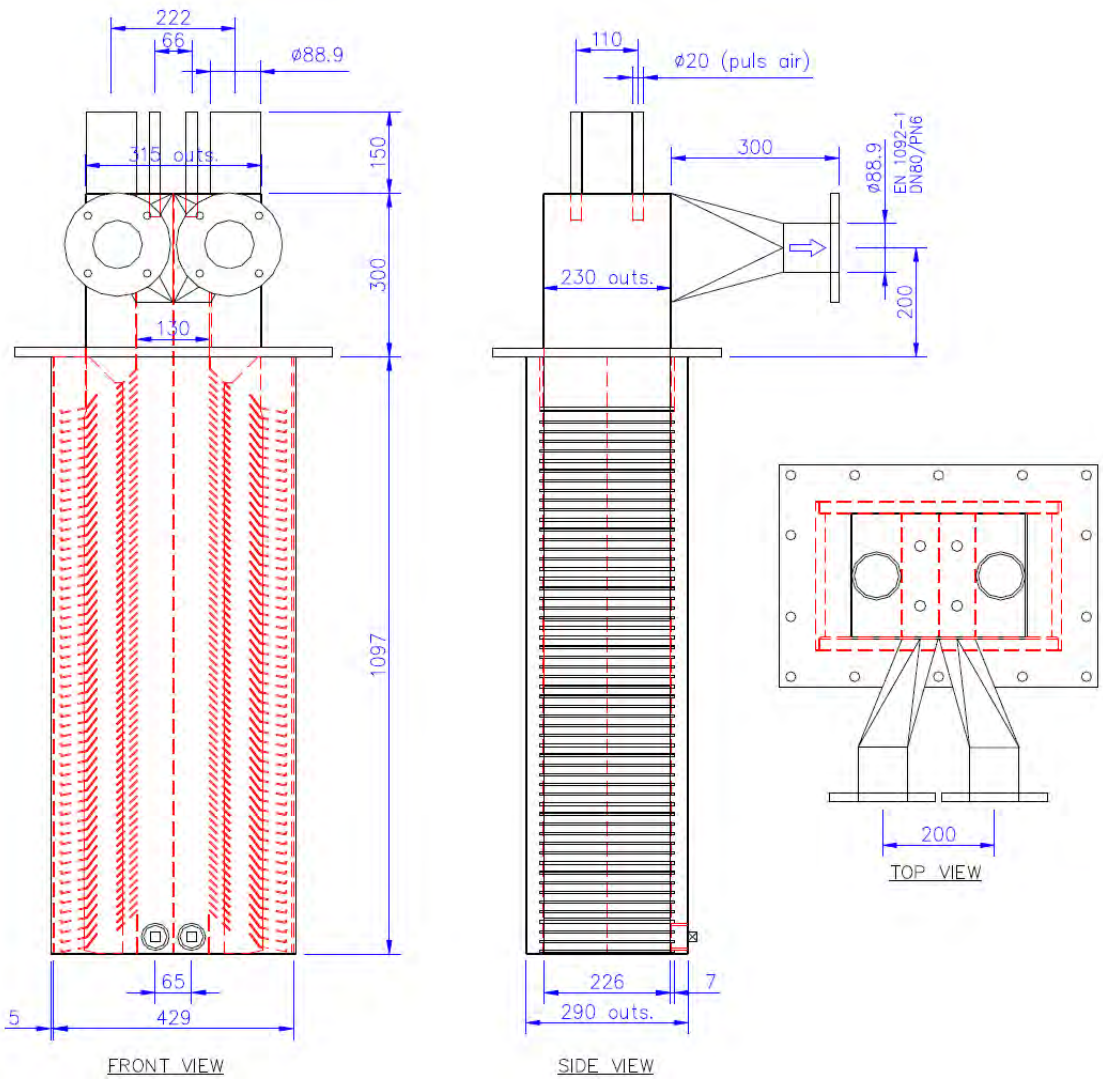

Figure D.22: Scaled up panel bed filter [mm]

Figure D.23: Scaled up filter and filter housing

Figure D.24: Scaled up filter module

Figure D.25: Mounting scaled up filter in Güssing

D.2.1 Scaled up results

Only three series of filtration experiments were done with the up-scaled filter. The experiments were done with a volumetric flow rate of 8 Nm^3/h at 525^oC. The gasification plant had some down time after approximately 3 hours during the first experimental series as shown in figure D.26. Figure D.27 shows the second series that went without any problems with the gasification plant. The data third series were wasted due to problems and shut down of the gasification plant. The plant was then shut down for about 3 weeks for maintenance and the filter testing was canceled in order to install the interface with the Solid Oxide Fuel Cell.

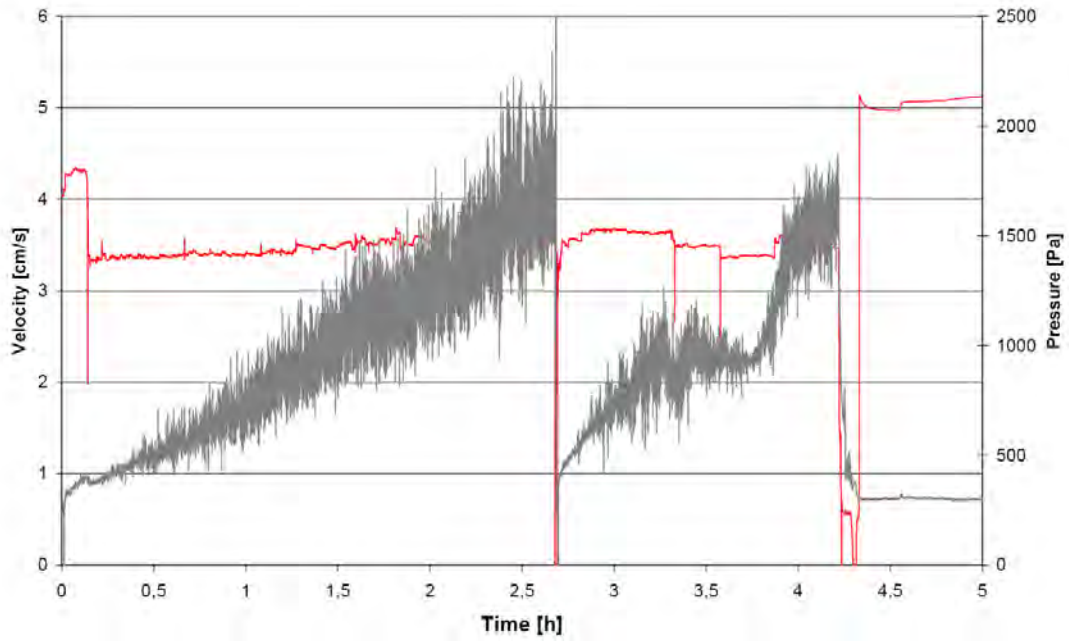

Figure D.26: Up scaled panel bed filter test #1

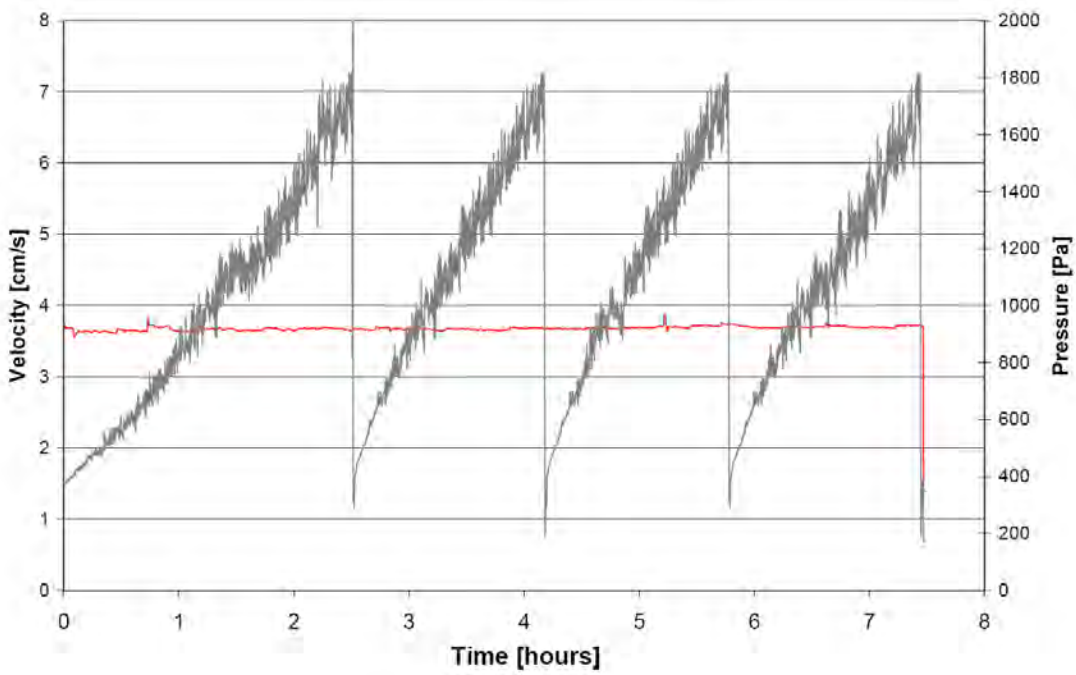

Figure D.27: Up scaled panel bed filter test #2

D.3 Axillary equipment

Figure D.28 shows the setup of the filter and fuel cell in Güssing. The producer gas from the gasifier is cooled from 900°C to 550°C in the pipe from the gasifier to the cyclone. After the filter the H_2S is removed with sorbent in the H_2S reactor. The flow split after the H_2S and the flow direction is regulated with valves.

The flow through the vacuum pump is cooled before the tar is cracked with acetone. The water is then removed with silica gel before the volume flow is measured with the calibrated nozzle (described in Appendix C) and sucked through the vacuum pump.

The flow to the fuel cell has to be delivered with a pressure slightly above atmospheric pressure. The pressure control loop is designed to increase the pressure by 0.1 bar by circulating the flow through two fans shown in figure D.29 and choking the flow with a valve. The gas to the fuel cell can then be bleed of on the pressure side of the fans. The loop has to be electrically heated to avoid tar condensation during startup, but well regulated to avoid the temperature to be increased further from the gas heating from the two 11 kW fans. Figure D.30 and figure D.30 show calculations on loop length versus heat loss and temperature and calculations of heat loss versus insulation thickness respectively [94]. The loop length was set to 7 meters as shown in figure D.32. The loop was then insulated with 5 cm Superwool and installed in Güssing as shown in figure D.33. The testing showed a long preheating time to get the fans up to 500°C, but steady operation temperature and a gas pressure increase of 0.1 bar as expected.

The flow to the fuel cell was measured by a V-cone and regulated with a valve before being heated to 920°C and delivered to the fuel cell.

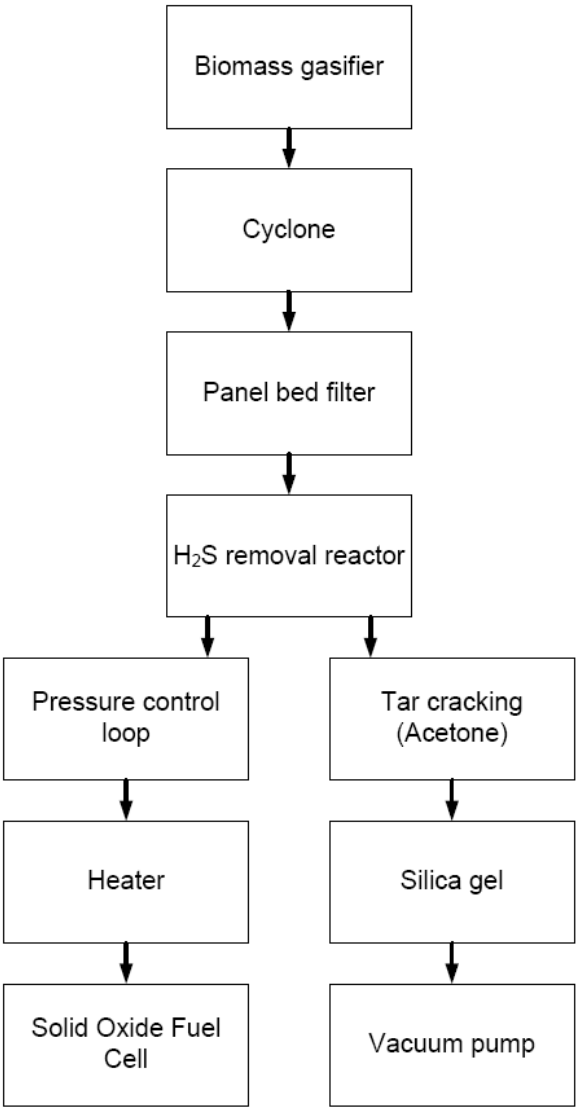

Figure D.28: Setup of filter and SOFC

Figure D.29: Fans

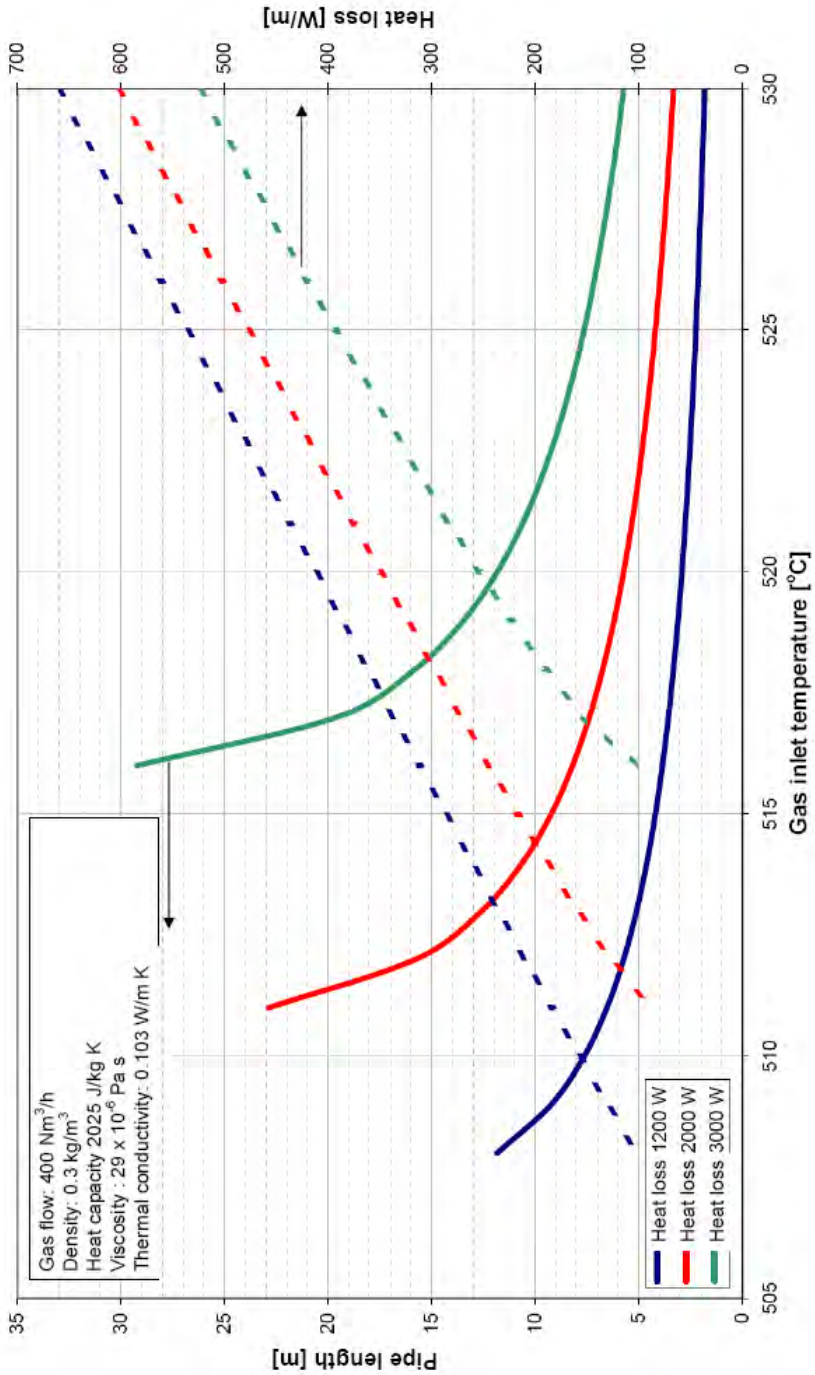

Figure D.30: Calculation of heat loss and loop length [94]

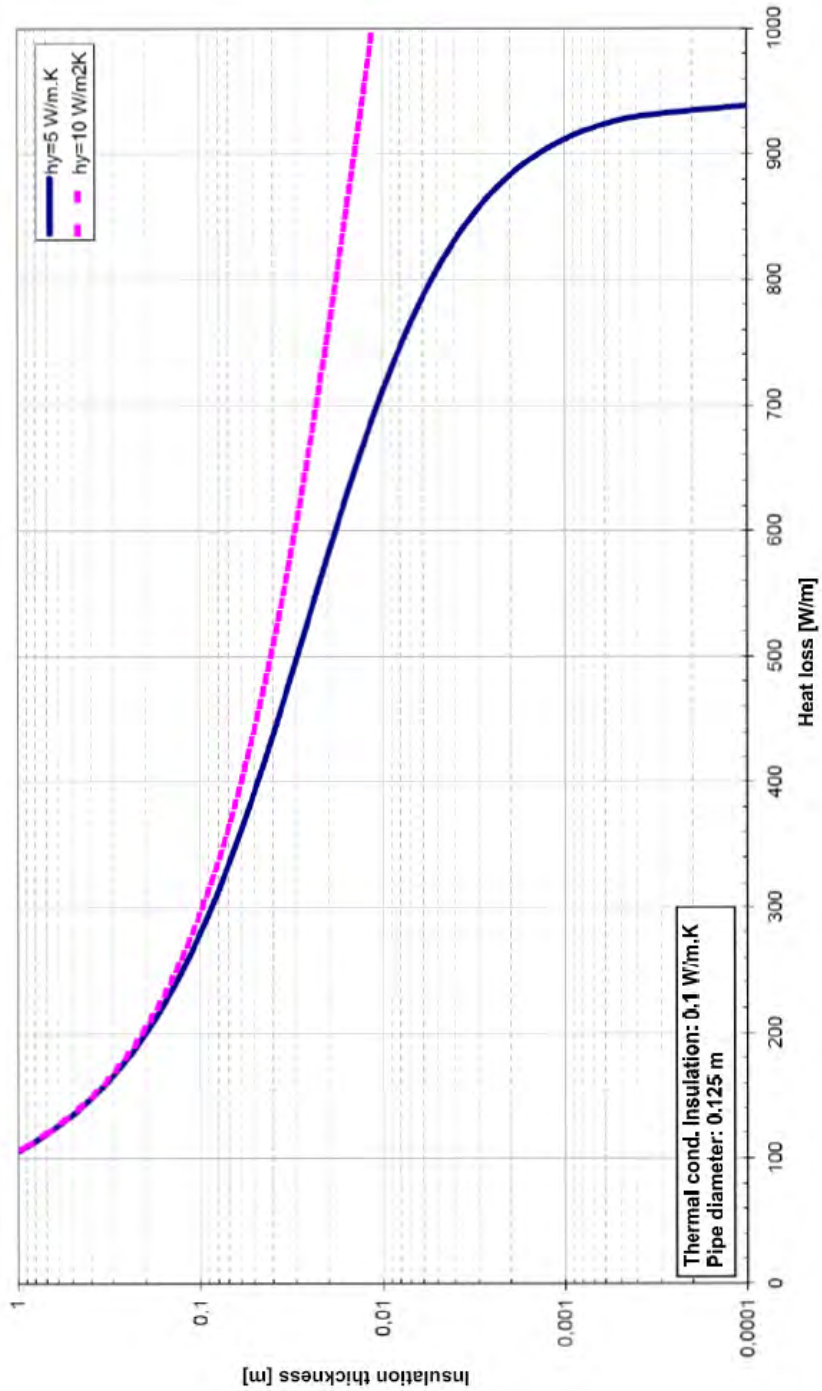

Figure D.31: Calculation of insulation thickness [94]

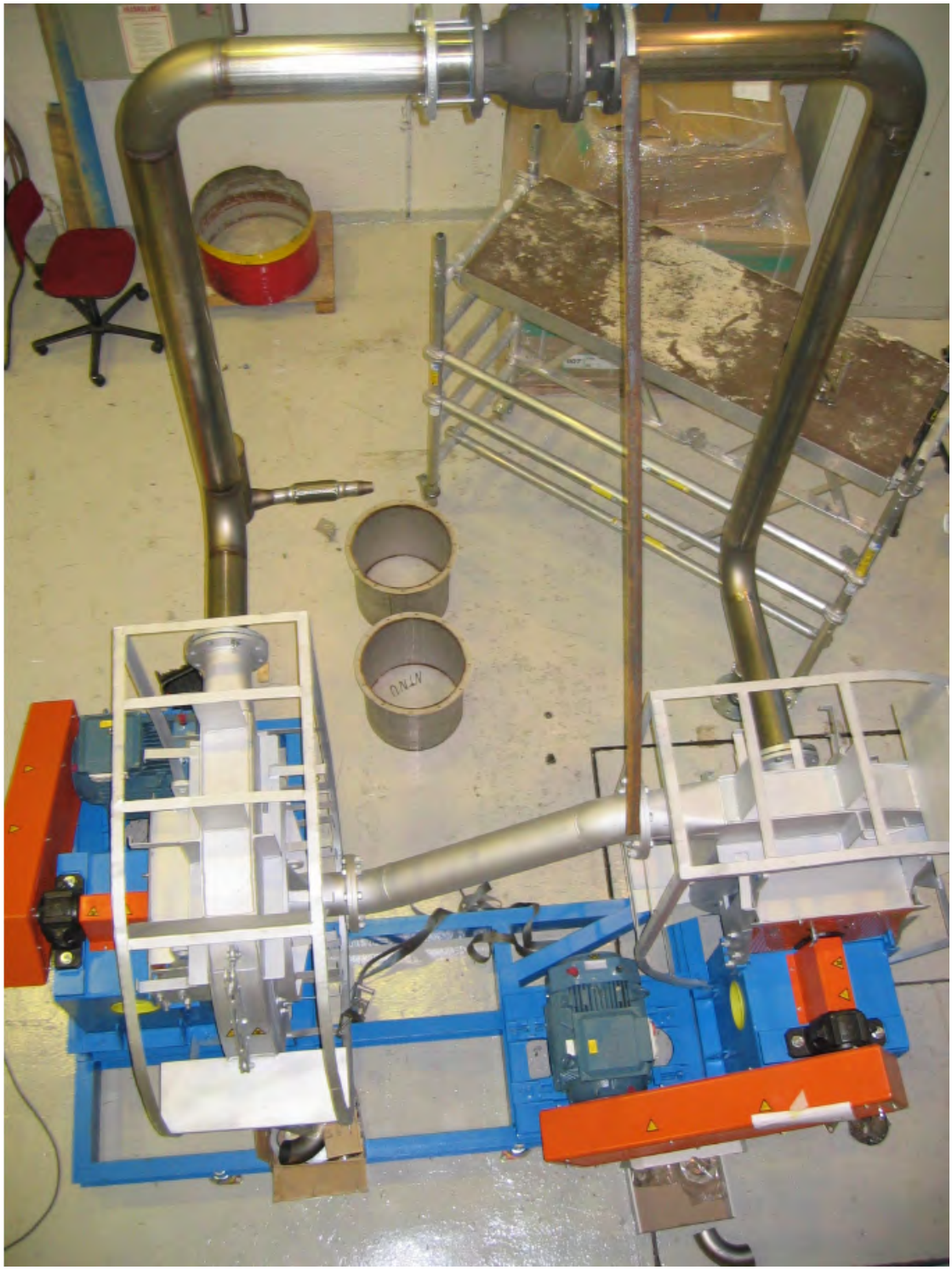

Figure D.32: Pressure control loop

Figure D.33: Loop with insulation in Güssing

Appendix E

Industrial scale filter

E.1 Equipment and setup

The demonstration plant filter setup was built to remove fly ash from the biomass furnace at Bjertnæs Sag AS, as shown in figure E.1. Figure E.2 shows the exiting cyclone and the fan used to control the combustion process. A slipstream was taken from the flue gas duct after the existing fan so as not to interfere with the combustion process. Figure E.3 shows the design for the filter house containing 3 filter modules, each designed for a maximum volume flow of 375 Nm^3/h. The maximum flow from the furnace was estimated to be 750 Nm^3/h when operating at 100%. This allows two of the filter modules to handle the entire flow when the third is closed during puffback. The filter modules were designed with a new puffback geometry as shown in figure E.4.

Figure E.5 shows the experimental setup where the numbers indicate the following axillary equipment:

1 Cyclone
The cyclone was used to lead the cleaned granular material sent up with the pneumatic sender down into the reservoir located above the filter housing.

2 Puffback valve
Asco SC G353.060 pulse valves was used. The pressure in the 3 pressure tanks located above the valve was manually adjusted and operated at 3.6 bar.

3 Cell feeder
The DMN-Westinghouse AML-150-1 cell feeder was used to measure the dust and granular material exiting the filter house and to act as a pressure barrier between the filter house and the sieve. The cell feeder was made of cast iron and could not handle alumina so quartz sand was used as granular material in the filter.

4 Sieve
the CSM 722 sifter MKII from Gerike had a screen aperture of 350 micron and separated the dust from the granular material. The sieve was also used to remove the fine fraction of the quartz sand before entering the filter.

5 Pneumatic sender
The dense phase conveyor Type PHFK-20 from Gerice was the smallest commercial available pneumatic conveyor we could find and was used to send up the granular material 6 meters to the cyclone. The sender came with an independent control unit STP12 that was modified and controlled via the master LabVIEW controll program.

6 The biomass furnace

Figure E.6 shows details of the sand reservoir and the sand distribution system above the filter housing. Figure E.7 and figure E.8 show the filter housing with and without the Rockwool insulation.

The flue gas from the filter house outlets (one from each filter module, but only one module was installed during these tests) of the filter goes down to one collecting manifold and out through the wall to the fan. The volume flow through each of the outlets are individually measured with a Micatrone MFS-C-100 flow sensor and regulated with a pneumatic valve. Figure E.9 shows an overview of the instrumentation. Compact Field Point was used for ADC and DAC while the controll program was programmed in LabVIEW.

Figure E.1: Furnace and fuel feeding system

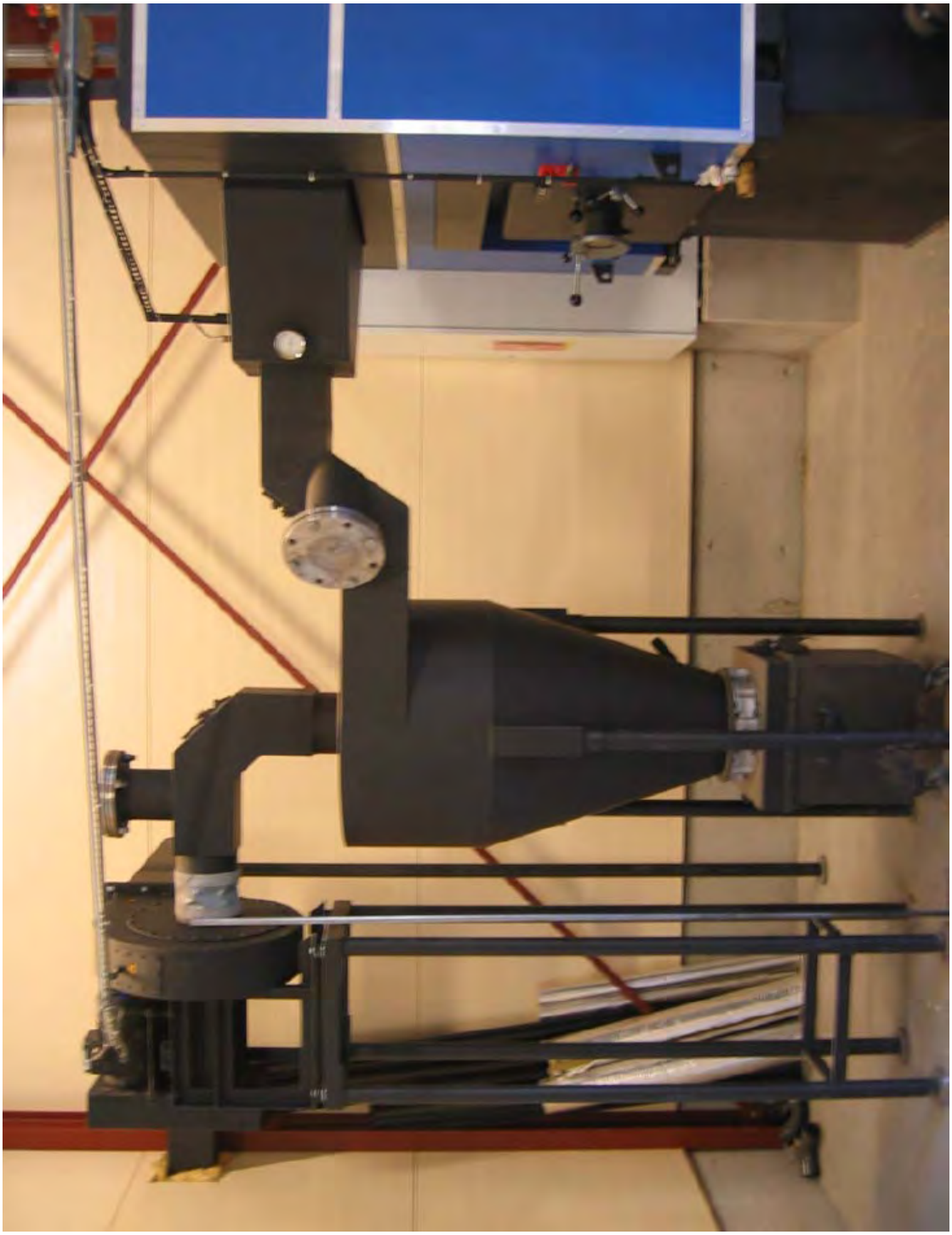

Figure E.2: Cyclone and fan

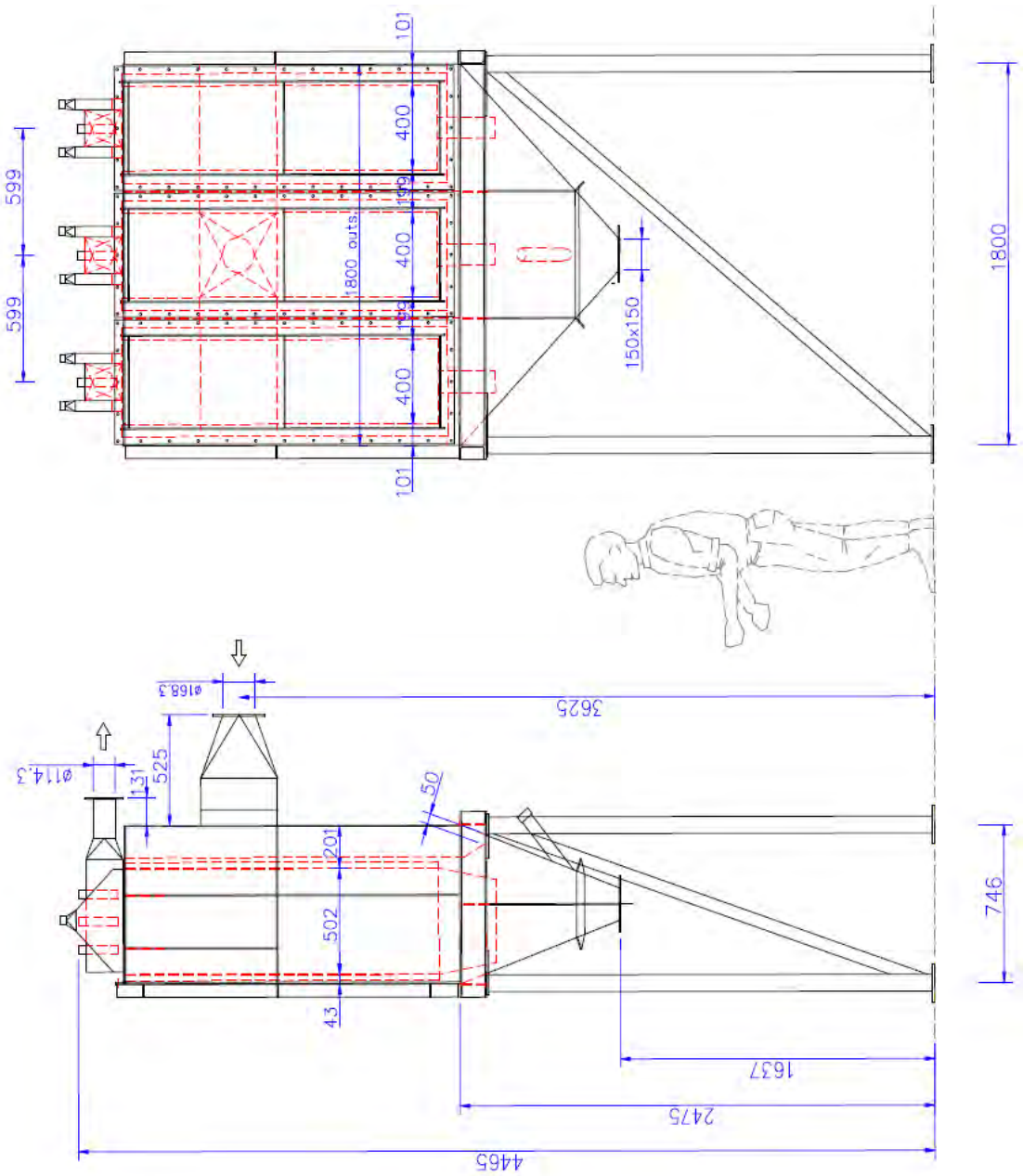

Figure E.3: Industrial scale filter housing [mm]

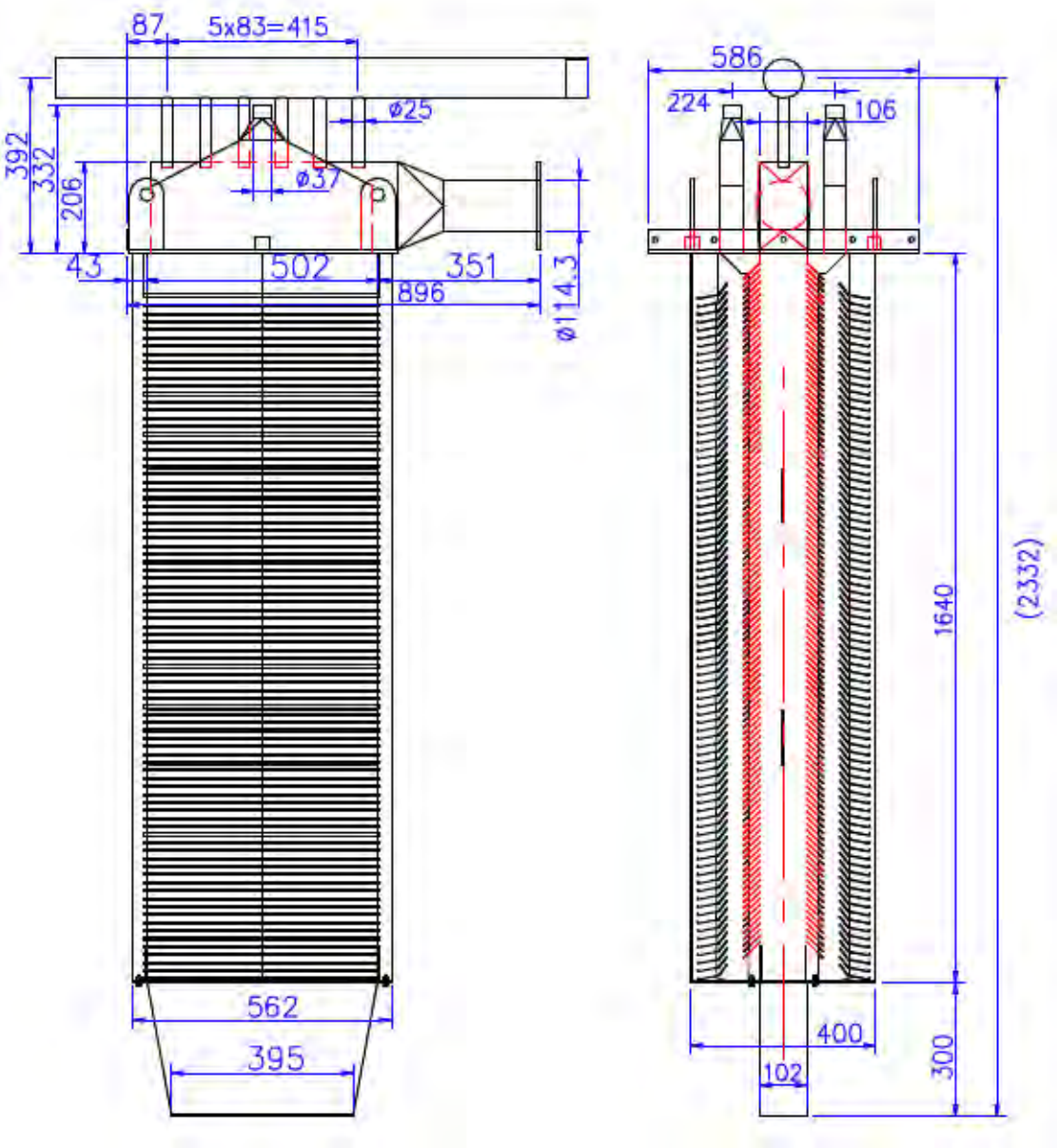

Figure E.4: Industrial scale filter moduls [mm]

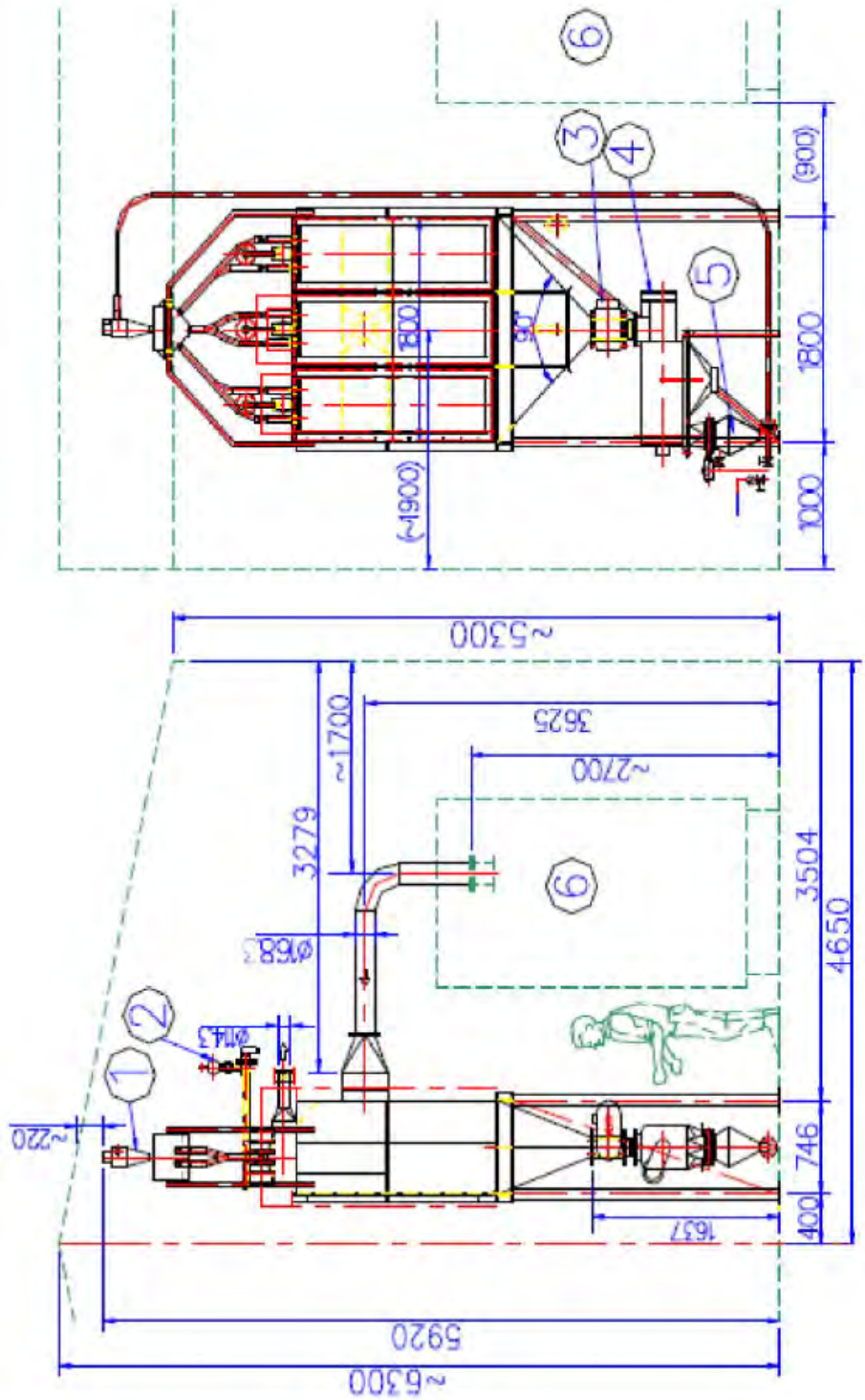

Figure E.5: Setup [mm]

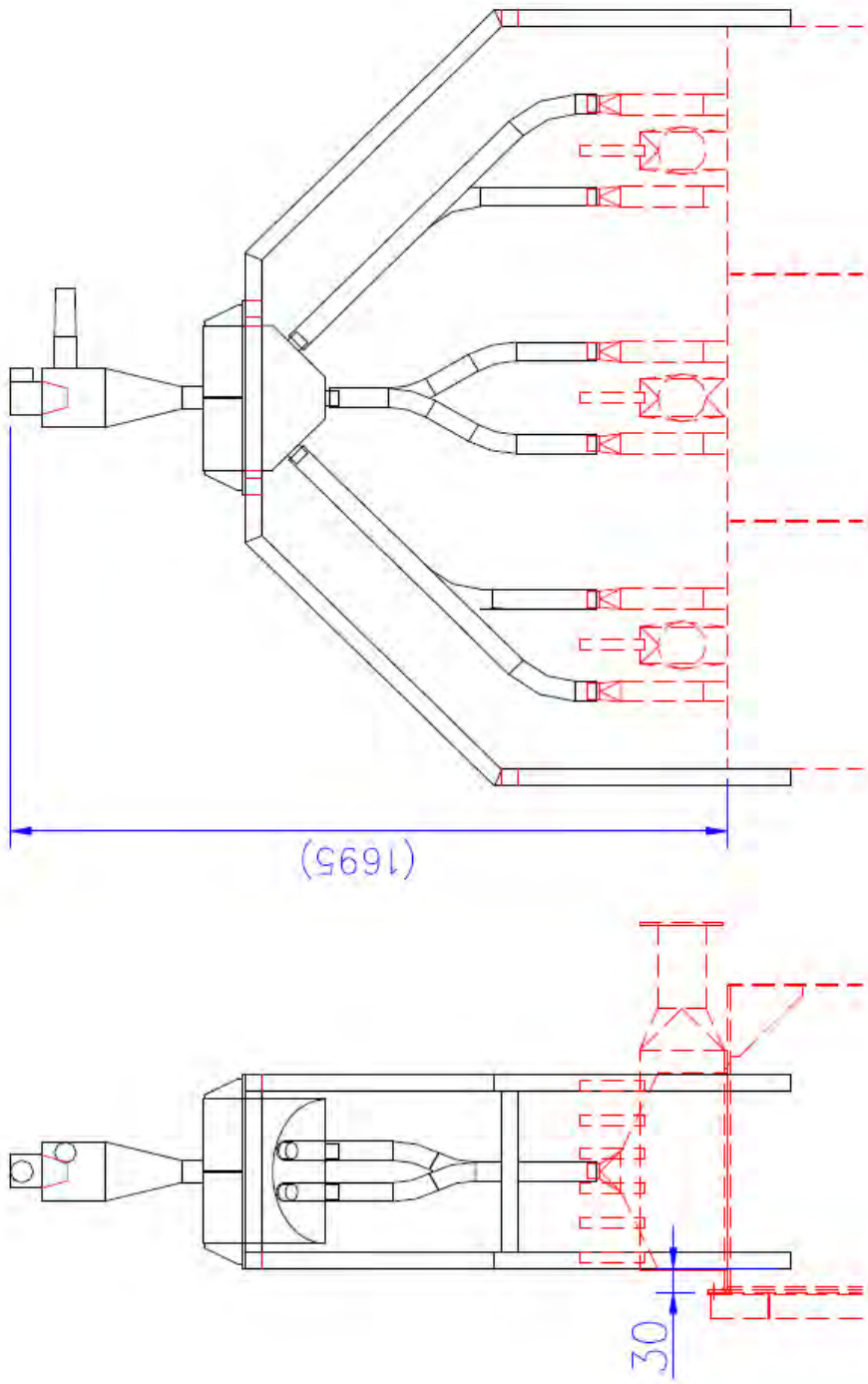

Figure E.6: Sand reservoir [mm]

Figure E.7: Filter without insulation

Figure E.8: Filter with insulation

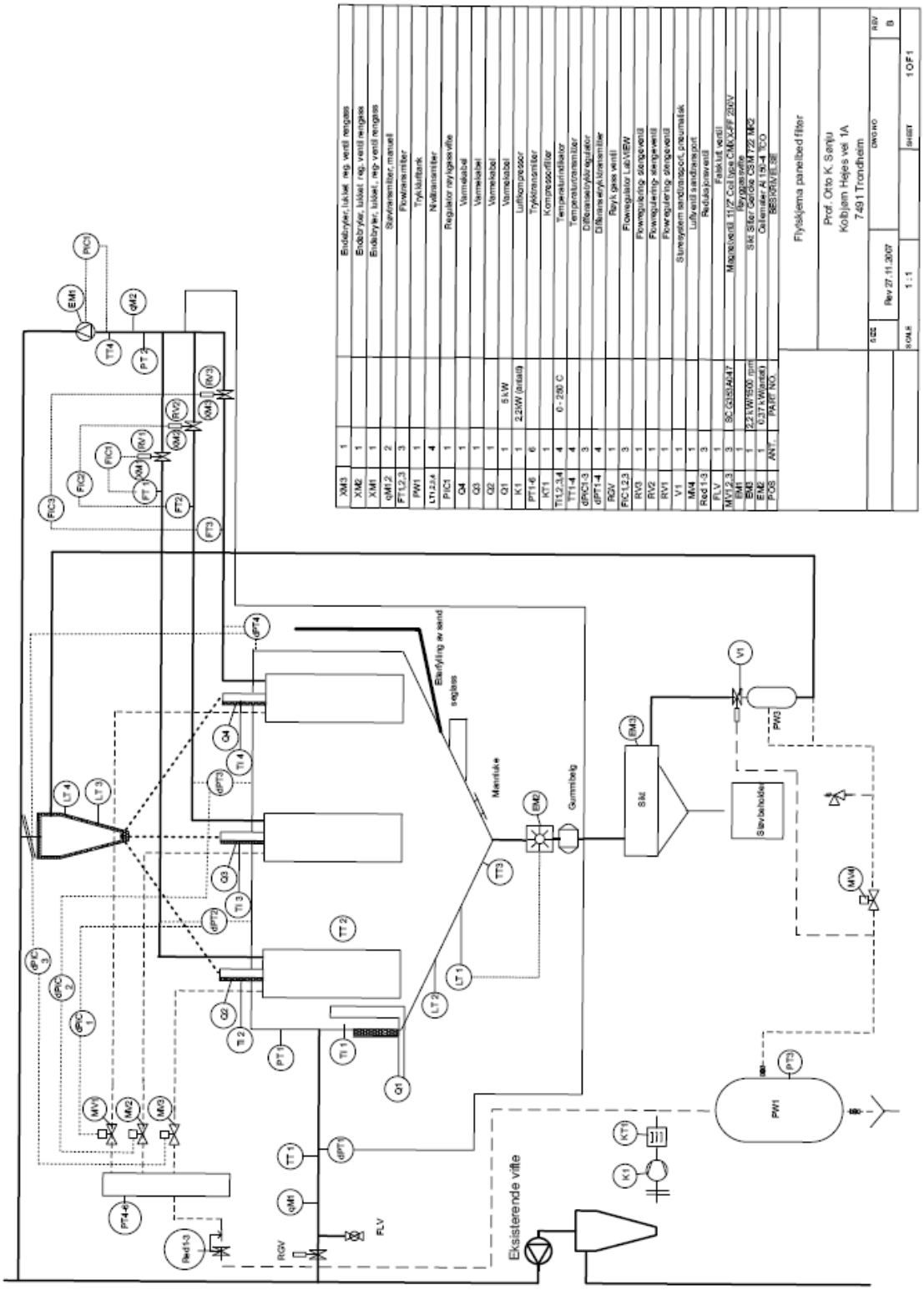

Figure E.9: Overview of instrumentation